DEVELOPING A NOVEL MODEL TO MEASURE DYNAMIC JOINT STIFFNESS OF L4/L5 JOINTS IN HUMAN LUMBAR SPINES USING AN INVERSE DYNAMIC APPROACH

by

Amir Hossein Moslehi

Submitted in partial fulfilment of the requirements for the degree of

Master of Applied Science

at

Dalhousie University
Halifax, Nova Scotia
April 2016

This thesis is dedicated to my parents, Majid and Touba, for their unconditional love and support over the years.

Table of Contents

LIST OF TABLES viii

LIST OF FIGURES x

ABSTRACT xiii

LIST OF ABBREVIATIONS USED xiv

ACKNOWLEDGMENTS xv

Chapter 1 INTRODUCTION 1

1.1. Purpose 6

1.2. Objectives 7

1.3. Hypotheses 8

1.4. Assumptions 8

1.5. Thesis Structure 9

Chapter 2 BACKGROUND LITERATURE 10

2.1. Low Back Pain & Spinal Stability 10

2.2. Joint Stiffness 14

2.3. Angle Measurements 19

2.3.1. Absolute Angle Measurements 19

2.3.2. Relative Angle Measurements 22

2.4. Dynamic vs. Quasi-Static Analysis 26

2.5. Abdominal Hollowing 28
2.6. Summary of Motivation 31
Chapter 3 METHODOLOGY 32
3.1. Research Design 32
3.2. Participants 32
3.3. Motion Markers Placement Protocol 33
3.4. EMG Sensor Placement Protocol 35
3.5. Normalization Exercises 36
3.6. Trunk Stability Test Protocol 37
3.7. TST Event Determination 40
3.8. General Data Acquisition 42
3.9. General Data Processing 43
3.9.1. Surface Electromyography 43
3.9.2. Kinematics 44
3.9.3. Kinetics 45
3.10. Objective 1 Methodology 48
3.10.1. Absolute & Relative Angle Calculations (Objective 1-b) 48
3.10.2. Dynamic vs. Quasi-Static Analysis (Objective 1-c) 51
3.10.3. Dynamic Analysis w/ and wo/ GRFs (Objective 1-d) 51
3.11. Objective 2 Methodology 52

3.11.1. Session I 53
3.11.2. Session II 54
3.11.3. Data Processing 55
3.11.4. Dependent Variables 58
3.11.5. Statistical Analysis 62
Chapter 4 OBJECTIVE 1 RESULTS 65
4.1. Introduction 65
4.2. Results 66
4.2.1. Absolute and Relative Angles Calculations (Objective 1-b) 66
4.2.2. Dynamic vs. Quasi-Static Analysis (Objective 1-c) 71
4.2.3. Dynamic Analysis w/ and wo/ GRF (Objective 1-d) 73
Chapter 5 OBJECTIVE 2 RESULTS 78
Introduction 78
5.2. Results 78
5.2.1. Normality Test Results 78
5.2.2. Participants' Demographics 79
5.2.3. Exercise Timing 79
5.2.4. Internal Oblique Muscles' Mean EMG Amplitude 80
5.2.5. Sagittal Plane L4/L5 Range of Motion 80
5.2.6. Sagittal Plane L4/L5 Joint Moment 83

5.2.7. Sagittal Plane L4/L5 Dynamic Joint Stiffness 85
Chapter 6 DISCUSSION 92
6.1. Objective 1 92
6.1.1. Objective 1.a 92
6.1.2. Objective 1.b 93
6.1.3. Objective 1.c 95
6.1.4. Objective 1.d 98
6.2. Objective 2 100
Chapter 7 CONCLUSION 108
7.1. Summary 108
7.2. Implications 112
7.3. Limitations 113
7.4. Future Research 113
7.5. Conclusion 114
BIBLIOGRAPHY 115
APPENDIX A DETAILED KINEMATIC & KINETIC MODEL 130
A.1. Segments' ACS & LCS 130
A.2. Rotational & Translational Matrices 136
A.3. Velocity & Acceleration 137
A.4. L4/L5 Joint Angle 140

A.5. Inverse Dynamics 142

APPENDIX B NORMALITY TEST RESULTS 149

APPENDIX C DYNAMIC VS. QUASI-STATIC ANALYSIS 152

APPENDIX D DYNAMIC MOMENT W/ AND WO/ GRF 155

LIST OF TABLES

Table 3-1: Dependent variables 62

Table 4-1: Comparison of thesis kinematic model and electrogoniometer 70

Table 4-2: Comparison of dynamic and quasi-static L4/L5 joint moments. 72

Table 4-3: Comparison of dynamic and quasi-static L4/L5 joint moments at the minima and maxima 73

Table 4-4: Comparison of dynamic sagittal plane L4/L5 joint moments with and without GRF in TST 1 and 3. 75

Table 4-5: Comparison of dynamic L4/L5 joint moments with and without GRF at the locations shown in Fig. 4-7 76

Table 4-6: Participants' mass, and their associated RMSE 77

Table 5-1: Participants information. 79

Table 5-2: Exercise timing for TST levels 1 and 3. 79

Table 5-3: IO muscles mean EMG amplitude in TST levels 1 and 3. 80

Table 5-4: Sagittal plane L4/L5 range of motion (ROM) in TST levels 1 and 3..... 82

Table 5-5: Sagittal plane L4/L5 joint moments at the minima and maxima in TST levels 1 and 3. 84

Table 5-6: The maximum and critical L4/L5 joint angle velocities 88

Table 5-7: Sagittal plane L4/L5 joint stiffness in TST levels 1 and 3. 90

Table C-1: Detailed comparison of dynamic and quasi-static sagittal plane L4/L5 joint moments in TST 1 152

Table C-2: Detailed comparison of dynamic and quasi-static sagittal plane L4/L5 joint moments in TST 3 153

Table C-3: Detailed comparison of dynamic and quasi-static L4/L5 joint moments at the minima and maxima in TST 1 153

Table C-4: Detailed comparison of dynamic and quasi-static L4/L5 joint moments at the minima and maxima in TST 3 154

Table D-1: Detailed comparison of dynamic sagittal plane L4/L5 joint moments with and without GRF in TST 1. 155

Table D-2: Detailed comparison of dynamic sagittal plane L4/L5 joint moments with and without GRF in TST 3. 156

Table D-3: Detailed comparison of dynamic L4/L5 joint moments with and without GRF at the locations shown in Fig. 4-7 in TST 1 156

Table D-4: Detailed comparison of dynamic L4/L5 joint moments with and without GRF at the locations shown in Fig. 4-7 in TST 3 157

LIST OF FIGURES

Figure 1-1: The ball and bowl model illustrating stability. 4

Figure 3-1: Marker set-up in the laboratory..... 34

Figure 3-2: Starting position of the participant in the motion trials. 38

Figure 3-3: Modified TST level 1..... 39

Figure 3-4: Modified TST level 3..... 40

Figure 3-5: Sagittal plane relative right hip joint angle in TST 1..... 41

Figure 3-6: Sagittal plane relative right hip joint angle in TST 3..... 41

Figure 3-7: Sagittal plane relative knee joint angle in TST 3..... 42

Figure 3-8: Pelvis free body diagram. 46

Figure 3-9: The electrogoniometer calibration equation obtained by plotting the angles versus the output voltages..... 49

Figure 3-10: Location of the motion capture system triads and the sensors of the electrogoniometer 50

Figure 3-11: Flowchart of the experimental procedure. 53

Figure 3-12: Flowchart illustrating the order in which the participants performed the experimental tasks..... 55

Figure 3-13: Comparison of ensemble averaged sagittal plane L4/L5 joint angle waveform in TST level 1, before and after low-pass filtering at 1.5 Hz using a Butterworth 4^{th} order recursive filter 57

Figure 3-14: The area where the mean EMG amplitude was calculated..... 59

Figure 3-15: Sagittal plane L4/L5 joint angle range of motion (ROM) in TST1 59

Figure 3-16: Sagittal plane L4/L5 joint angle range of motion (ROM) calculation in TST3. 60

Figure 3-17: Calculation of the L4/L5 joint moments at the minima and maxima in TST level 1. 61

Figure 3-18: Calculation of the L4/L5 joint moments at the minima and maxima in TST level 3. 61

Figure 4-1: Comparison of absolute angle measurements between the motion camera system and inclinometer for the left shank. 67

Figure 4-2: Comparison of absolute angle measurements between the motion camera system and inclinometer for the right shank 67

Figure 4-3: Comparison of absolute angle measurements between the motion camera system and inclinometer for the left thigh 68

Figure 4-4: Comparison of absolute angle measurements between the motion camera system and inclinometer for the right thigh 68

Figure 4-5: Comparison of the L4/L5 joint relative angle measured by the developed kinematic model and the electrogoniometer 70

Figure 4-6: Ensemble averaged dynamic and quasi-static L4/L5 joint moments in the sagittal plane in TST 1 and TST 3. 71

Figure 4-7: Comparison of ensemble dynamic sagittal plane L4/L5 joint moment with and without GRF in TST 1 and TST 3. 74

Figure 4-8: Plots of RMSE versus participants' mass in TST 1 and TST 3 77

Figure 5-1: Ensemble averaged sagittal plane L4/L5 joint angle for all the participants in TST 1 and TST 3 83

Figure 5-2: Ensemble averaged sagittal plane L4/L5 external joint moment for all the participants in TST 1 and TST 3 85

Figure 5-3: A representative sagittal plane dynamic L4/L5 joint stiffness in TST 1 91

Figure 5-4: A representative sagittal plane dynamic L4/L5 joint stiffness in TST 3 91

Figure A-1: Pelvis width, the locations of RASIS and LASIS, and the coordinate system used for estimating the HJCs. 132

Figure A-2: The location of the cervical joint center..... 134

Figure A-3: Leg's triad. 136

Figure A-4: Free body diagram of a person at the starting position of the Trunk Stability Test protocol exercises..... 142

Figure A-5: Free body diagram of foot and shank..... 143

Figure A-6: Free body diagram of the thigh. 145

Figure A-7: Free body diagram of pelvis..... 146

ABSTRACT

Joint stiffness has been claimed as the main component providing stability to human spines during different daily activities. As a result, researchers have developed various models to calculate spinal joint stiffness during performance of different functional tasks. However, to date, the models in the literature have estimated spinal joint stiffness using only discrete measures during dynamic tasks, and do not consider temporal changes. Therefore, the main objective of this thesis was to address this gap in the literature by developing equations to estimate dynamic L4/L5 joint stiffness in the sagittal plane, and to use these equations to estimate sagittal plane dynamic L4/L5 joint stiffness during two different controlled dynamic tasks under two different conditions (performing the tasks with and without abdominal hollowing (AH)). Ten healthy men between the age of 20 and 30 years old with no history of low back pain were recruited to perform two modified levels of Trunk Stability Test protocol (levels 1 and 3) with and without AH. The results of this study revealed that AH resulted in significantly ($p < 0.05$) higher dynamic L4/L5 joint stiffness and lower L4/L5 joint angle range of motion, but no significant effect on the sagittal plane L4/L5 joint moments.

LIST OF ABBREVIATIONS USED

ACS: Anatomical Coordinate System

AH: Abdominal Hollowing

ANOVA: Analysis of Variance

EMG: Electromyography

FBD: Free Body Diagram

GCS: Global Coordinate System

GRF: Ground Reaction Force

IO: Internal Oblique

L4/L5 joint: The joint between the lowest two vertebrae of the lumbar spine.

L4/L5 (relative) joint angle: This term refers to the relative angular motion of pelvis to trunk around the L4/L5 joint axis

LCS: Local Coordinate System

MVIC: Maximum Voluntary Isometric Contraction

NAH: No Abdominal Hollowing

RMSE: Root Mean Squared Error

ROM: Range of Motion

TrA: Transversus Abdominis

TST: Trunk Stability Test

ACKNOWLEDGMENTS

Firstly, I would like to express my sincere gratitude to my supervisor Dr. Cheryl Kozey for the continuous support of my thesis, for her patience, motivation, and immense knowledge. Her guidance helped me in all the time of research and writing of this thesis.

I would also like to thank the rest of my thesis committee, Dr. John Kozey and Dr. Janie Astephen Wilson, for their insightful comments and encouragement. Additionally, I am very grateful to Dr. Derek Rutherford for allowing me to use the equipment in the Joint Action Research laboratory for my thesis, and for being very kind in answering my questions.

A very special thanks goes to Adam Quirk for his help with my thesis data collections, and for kindly answering my biomechanics questions during the course of my study. I was very fortunate to be sharing a laboratory and grad office with him.

My sincere thanks also goes to Mr. James Crouse for providing exceptional technical support in the laboratory during my thesis and other research projects.

Last but not least, I would like to thank my parents, Majid and Touba, and my brothers, Hamid and Mojtaba, for their unconditional support throughout my Masters program and my life in general.

I would like to acknowledge Natural Sciences and Engineering Research Council for funding the study.

CHAPTER 1 INTRODUCTION

Low back pain (LBP) is a common and significant cause of work and social loss and makes up approximately 85% of all back pain cases (i.e. cervical, thoracic, and lumbar pain) (Chang, 2008). Surveys show that about 60-80% of the population in industrialized societies suffer from low back pain at least once in their lifetime (APTA, 2012; Asher, 2013), and that approximately 20-30% of people suffer from LBP at any given time (ASDA, 2009). LBP is the leading cause of lost work, which results in tremendous economic burden on individuals, industries, and governments. For instance, in the United Kingdom, LBP is the most common cause of disability in young adults, resulting in more than 100 million days of lost work per year (Duthey, 2013). In the United States, this number is estimated to be about 149 million, with an annual cost ranging from $100 to $200 billion (ASDA, 2009; Duthey, 2013). In 2008, due to the high prevalence of LBP among Australian adults, researchers lobbied the government to name back pain as a National Health Priority Area, since it was one of the leading causes of lost work and long-term disability (Briggs & Buchbinder, 2008). While LBP can happen to people of any age, it is more common in those aged 30 to 60 years who have a sedentary lifestyle or perform heavy labor (Statistics Canada, 2006). LBP is second only to upper respiratory disease as a cause of work loss. In fact, the medical costs and costs for LBP compensation at work are estimated to be greater than the total cost of all other work injuries (ASDA, 2009). Due to the complex nature of lumbar spine anatomy, precise diagnosis of LBP is difficult, which makes treatment challenging. Hence, in the majority (i.e., about 85 to 90%) of cases, LBP is labeled as “non-specific”, meaning that the exact cause of the pain is unknown (Borenstein & Callin, 2012).

Although spinal instability has been theorized to be one of the main causes of low back pain (McGill, 2001), stability is still not well defined or understood in the literature (Reeves, Narendra, & Cholewicki, 2007). In spinal biomechanics, there is no accepted definition of spinal stability, and therefore biomechanists have used different definitions based on their context of research. However, there are two general categories of spinal stability that form the basis for current spinal stability analyses: mechanical stability and clinical stability. Mechanical stability was pioneered by Bergmark in 1989 when he developed a simple mathematical model of the spine by which he was able to mathematically formulize spine stability (Bergmark, 1989). In his model, he used joint stiffness and 40 trunk muscles to formulize spine stability. Shortly after that, Panjabi introduced clinical stability by developing a theoretical model of the spine in humans (Panjabi, 1992, 2003, 2006; Panjabi, Abumi, Duranceau, & Oxland, 1989). Panjabi's spinal stability model included three independent subsystems which work together to provide stability for the spine. These subsystems include a passive system (i.e. vertebrae, facet articulations, intervertebral discs, spinal ligaments, joint capsules, and the passive mechanical properties of the muscles), an active system (i.e. muscles and tendons), and a neural control system (i.e. neural control centers (brain and spinal cord), and the various force and motion transducers embedded in the ligaments, tendons, and muscles). Both Bergmark's and Panjabi's models were based on similar components. In fact, they have both introduced the three subsystems described above (i.e. passive, active, and neural control) as integral parts of the spine stabilizing system. Panjabi supports Bergmark's model with a more clinically relevant model of how spine instability can cause injury, and create pain and discomfort. Moreover, they have both acknowledged the importance

of muscular structures in creating spine stiffness to maintain spine stability during different tasks. However, there are some differences in basic definitions of mechanical and clinical stability models. For example, under mechanical stability, stability is an absolute term meaning that spine is either stable or not stable. On the other hand, clinical stability is related to the amount of deformation in a loaded spine. Hence, unlike mechanical stability, clinical stability is continuously variable and the spine can be more or less stable under loaded conditions. Moreover, Bergmark's mechanical stability only analyzes stability under static environments and describes stability requirements under static postures and loads. Therefore, Bergmark's model is not able to explain stability requirements of a person under dynamic conditions where they move from one posture to another.

To simplify the concept of spine stability, stability has often been visualized using a ball and bowl analogy (McGill, 2001; Panjabi, 2003). This analogy utilizes potential energy (PE) in the form of PE = mass × gravity × height (Figure 1-1). When the ball is placed inside a bowl and a force is applied to the ball, the system is stable if the ball rises up the side of the bowl and then returns to rest at the bottom of the bowl, where the potential energy is minimum (i.e., height is minimum, and therefore PE is minimum). As mentioned by Bergmark (1989), "stable equilibrium prevails when the potential energy of the system is minimum". Hence, we can determine the stability of the system by analyzing the energy state of the system before and after perturbation. As can be seen in this figure, when the bowl is deeper and/or the sides of the bowl are steeper, the system is potentially more stable. This is because with the deeper bowl or steeper sides, the ball is

more likely to return to a minimal potential energy state, and hence, be more stable following a perturbation.

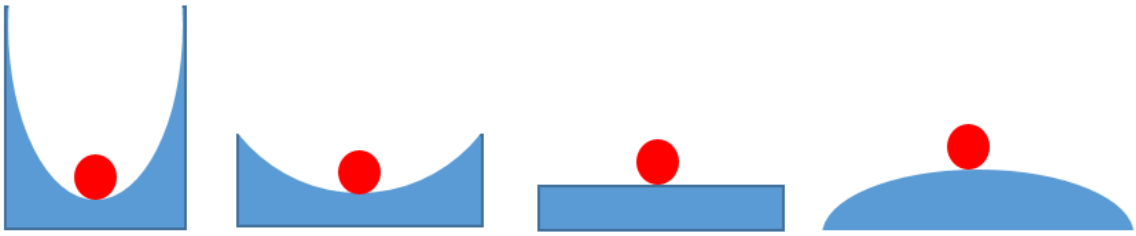

Figure 1-1: The ball and bowl model illustrating stability. (A) is the most stable, whereas (D) is the least stable system. Increasing the deepness of the bowl and the steepness of the sides will result into a more stable system because the ball will have much less chance of rolling out of the bowl during perturbation. Reprinted with permission from (McGill, 2001).

Spinal joints translate and rotate in three dimensions, leading to a six-dimensional ball and bowl system for each joint. The human body has six lumbar joints, so we will need a 36-dimensional ball and bowl system to represent the entire lumbar spine. Thus, if the height of the bowl is lowered such as in Fig. 1.1(b), the ball can roll out of the bowl causing an instable system. Clinically, instability in one or more of these 36 dimensions can be caused by a muscle with inappropriate stiffness, or a damaged passive tissue with impaired stiffness (McGill, 2001).

The potential energy used in the ball and bowl model is called gravitational potential energy, which is useful in the simplification of the concept of stability. However, for the human body, the elastic potential energy is used, which is calculated in terms of stiffness (k) and deformation of the elastic element such as muscle or joint's passive capsules and ligaments (x): $PE = 0.5 \times k \times x^2$. In this case, unlike the gravitational potential energy,

higher elastic potential energy leads to a more stable system. As can be seen in this equation, the higher the stiffness (k), the higher the potential energy, and hence, the greater the stability (i.e., deep bowl with steep sides (Fig. 1.1(a))). Therefore, we can conclude that stiffness is related to stability, and that stability is increased by increasing stiffness.

It has been claimed that increasing the muscle activity causes a quick and non-linear increase in joint stiffness, so that even moderate levels of muscle activity create stiff and stable joints. (McGill, 2001) Moreover, the soft tissues around the joints themselves possess inherent passive stiffness that is mostly attributed to the joint capsules and ligaments. Passive components become especially important toward the end of range of motion. Based on the Panjabi model, the motor control system provides joint stability through muscle activation, and, to a lesser extent, passive stiffness in the neutral spine or not at extreme ranges. However, when the neural control system becomes impaired, the system can cause inappropriate levels of muscle activation and force and thus create inappropriate stiffness (Panjabi, 1992, 2003, 2006). In the example of the ball and bowl model, this will cause the ball to roll out of the bowl, resulting in an unstable system.

As described in the previous paragraphs, joint stiffness is an important component of spinal stability. Hence, many researchers have attempted to calculate joint stiffness using various methods including electromyography (EMG) assisted muscle modelling (Cholewicki & McGill, 1996; Grenier & McGill, 2007; Kavcic, Grenier, & McGill, 2004), quick reflex method (Bazrgari, Nussbaum, & Madigan, 2012; Brown & McGill, 2009; Cholewicki, Lee, Peter Reeves, & Morrisette, 2010; Granata & Rogers, 2007), and moment vs. joint angle approach (Beach, Parkinson, Stothart, & Callaghan, 2005; Green,

Grenier, & McGill, 2002; McGill, Seguin, & Bennett, 1994; Parkinson, Beach, & Callaghan, 2004). Each method uses different algorithms and inputs in order to calculate joint stiffness. Hence, different researchers may use different approaches to measure joint stiffness in their study. The one and perhaps the most important gap that has been found in the literature is that no study has measured dynamic joint stiffness of spine in a dynamic task. In other words, researchers have only looked at discrete measures of joint stiffness. Therefore, this study has attempted to address this gap by developing a kinematic and kinetic model that measures dynamic joint stiffness of spine during a dynamic task. This will allow us to observe the change in joint stiffness of lumbar spine (i.e. amplitude and pattern) during an entire dynamic task.

1.1. PURPOSE

The purpose of this study was twofold. First, to develop a sagittal plane kinematic and kinetic model of the spine, pelvis and lower limb; and second, using the L4/L5 joint angle motion and L4/L5 moment changes, calculate a measure of dynamic joint stiffness at the L4/L5 joint of human spines. To achieve these purposes, motion, inertial properties, and ground reaction forces were recorded during two levels of a modified trunk stability test (TST). Then, the relative joint angle of L4/L5 vertebrae relative to the pelvis (**referred to herein as the relative L4/L5 joint angle**) were calculated and using a bottom-up inverse dynamic approach, the dynamic joint moments about L4/L5 joint were calculated. Finally, dynamic joint stiffness of L4/L5 were estimated using the slope of joint moment vs. joint angle plot.

1.2. OBJECTIVES

Due to the developmental nature of the project, a number of objectives were identified to develop the foundation to address the main objective (2).

1. Develop methodology to estimate sagittal plane dynamic joint stiffness at L4/L5 joint. This included the following sub-objectives:

    a) Implement a kinematic and kinetic model using a linked segment model of the trunk, pelvis, and the lower limbs.

    b) Confirm the reasonability of the kinematic model by calculating the relative L4/L5 joint angle (as defined above) and the absolute angular displacements of the thighs and legs. Then, check their agreement with the values measured by other angle measurement systems (i.e. digital inclinometer for absolute angles, and electrogoniometer for relative angles).

    c) Calculate the L4/L5 joint moments dynamically and quasi-statically, and estimate the effect of inertial factors to net resultant joint moment at the L4/L5 joint.

    d) Calculate dynamic joint moments of L4/L5 with and without ground reaction forces, and estimate the effect of the ground reaction forces on the net resultant joint moment at the L4/L5 joint.

The main objective of this study was as follows:

2. To compare sagittal plane dynamic L4/L5 joint stiffness between two different dynamic controlled tasks (TST 1 and 3) with each task performed under two different conditions (with and without abdominal hollowing).

    a) Compare sagittal plane relative L4/L5 joint angles and L4/L5 moments, and the activation amplitudes of the internal oblique muscles between tasks and condition.

1.3. HYPOTHESES

The main hypotheses of this study were twofold. Studies have shown that performing the abdominal hollowing (AH) increases the initial abdominal muscle activities. Hence, the first hypothesis of this study is that abdominal hollowing leads to greater dynamic L4/L5 joint stiffness during controlled dynamic tasks. The second hypothesis of this study is that due to the added knee extension in one of the two dynamic tasks in the study (i.e. modified TST level 3), there will be larger moment magnitude and higher overall dynamic joint stiffness at the L4/L5 joint in the modified TST level 3 compared to the other task (i.e. the modified TST level 1).

1.4. ASSUMPTIONS

The assumptions of this study are:

- That minimal movement occurred between the kinematic markers and skin during the experimental tasks (controlled by using tight straps for triads, and double sided tapes for single markers). Moreover, the movement between EMG electrodes and skin was minimal.

- That the same kinematic marker and EMG electrode placement were performed for each participant.
- That no significant learning effect occurred between trials. This was achieved by familiarization and practice sessions before the testing session, and randomization of conditions.
- That fatigue was not be present during the testing (controlled by giving periodic rest breaks between trials).

1.5. THESIS STRUCTURE

This thesis is comprised of seven chapters. Chapter 1 provides an introduction to the study and describes the thesis's purpose, objectives, hypotheses, and assumptions. Chapter 2 examines the relevant background literature regarding spinal stability and spinal joint stiffness. Chapter 3 provides the detailed methodology which was used to address the objectives and sub-objectives of this thesis. Chapters 4 and 5 present the results related to the Objectives 1 and 2 of this thesis respectively. Chapter 6 provides a discussion of the results presented in Chapters 4 and 5. Finally, Chapter 7 concludes the thesis by providing a summary of the results, implications, limitations, and directions for future research.

CHAPTER 2 BACKGROUND LITERATURE

2.1. LOW BACK PAIN & SPINAL STABILITY

Low back pain (LBP) is a very common musculoskeletal disorder which imposes a huge economic burden on individuals and societies (APTA, 2012; Duthey, 2013). The spine is a complex multi-segment structure that supports the head and trunk during posture and movements. It also contains and protects the spinal cord, nerve roots, and arteries (Izzo, Guarnieri, Guglielmi, & Muto, 2013). The lower region of the spine, known as the lumbar spine, is responsible for supporting the trunk and for transmitting compressive and shear forces to the lower body during daily activities. However, it has been reported that thoracolumbar and lumbar parts of the spine devoid of musculature, buckle under just 20 and 90 N compressive loads, respectively (Crisco, Panjabi, Yamamoto, & Oxland, 1992). On the other hand, it has been estimated that the spine can experience a compressive load of about 6000 N during heavy tasks, and a load of around 18000 N during competitive power lifting (Cholewicki, McGill, & Norman, 1991; McGill & Norman, 1986). Hence, one can conclude how important the role of muscles is in providing support for the spinal column during everyday tasks. It may be the complex anatomy of the spine and of its surrounding musculature and tissues that makes the etiology of low back pain unknown to date.

Spinal instability is claimed to be the main cause of low back pain and is still not well defined or understood. The fact that there are many interpretations and definitions about spinal stability helps us understand why Reeves et al. (2007) have made an analogy similar to the story of the six blind men and the elephant. In this poem, the blind men, depending on what part of the elephant they had touched, assumed the elephant to be a

wall (side), spear (tusk), snake (trunk), tree (leg), fan (ear), or rope (tail) (Reeves, Narendra, & Cholewicki, 2007). From this, we can see how different experiences can result in different perceptions and, by analogy, understand why various researchers and clinicians have provided different definitions of spinal stability, and why different interpretations of low back pain have been made.

Stability is one of the most important concepts that is used to characterize any systems. For a system to function properly and to achieve its goals, the system needs to be stable. In spine biomechanics, stability of spine is crucial so that spine can move and sustain loads without getting injured (Reeves et al., 2007). As mentioned in the preceding paragraph, there are various definitions for spine stability. The term mechanical stability was pioneered by Bergmark in 1989 which is defined as the spine's ability to maintain static equilibrium under loaded positions. Similar to mechanical structures, if the spine is not able to meet equilibrium conditions, it will buckle and become unstable. Therefore, under mechanical terms, the spine can be either stable or unstable at any point in time (Bergmark, 1989). In his model, Bergmark evaluated spine stability by analyzing the potential energy of the system and attempted to identify the conditions for the mechanical stability of the human lumbar spine. In order for a system (e.g., a spine) to meet the conditions of static equilibrium, the sum of the resulting force and the resulting moment acting on the system have to be zero.

$$\sum \text{Force} = \text{mass} \times \text{linear acceleration} = 0 \qquad \text{Equation 2.1}$$

$$\sum \text{Moment} = \text{moment of inertia} \times \text{angular acceleration} = 0 \qquad \text{Equation 2.2}$$

These equilibrium conditions must be met for the entire system and all components that it contains. However, even if the spine meets the equilibrium conditions, it can still collapse and become unstable. In other words, satisfaction of the conditions of the equilibrium is necessary but not sufficient, and hence, mechanical stability must also be maintained. For instance, if we lean on a piece of rod, the rod may look straight and stable, but if the force on the rod exceeds a certain value, the rod may bend. Furthermore, even though the bent rod meets the conditions of static equilibrium (i.e., the net force and moment are zero) and it does not break, it still does not satisfy the conditions of mechanical stability. This is because equilibrium is an absolute term while stability is a relative concept meaning that a system such as spine can be more or less stable if the equations of static equilibrium are not met.

Stability of the spine has also been explained by the concept of potential energy which is often visualized by a ball and bowl analogy (McGill, 2001; Panjabi, 2003; Reeves et al., 2007). In this analogy, a ball is placed inside a bowl, and the shape of the bowl will indicate whether or not the system is stable. For example, if a bowl is very shallow, under small perturbations, the ball can roll off the bowl indicating an unstable system. In the other hand, if the ball is placed inside a deep bowl with steep sides, the ball will roll up the sides of the bowl but then will come back into the resting position where the potential energy is zero. This second bowl ball and bowl example depicts a stable system.

Another important type of spinal stability is clinical stability which was first introduced by Panjabi in 1978. According to White and Panjabi (1978), clinical stability is defined as "the ability of the spine under physiologic loads to limit patterns of displacement so as not to damage or irritate the spinal cord or nerve roots and, in addition, to prevent

incapacitating deformity or pain due to structural changes. Any disruption of the spinal components (ligaments, discs, facets) holding the spine together will decrease the clinical stability of the spine. When the spine loses enough of these components to prevent it from adequately providing the mechanical functions of protection, measures are taken to re-establish the stability" (White & Panjabi, 1978).

One important difference between mechanical stability and clinical stability is that clinical stability can be more or less stable, however, in mechanical stability, the spine is either stable or unstable. Clinical stability is composed of three subsystems: passive, active, and neural control subsystems. The passive subsystem consists of vertebrae, facet articulations, intervertebral discs, spinal ligaments, joint capsules, and the passive mechanical properties of the muscles. The components of the passive subsystem do not contribute to the spinal stability significantly during the neutral position. It is actually toward the ends of the spinal ranges of motion that the ligaments start to resist the spinal motion. During the neutral position, the passive components function as transducers to measure the vertebral positions and motions. This subsystem is called passive, since it does not produce active force by itself but is dynamically active in monitoring the transducer signals.

The active subsystem includes the muscles and tendons surrounding the spinal column. The components of the active subsystem provide the required stability especially by means of forces produced in muscles. The amount of force produced in each muscle is measured by the force transducers that are embedded in the tendons. Hence, according to Panjabi's model, this aspect of the tendons is considered as a part of the neural control subsystem.

The neural subsystem includes the neural control centers and the various force and motion transducers embedded in the ligaments, tendons, and muscles. The purpose of the neural subsystem is to receive information from the various transducers, determine the requirements for the spinal stability, and then cause the active system to achieve these requirements. Each muscle's tension is measured and adjusted until the required stability is fulfilled. These requirements are dependent on the person's dynamic posture, which is a variation of lever arms and inertial loads of different masses and external loads.

Under normal conditions, the function of this stabilizing system is to provide stability to the spine during various stability demands caused by changes in the spinal posture, along with static and dynamic loads. Injury and degeneration or disease of any of the subsystems may lead to the dysfunction of the spinal stability system. When the neural control subsystem becomes aware of deficiencies in other subsystems, it may attempt to compensate by initiating changes in the active subsystem. Even though the stability of the spine may become restored, the consequences of these changes to the active subsystem may be harmful to each component of the spinal stability system. For instance, accelerated degeneration of the various components of the spinal column, muscle spasm, injury, and fatigue may take place in the body as a result of the spinal system's dysfunction. Over time, these may lead to chronic dysfunction and pain.

2.2. JOINT STIFFNESS

After Bergmark developed mechanical stability, it was determined that in order to maintain spine stability, spine stiffness is required to prevent low back injuries (Bergmark, 1989). This and other studies suggested that the lack of spine stiffness is associated with low back injuries. Hence, the researchers have tried to develop

rehabilitation protocols to retrain the central nervous systems to increase muscle recruitment which in turn will improve spine stiffness (McGill, 2001, 2004). In the example of ball and bowl system, spine stiffness makes the walls of the bowl steeper which makes it harder for the ball to roll off the bowl under perturbations. Therefore, increasing spine stiffness will increase stability of the spine, decrease the displacement of vertebrae, and reduce the risks of low back injury (Reeves et al., 2007).

Many biomechanists have attempted to quantify spine stiffness using various methods. Some of the methods that measure spine stiffness include quick reflex method (Bazrgari et al., 2012; Brown & McGill, 2009; Cholewicki, Juluru, Radebold, Panjabi, & McGill, 1999; Cholewicki et al., 2010; Granata & Rogers, 2007) EMG assisted muscle modelling (Cholewicki & McGill, 1996; Grenier & McGill, 2007; Kavcic et al., 2004), and moment vs. joint angle approach (Beach et al., 2005; Green et al., 2002; McGill et al., 1994; Parkinson et al., 2004).

In the quick reflex method, trunk stiffness and damping are calculated using trunk kinematic response to a sudden load release (i.e. quick release). In this technique, the trunk is modeled as a mass-spring-damping system with one or two degrees of freedom (DOF). The load is connected to the upper torso of the participants through a harness on the chest, and is released at a random time. Then the participant has to react to the load release by actively contracting their trunk muscles in order to maintain their spine stability. The angular displacement of the trunk relative to pelvis from the point of load release to maximum trunk deflection is captured using motion sensors, and then will be used as input to an equation that describes a one or two DOF mass-spring-damping system. Equation 2.3 illustrates a one DOF system:

$I\theta'' + B\theta' + K\theta = mgLsin\theta$ Equation 2.3

Where θ is the angular response of the trunk, I is trunk's inertia, B is trunk's damping, and K is trunk's stiffness. Moreover, mg is the weight of the trunk, and L is the distance measured from L4 to T9 of spine (Cholewicki et al., 2010). Using this model, we can only obtain discrete trunk stiffness values which are calculated over a certain period of time from the point of load release to the point of maximum trunk deflection. Hence, this approach cannot be utilized for studies in which the objectives are to calculate dynamic stiffness.

In the EMG assisted model, the EMG data from various trunk muscles can be used as input for an EMG assisted optimization algorithm to calculate stiffness of individual trunk muscles. Then using a "muscle Jacobian matrix", joint stiffness of the spine is calculated. Mathematically, "muscle Jacobian matrix" relates the muscle's length change to the joint's angular displacement (Zatsiorsky, 2002). The advantage of this approach is that using this method we can calculate dynamic joint stiffness in the spine, however, we cannot obtain surface EMG data from the deep muscles of the trunk and hence, assumptions regarding their EMG activities must be made. Moreover, todays EMG assisted models are very complex, and hence designing one is very challenging, time-consuming, and is beyond the scope of this study. Finally, although this technique is capable of calculating dynamic joint stiffness, up until now it has not been used to determine the dynamic joint stiffness of spine during different tasks.

The third method to calculate joint stiffness is the derivative of joint moment divided by joint angle (i.e. $\Delta M/\Delta\theta$) which has been used by various biomechanists (Beach et al., 2005; Green et al., 2002; McGill et al., 1994; Parkinson et al., 2004). Although

researchers only calculated discrete stiffness values using this method, this approach is capable of calculating dynamic joint stiffness because both dynamic joint moment and joint angular displacement can be calculated using the inverse dynamics and linked-segment method.

In summary, stiffness calculation using the quick reflex technique is only capable of estimating discrete stiffness values and cannot measure dynamic stiffness. Moreover, although EMG assisted approach has the capability of calculating dynamic stiffness, none of the researchers have used this technique to compute dynamic spinal joint stiffness. Additionally, surface EMG cannot be collected from the deep muscles of the trunk, and hence assumptions must be made regarding their activation patterns during a dynamic task. Also, designing a sophisticated EMG assisted model used by other researchers is very complex and challenging, and for that reason it is outside the scope of this study. Therefore, this study will use derivative of joint moment divided by joint angle (i.e. $\Delta M/\Delta\theta$) to measure dynamic joint stiffness at L4/L5 joint of spine. This study aimed to develop a kinematic and kinetic model which will estimate joint moments and angles at the L4/L5 joint of lumbar spine through a linked segment model and inverse dynamic technique. By this method, we can obtain joint moments and angles at the L4/L5 joint of spine, and then using the slope of joint moment versus joint angle, we can estimate dynamic joint stiffness. This thesis will be novel in the sense that it will be the first study that calculates dynamic joint stiffness in lumbar spine during a dynamic task. Other researchers have only calculated discrete measures which does not allow an examination of the change in stiffness during an entire dynamic task.

The motivation for examining dynamic joint stiffness is in part based on the findings that muscle activation patterns of the trunk musculature have time-varying changes which presumably results in temporal changes in active stiffness and thus joint stiffness during the performance of a dynamic task. Several studies show changes in trunk muscle activation patterns between those with and those without chronic low back pain during walking (Lamoth, Meijer, Daffertshofer, Wuisman, & Beek, 2006), exercise tasks (Hubley-Kozey & Vezina, 2002a) and trunk motions (Lariviere, Gagnon, & Loisel, 2000). Other studies from our laboratory showed that abdominal and back extensor patterns differed among different levels of a trunk stability test protocol that was aimed to improve dynamic spinal stability (Davidson & Hubley-Kozey, 2005). Furthermore, our studies showed that the abdominal and back muscle activation patterns were different between healthy individuals and those who were deemed recovered from low back injury (Moreside, Quirk, & Hubley-Kozey, 2014), and also between young and older adults (Hubley-Kozey, Hanada, Gordon, Kozey, & McKeon, 2009; Quirk & Hubley-Kozey, 2014). In all cases the pelvis motion was minimized which required the abdominal muscles to respond to the changes in the counterbalancing force requirements of the abdominal muscles to minimize pelvic motion. The minimized pelvic motion ensured that the continuously changing moments on the trunk during the dynamic tasks were mainly created by the external load and not changes in trunk motion (Hubley-Kozey, Butler, & Kozey, 2012; Hubley-Kozey et al., 2009; Hubley-Kozey, Moreside, & Quirk, 2014). Finally, a preliminary study investigated the differences in trunk muscular activation patterns of a group of healthy individuals with no low back pain between those who minimized their pelvic motion and those who did not (Moslehi & Hubley-Kozey, 2014).

The results of this study showed that the abdominal and back extensor muscle activation patterns differed between those who minimized their pelvic motion and those who did not. Furthermore, this study showed differential abdominal and back extensor responses to the dynamic perturbations during the tasks which included raising, extending, and lowering the legs, suggesting the need to investigate the spinal stiffness for the entire duration of the dynamic tasks rather than just calculate a discrete value over a specific period of time (Moslehi & Hubley-Kozey, 2014).

2.3. ANGLE MEASUREMENTS

2.3.1. Absolute Angle Measurements

In using the linked segment model and inverse dynamics technique, the body segments absolute angles during a task are utilized to calculate segments angular velocities and accelerations. Then, the segments angular velocities and accelerations are used to determine the time rate of change of the body segments' angular momentum and are incorporated into joint moment equations (Robertson, Caldwell, Hamill, Kamen, & Whittlesey, 2013). Therefore, it is important to ensure that a developed kinematics model in a study records the body segments absolute angles accurately.

Studies commonly use motion capture systems to record humans motion during different dynamic tasks (Myer, 2009). Using a linked segment model and the data obtained from the motion capture system, kinematic models can be developed to calculate the body segments absolute angles. To ensure that the developed kinematic models measure the body segments absolute angles correctly, the angle measurements are often compared against the ones obtained from other instruments.

Inclinometers are a common tool in the laboratories and clinics to measure the absolute angles of the body segments. Various studies have tested the validity and reliability of the inclinometers measurements when measuring body segments absolute angles. For instance, Saur et al. measured lumbar spine's range of motion during trunk flexion and extension by means of inclinometers and radiographic (fluoroscopy) technique as the criterion tool. Their results showed high correlation between the two techniques reporting that inclinometers are highly reliable and valid in measuring lumbar spine's range of motion and trunk's absolute flexion angles (Saur, Ensink, Frese, Seeger, & Hildebrandt, 1996). Another study measured the cervical range of motion, a rather complex motion, by means of a three dimensional ultrasound motion device as the criterion, and an inclinometer. Their results showed good agreement of cervical range of motion measurement between the two devices (intra-class correlation (ICC) >0.93 for concurrent validity). The authors reported that inclinometers are reliable devices in measuring angles (ICC > 0.90 for intra-device reliability for both devices) and suggested them for use in routine clinical orthopedic work (Malmstrom, Karlberg, Melander, & Magnusson, 2003). A different study investigated the concurrent validity of scapular plane shoulder elevation measurements using an inclinometer and a goniometer. Their results indicated excellent concurrent validity between the two measurement systems with an ICC value of 0.94. Furthermore, the 95% limits of agreement in their study suggested that the difference between inclinometer and goniometer can be expected to vary by up to ±11 degrees in scapular plane shoulder elevation measurements (Kolber, Fuller, Marshall, Wright, & Hanney, 2012). A similar study investigated the reliability of inclinometers in active shoulder range of motion measurements (i.e. active flexion, abduction, external rotation,

and internal rotation), and reported that inclinometers are reliable instruments during shoulder range of motion measurements (Kolber, Vega, Widmayer, & Cheng, 2011). Herrero et al. measured the hip abduction angle using an inclinometer and a goniometer in children with cerebral palsy. Their results indicated high intra-examiner reliability for both devices (i.e. ICC > 0.80 for goniometer; ICC > 0.85 for inclinometer), however the inter-examiner (i.e. five examiners) reliability was low for the goniometer (ICC = [0.38-0.48]) while it was high for the inclinometer (ICC > 0.97). Hence, the authors in this study concluded that inclinometers are highly reliable tool in measuring hip abduction angles in children with cerebral palsy (Herrero, Carrera, Garcia, Gomez-Trullen, & Olivan-Blazquez, 2011). In a different study, however, both the intra-examiner and inter-examiner (with two examiners) reliability for hip extension measurements between goniometer and inclinometer were high (ICC = 0.91-0.93 for intra-examiner; ICC = 0.86-0.92 for inter-examiner). These results indicated that both these devices are reliable tools in measuring hip extension angles (Clapis, Davis, & Davis, 2008). Lastly, the lower limb absolute angles were measured using three different measurement devices (pendulometer type inclinometer, electronic inclinometer, and electrogoniometer) during straight leg raise motion. While the ICC and the standard error of measurement (SEM) were not calculated for the electronic inclinometer, these values were determined for the pendulometer type inclinometer (ICC = 0.95-0.98; SEM = 0.54^{o} – 1.22^{o}). Furthermore, the mean lower limb absolute angles difference between the two types of inclinometer was 1.5^{o}. Also, the mean difference between the inclinometers and the electrogoniometer was about 10^{o}. The authors concluded that the use of an inclinometer is more suitable for measuring lower limb absolute angles during straight leg raise exercise compared to the

electrogoniometer since the inclinometer better matches the construct of limb motion during this exercise (Boyd, 2012). One major drawback with this study was that the electrogoniometer was placed on the lateral aspect of the hip joint, and hence, the output from this device is the relative hip joint angle, and not the lower limb absolute angles. Thus, special care should be taken when comparing the outputs from the electrogonimeter and inclinometers as they measure different types angles during a motion (i.e. relative hip joint angle versus lower limbs absolute angles).

Based on the preceding paragraph, the inclinometers are reliable tools in measuring the body segments absolute angles. However, a major drawback with using these devices is that unlike the motion capture systems, the inclinometers cannot be used to measure angles during dynamic motion. As mentioned previously, when developing a kinematic model to measure body segments absolute angles, it is important to test the validity of the measurements to ensure that the angles are calculated accurately. Therefore, studies that use motion capture systems to calculate body segments absolute angles can utilize inclinometers to check the agreement of the angle measurements between the two methods.

2.3.2. Relative Angle Measurements

In this study, the relative L4/L5 joint angle was used to calculate the dynamic L4/L5 joint stiffness. Therefore, it was necessary to make sure that the kinematic model in this study measured the relative L4/L5 joint angle correctly. One way to do this was to measure the relative L4/L5 joint angle with a tool other than the developed kinematic model, and then check the agreement of the measurements between the two methods.

Electrogoniometers are a common device in the laboratories and clinics that are used to measure the relative joint angles during both static and dynamic motions. Various studies in the literature have used electrogoniometers to measure humans' relative joint angles, and to compare this device with other instruments. In one study, the authors utilized a flexible electrogoniometer and a potentiometric goniometer to measure ankle and knee relative joint angles, and then compared the results together (Tesio, Monzani, Gatti, & Franchignoni, 1995). For the ankle and knee joints, the participants performed ten trials of dorsi-plantar flexion and six trials of knee flexion extension respectively. Their results indicated that for the ankle joint, two output from the two instruments vary by 19% to 40%. Similarly, for the ankle joint, the outputs varied 24% to 32%. The authors claimed that due to inflexibility of the potentiometric goniometer's arms, the potentiometric goniometer tended to underestimate the joint angles whereas in the electrogoniometer, the sensors are connected to each other by a flexible cable, and hence, they are free to move as the knee and ankle joint angles change (Tesio et al., 1995). In another study, the researchers measured various joint angles (i.e. knee, hip, elbow, and shoulder) by a goniometer, a Leighton flexometer, and an electrogoniometer. Then, they compared the outputs from the three instrument. Their results showed that the outputs from the goniometer and the flexometer were correlated and were in high agreement. However, the output from the electrogoniometer was poorly correlated with both the goniometer and the flexometer. The authors indicated that one of the reasons that the output from the electrogoniometer was not correlated with the other two instruments was that the cable containing the strain gauge was frequently bent during the exercises. Moreover, the authors noticed that during shoulder extension and abduction, the electrogoniometer's

endblocks rotated during the motion which introduced crosstalk to the measurements. Lastly, it was noted that the electrogoniometer performed best when its endblocks were placed directly on skin. However, since this study was comparing the joint angles while the participants were wearing different clothing, the slight movements of the endblock over the clothing could potentially lead to inaccurate results (Adams & Keyserling, 1993). In a different study, the ankle joint's motion during gait was assessed by an electrogoniometer in both sagittal and frontal plane. Their results showed that the sagittal plane angles were similar to the ones measured by potentiometric goniometers and motion capture systems in the literature. However, the inversion angles measured in the frontal plane were higher than those reported in the literature. One potential reason for measurement errors in the frontal plane is that the location of the axis around which the subtalar inversion and eversion movements occur is still controversial in the literature as it differs greatly among individuals (Moriguchi, Sato, & Gil Coury, 2007). Bronner et al. compared an electrogoniometer with a digital protractor. The measurements were taken from -140^{o} to +140^{o} in 10^{o} stepped intervals. The results indicated high correlations ($r \geq 0.998$) and low standard error of measurement (SEM $\leq 3.65^{o}$) between the two devices. The study also investigated the agreement of hip, knee, and ankle joint angle measurements in the sagittal plane between an electrogoniometer and a five-camera motion capture system (Vicon, Oxford Metrics, Oxford, UK) during several dance moves. The results revealed high reliability of electrogoniometer ($r \geq 0.983$; SEM $\leq 3.49^{o}$), and high correlation between the electrogoniometer and the motion capture system measurements ($r \geq 0.949$; SEM $\leq 6.80^{o}$) (Bronner, Agraharasamakulam, & Ojofeitimi, 2010). Another study also compared the agreement of joint angles between

electrogoniometers and motion capture system, with the motion capture system being the criterion measure. In this study, five participants were asked to walk with their self-selected speed while their knee flexion angle was recorded by both an electrogoniometer and a five-camera motion capture system (Vicon, Oxford Metrics, Oxford, UK). The results indicated high agreements of temporal knee flexion angle patterns between the electrogoniometer and the motion capture systems. The mean difference in left knee flexion angle range of motion was 0.6º between the two systems. For the right knee, the mean difference was 0.8º (Rowe, Myles, Hillmann, & Hazlewood, 2001). This study also investigated the electrogoniometer's crosstalk which occurs when the human's joint is exposed to movement in more that one plane (i.e. joint angle measurement during simultaneous flexion/extension and abduction/adduction, or when the endblocks are twisted). When the enblocks were twisted along the long axis of the device from -60º to +60º, there was a systematic error of 3% (1.5º) in a 60º range. In another test, the electrogoniometer went through flexion/extension from -120° to +120° while being abducted and adducted at different angles (-40º, -20º, 0º, +20º, and +40º). The results showed that the measurement errors increased as both the flexion/extension and abduction/adduction angle increased. The maximum error in this test was 8% (10º) (Rowe et al., 2001).

Overall, and based on the preceding paragraph, the electrogoniometers are reliable tools in measuring the relative human joints angles during both static and dynamic motions. However, if these devices are not used properly, they can produce erroneous angle measurements. For instance, it has been shown that moving the body segments around a joint in more than one plane of motion results in crosstalk in the measurements (Rowe et

al., 2001). Furthermore, the endblocks of the electrogoniometers must be applied directly on the skin rather than on clothing to eliminate the endblocks/skin motion artifact (Adams & Keyserling, 1993). Lastly, over-flexion or extension and bending of the strain gain inside the connecting cable of the electrogoniometers can produce errors in the measurements (Adams & Keyserling, 1993). Hence, the researchers should use these devices during motions in which the possible over-flexion or extension of the strain gauge is minimized.

2.4. DYNAMIC VS. QUASI-STATIC ANALYSIS

Human joint forces and moments which are generated by the muscles and passive soft tissues provide invaluable information about the biomechanics of humans motion during different tasks (Winter, 2009). As a result, the estimation of the joint forces and moments has always been a topic of interest for the biomechanists.

Overall, there are two techniques to calculate the joint moments during a dynamic task: dynamic analysis and quasi-static analysis. The difference between the two methods is that in the quasi-static analysis, the body segments acceleration and inertial terms are removed from the inverse dynamic model in order to simplify and speed up data processing.

Various studies in the literature have compared the dynamically and quasi-statically determined joint moments during different tasks to understand the effect of removing the acceleration and inertial terms on the joint moments. In 1985, McGill et al. compared the dynamic and quasi-static L4/L5 joint moment during a lifting task in sagittal plane. Their results showed that on average, the dynamic analysis produced 19% higher peak joint moment compared to quasi-static analysis (McGill & Norman, 1985). Furthermore, it was

found that the quasi-static analysis underestimates the joint moment magnitude during the minima and maxima of the dynamic joint moments. In another lifting study, Wood et al. investigated a lifting task with straight leg and back in which the motion was performed with a moderate speed with an average trunk angular velocity of 60^{o} per second with a maximum of 74^{o} per second. The results of this study showed that the quasi-static analysis underestimated the peak joint moments magnitude during the motion by about 24% (Wood & Hayes, 1974). In 1984, Freivalds et al found that the inertial terms in dynamic analysis can increase the L5/S1 joint loads by up to 40% during different lifting tasks compared to the quasi-statically determined joint loads (Freivalds, Chaffin, Garg, & Lee, 1984).

The effect of the acceleration and inertial terms on other humans' joints during different dynamic tasks was also investigated. Krabbe et al. showed that during running at 5 m/s, although the effect of acceleration and inertial terms on the ankle joint's forces and moments is negligible, the proximal joints' kinetics (i.e. knee and especially the hip joints) are significantly affected by these terms, and hence, they should not be neglected for the knee and hip joints (Krabbe, Farkas, & Baumann, 1997). Wu et al. compared the dynamic and quasi-static joint loads (i.e. forces and moments) at the ankle, knee, and hip during slow (1.13 (0.06) m/s), normal (1.36 (0.05) m/s), and fast (2.15 (0.13) m/s) walking, and running (3.87 (0.16) m/s). Their results showed that at the more proximal joints (i.e. at the knee, and especially at the hip), the effect of neglecting the acceleration and inertial terms were more significant. Furthermore, as the speed of walking increased, the effect of acceleration and inertial terms on all joints became larger and more important (Wu & Ladin, 1996). Another study compared the dynamically and quasi-

statically determined joint forces and moment at different joints of the humans' bodies during rising from a chair. Their results revealed that the acceleration and inertial terms make up less than 1% of the total ankle and knee joint forces and moments, and hence can be neglected. For the hip joints, the contribution of these terms to the forces and moments was less than 10% whereas for the lumbar spine joint, this contribution was about 18% (Hutchinson, Riley, & Krebs, 1994).

Overall, the studies in the literature have shown that the quasi-static analysis significantly underestimates the lumbar spine joint moment magnitude during the minima and maxima of the moment waveforms. Furthermore, as the speed of motion during a dynamic task is increased, the effect of the acceleration and inertial terms exclusion from the dynamic analysis becomes more significant on the joint moments.

2.5. ABDOMINAL HOLLOWING

To increase the lumbar spine joint stiffness, and hence stability, different trunk muscle activation techniques such as abdominal hollowing and bracing have been proposed in the literature.

In 1999, Hodges et al. showed that in the healthy individuals, the deep abdominal muscles of transversus abdominis (TrA) were activated a fraction of a second ahead of the upper limb movements. On the contrary, in the individuals with LBP, the study found out the TrA had a delayed onset time (Hodges & Richardson, 1999). This and similar other findings were the basis for the work of Richardson and et al. to create a rehabilitation program, known as abdominal hollowing, which would retrain the perturbed motor patterns of TrA muscles in patients with LBP (Richardson, 1999). To perform an abdominal hollowing exercise, the patients would draw the lower area of the

stomach in and toward their ribcage. In a study in 2002, Richardson et al. showed that abdominal hollowing resulted in lower sacroiliac joint laxity claiming that abdominal hollowing would be a good exercise for increasing sacroiliac stability (Richardson et al., 2002). While abdominal hollowing causes increased muscle activation in TrA muscles, it has smaller effect on the rectus abdominis (RA), internal (IO) and external oblique (EO) muscles indicating that the main focus of the abdominal hollowing is indeed the deep abdominal muscles (Urquhart, Hodges, Allen, & Story, 2005).

In contrast to Robertson and Hodges group who have advocated for abdominal hollowing as a suitable therapeutic exercise for people with LBP, McGill et al. introduced "abdominal bracing" which would require the individuals to perform a mild contraction of the abdominal wall to increase spinal stability (McGill, 2007). Compared to the abdominal hollowing which primarily targets the deep muscles of TrA, the abdominal bracing engages all the core abdominal muscles. When done correctly, abdominal bracing would not cause a geometric change in abdominal wall, and unlike abdominal hollowing, the patient would not draw in their abdominal muscles. Instead they would activate their abdominal muscles making them stiff (the analogy for this exercise would be contracting the abdominal muscles as if someone wants to punch us in the stomach).

The first main difference between abdominal hollowing and bracing is the number of muscles involved in each exercise. While abdominal hollowing only trains the TrA muscles, in abdominal bracing all the three layers of the abdominal wall are co-activated resulting in more stability (McGill, 2007). In fact, a quantitative study by Grenier and McGill has shown that compared to abdominal hollowing, abdominal bracing would lead to a significantly higher stability index in a person standing upright. Furthermore, it was

shown that holding loads in hand while standing would drop the stability index to negative levels indicating that instability is possible (Grenier & McGill, 2007).

The second difference between abdominal hollowing and bracing is their ability to minimize pelvic motion or trunk deflection due to external loads. In 2007, Vera-Garcia and et al. measured the trunk deflection as a result of sudden perturbations to the trunk, and compared the results between abdominal hollowing and abdominal bracing. The results showed that abdominal hollowing was not effective in minimizing the trunk deflection whereas in abdominal bracing the trunk movement was reduced. This study also showed that abdominal bracing was more successful in stabilizing the trunk during the perturbations (Vera-Garcia, Elvira, Brown, & McGill, 2007). In contrast to findings of McGill et al., other studies have shown that abdominal hollowing is an effective technique to reduce the pelvic motion during different tasks. For instance, studies have shown that abdominal hollowing significantly reduces the anterior pelvic tilt by 7^{o} (i.e. statistically significant) during prone hip extension (Oh, Cynn, Won, Kwon, & Yi, 2007), and by 1.8^{o} (i.e. statistically significant) during controlled lifting task (Butler, Hubley-Kozey, & Kozey, 2007).

In the studies from our laboratory, it was shown that abdominal hollowing helped the study participants minimize their pelvic motion during different dynamic tasks including tasks similar to ones in this thesis (Hubley-Kozey et al., 2012; Hubley-Kozey et al., 2009; Hubley-Kozey et al., 2014). Therefore, and based on the preceding paragraphs, after developing a model to calculate dynamic L4/L5 joint stiffness, the participants were asked to perform the study exercises with and without abdominal hollowing to verify

whether this muscle activation technique has a significant effect on the lumbar spine joint stiffness and hence stability.

2.6. SUMMARY OF MOTIVATION

As described earlier in this chapter, spinal instability is thought to be a major contributor to low back injuries. Moreover, as explained before, the most important component of stability is spinal stiffness, hence insufficient stiffness may result in instability. Many researchers have attempted to quantify stiffness by means of sophisticated biomechanical models. However as explained above, to our knowledge, no one has provided dynamic profiles of spinal joint stiffness during dynamic tasks. Biomechanists have only calculated discrete values over a certain period of time during dynamic tasks. The novel aspect of this study was to develop a method to capture the time-varying changes in stiffness during a fundamental task.

CHAPTER 3 METHODOLOGY

3.1. RESEARCH DESIGN

This pilot study was designed to determine if there were differences in dynamic joint stiffness between two tasks with different loading demands under two conditions. Three dimensional segment motion was captured using a passive marker motion capture system, inertial properties were determined from body segment marker locations and Dumas et al.'s anthropometric model (Dumas, Cheze, & Verriest, 2007), and ground reaction forces were captured using a force platform from ten young and healthy male participants with no history of low back pain (LBP). Using these data, a dynamic measure of joint stiffness at L4/L5 joint was developed and calculated. In this study, the body segment inertial properties and data processing procedure–except for dynamic L4/L5 joint stiffness, and L4/L5 joint moment and relative angle–was developed and described in three dimensions to enable future studies in our laboratory to analyze dynamic joint stiffness in three dimensions during different dynamic tasks. The exercises for this study were designed such that main movement was done in the sagittal plane, and hence, this study focuses on dynamic L4/L5 joint stiffness in the sagittal plane only.

3.2. PARTICIPANTS

Participants for this study included ten healthy men between the ages of 20-30 years. There is evidence of differences in trunk muscle activation patterns between men and woman performing a variety of tasks (Anders, Brose, Hofmann, & Scholle, 2007; Anders, Wagner, Puta, Grassme, & Scholle, 2009; Granata, Orishimo, & Sanford, 2001; Hubley-Kozey et al., 2012; Marras, Davis, & Jorgensen, 2003) including a task similar to the exercises in this study (Dahn, 2012). Therefore, due to the developmental nature of

this work, the small sample size, and in order to reduce the variability, only one sex (i.e. men) was recruited for this study. The participants had no history of LBP, and were recruited through posters and emails at Dalhousie University. Inclusion and exclusion of study participants were done through a health-screening questionnaire. Exclusion criteria included any cardiovascular, neurological or other musculoskeletal problems that would place participants at risk or prevent them from completing the study tasks correctly. The participants that were included in the study signed a consent form approved by Dalhousie University Health Sciences Research Ethics Board (REB#: 2015-3629). Also, their age, sex, mass, and height were recorded. Furthermore, the participants were instructed to wear gym t-shirt and shorts, and to remove their shoes during data collections.

3.3. MOTION MARKERS PLACEMENT PROTOCOL

For this study, the motion data was captured using Qualisys™ motion capture system (Qualisys™, Gothenburg, Sweden) by placing passive reflective sensors on trunk, pelvis, and legs. Figure 3-1 illustrates the location of these markers. Markers were placed bilaterally on lateral femoral epicondyle (LE), lateral malleolus (LM), anterior superior iliac spine (ASIS), posterior superior iliac spine (PSIS), medial femoral epicondyle (ME), medial malleolus (MM), calcaneus (CAL), 1st metatarsal head (MH1), and 5th metatarsal head (MH5), suprasternale (SUP), and 7th cervicale (C7). Also, triads were placed on trunk, pelvis, thighs, and shanks segments. The location of single markers were used to create anatomical coordinate systems for trunk, pelvis, thigh, and shank (Dumas et al., 2007). The markers on the feet were used to estimate their center of masses (COM). For this study, the angle between feet and shank was assumed to be constant during the tests, and therefore, shanks and feet were combined and assumed as one segment.

Nevertheless, the participants were monitored during the experiment to ensure that they kept the shank-foot angle constant while performing the tasks. Once all markers were placed, the participants were instructed to stand in a neutral position, and then a one-second calibration trial was collected which was utilized as a reference position. This data was used to calibrate the position of the single markers relative to the location of the triads. Following the static standing trials and prior to the motion trials, all markers–except the triads and the marker on right LM–were removed.

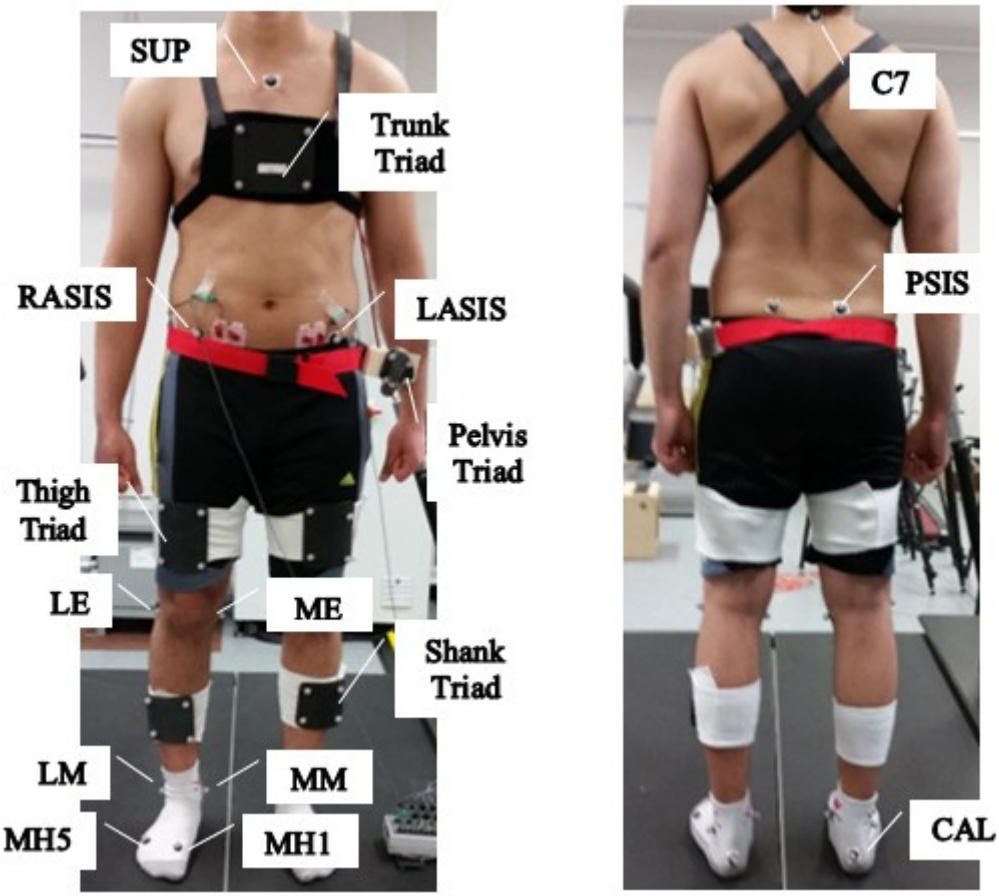

Figure 3-1: Marker set-up in the laboratory. LE: lateral femoral epicondyle, LM: lateral malleolus, RASIS (LASIS): right (left) anterior superior iliac spine, PSIS: posterior superior iliac spine, ME: medial femoral epicondyle, MM: medial malleolus, CAL: calcaneus, MH1: 1st metatarsal head, MH5: 5th metatarsal head, SUP: suprasternale, C7: 7th cervicale.

Using the motion sensors shown in Fig. 3-1, a three-dimensional kinematic and kinetic model was developed, however for this study, only movement in the sagittal plane was analyzed. For more detail regarding this model, please refer to Appendix A.

3.4. EMG Sensor Placement Protocol

The experimental tasks for Objective 2 of this thesis were performed under two conditions: with and without abdominal hollowing (AH). Activation of transversus abdominis has been reported to increase spinal stability by reducing the sacroiliac joint laxity (Richardson et al., 2002). Therefore, it is of interest to measure the angular motion of pelvis and L4/L5 dynamic joint stiffness when participants do not activate their transversus abdominis muscles, and then compare the results to when they do. To ensure that participants activated their transversus abdominis muscles during the abdominal hollowing conditions, EMG electrodes were placed bilaterally on left and right internal oblique muscles (IO). Although abdominal hollowing has been designed to target the deep muscles of transversus abdominis and lumbar multifidi (Richardson, 1999; Richardson et al., 2002), IO muscle has been shown to be a synergist of transversus abdominis (Juker, McGill, Kropf, & Steffen, 1998) and therefore it could be used as a good indicator of whether or not the participants performed abdominal hollowing during tasks.

A standardized protocol based on previous work was used to capture EMG data of the IO muscles (Butler, Hubley-Kozey, & Kozey, 2013). Each IO muscle was located at center of a triangle formed by inguinal ligament, lateral border of rectus sheath, and the line between the two anterior superior iliac spines (ASIS) (Ng, Kippers, & Richardson, 1998). Prior to electrodes placement, skin was prepared by shaving with a disposable razor and

abrading with 70% alcohol wipes resulting in a skin/amplifier impedance ratio of <0.1%. Ag/AgCl surface electrodes (10 mm diameter, Red Dot™, 3M™, London, Ontario, Canada) were placed in a bipolar configuration along the muscle fiber orientation of right and left IO muscles with an inter-electrode distance of 20 mm. One ground surface electrode was placed over the lateral side of iliac crest. To address anatomical differences between the participants, and to validate EMG signals and adjust gain settings, minor adjustments in electrode placements were made by palpation and a series of submaximal isometric contraction including trunk lateral bending and trunk flexion coupled with axial rotation (Butler, Hubley-Kozey, & Kozey, 2009).

3.5. NORMALIZATION EXERCISES

Following the surface EMG electrodes placement, a participant bias trial of resting muscle activity was collected for one second with the participants lying in a relaxed supine position. Then, the participants were instructed to perform a series of standardized exercises that required maximum voluntary isometric contraction (MVIC) (Butler, Hubley-Kozey, et al., 2009). The MVIC exercises enabled us to express the IO muscle activation patterns as a percent of MVIC by normalizing the EMG data to the maximum EMG activation amplitudes. In order to maximally activate internal oblique muscles, the participants were instructed to perform side lying lateral flexion (right and left) coupled with ipsilateral hip hike and seated axial rotation (right and left) (Butler, Hubley-Kozey, et al., 2009). Each normalization exercise was done in two trials (i.e. eight trials in total) with each trial lasting three seconds. To prevent muscle fatigue, a two-minute rest was given to the participants between each trial. During these normalization exercises, all participants were given standard verbal encouragement to elicit maximum effort during

each trial (Ng, Parnianpour, Kippers, & Richardson, 2003). Moreover, to prevent movement during the normalization exercises and to ensure the participants' safety, participants were secured to the laboratory's bed using non-elastic straps. At the end of session two, a system bias trial was collected to correct the EMG data. Following the normalization exercises, the experimental tasks (see section 3.6) were performed.

3.6. TRUNK STABILITY TEST PROTOCOL

The experimental tasks that were used in both Objectives 1(a, c, and d) and 2 of this thesis included two levels of a modified trunk stability test (TST) protocol. Furthermore, the tasks were performed in random order to minimize the effects of learning and fatigue. The TST tasks were previously described in studies from this laboratory, and were performed to provide a dynamic challenge to lumbar spine so that the trunk musculature had to respond to constant changes in load (i.e. leg lifting, lowering, and extension) moments (Hanada, Hubley-Kozey, McKeon, & Gordon, 2008; Hubley-Kozey & Vezina, 2002b; Moreside et al., 2014). The TST exercises in these previous studies were done using single-leg lifting tasks which created dynamic moments in sagittal, frontal, and transverse planes. Since in this study the focus was on sagittal plane movement and sagittal plane dynamic stiffness, the TST protocol was modified such that the tasks were performed in only one plane (i.e. sagittal plane) by moving right and left legs simultaneously.

Since the force platform in the laboratory does not have a physical button to "zero" the force plate data (i.e. remove offset from the force plate's measurements), a one-second calibration trial was collected prior to the experimental tasks where no load was applied

to the force plate. The data from the force plate calibration trial was then used to remove any offset from the force plate data during the experimental tasks.

The participants were instructed to lie on a force platform in supine position with their ASIS aligned with the proximal edge of the force plate, and their feet on a foot switch trigger. Figure 3-2 illustrates the starting position of the participants with respect to the force plate and foot switch prior to the motion trials. By taping a piece of aluminum tape to right foot of the participants, the foot switch trigger helped determine the start and end of the experimental tasks. The foot switch trigger board was placed about 3cm above the force plate so that only the ground reaction forces acting on the pelvis were recorded.

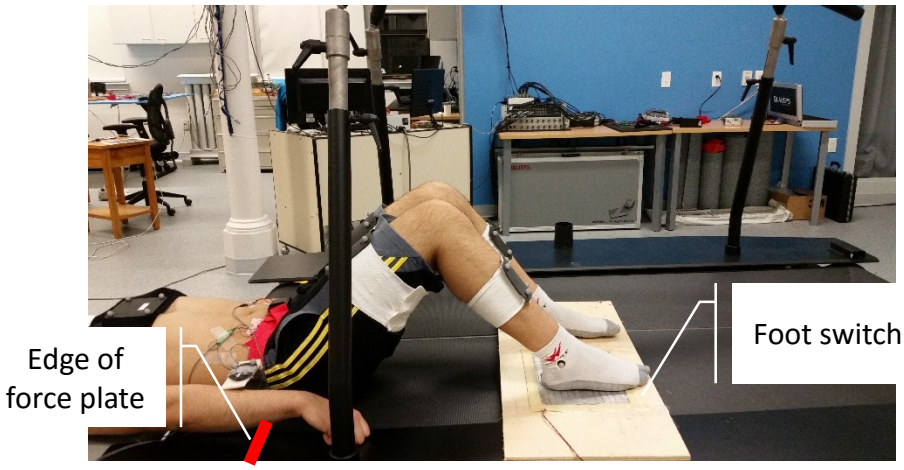

Figure 3-2: Starting position of the participant prior to the start of the motion trials.

Participants performed each exercise three times while taking one-minute rests in between trials to minimize fatigue. Figure 3-3 illustrates the modified version of TST level 1. As shown in this figure, the participants were instructed to lie down in a supine position with their knee flexed to 90^{o} and their pelvis over a force platform to capture ground reaction forces (GRFs) from pelvis during the experimental tasks. To ensure

proper placement of pelvis on the force platform, a researcher guided the participants to align their ASIS with proximal end of the force platform (see Fig. 3-2). The participants started the task by lifting both legs at the same time to 90º hip flexion while maintaining their knees flexed at 90º (Phase 1). This phase took one second. In the second and final phase, the participants lowered both their legs simultaneously back to the starting position (Phase 2). This phase again took one second. To ensure standard timing for each participant and each trial, time was recorded by a timer and was monitored on the computer. Moreover, a research assistant constantly monitored the participant's motion to ensure standard timing for each phase for the all the participants.

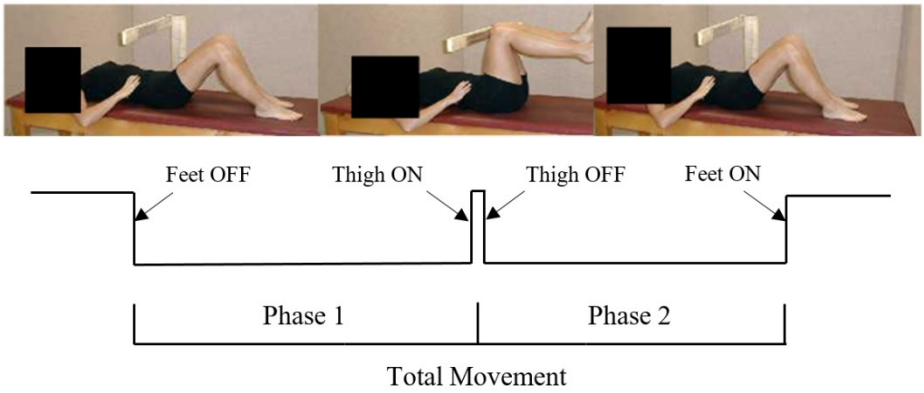

Figure 3-3: Modified TST level 1.

Figure 3-4 depicts the modified version of TST level 3. As illustrated in this figure, the TST level 3 is similar to TST level 1, except that in TST level 3 and after phase 1, the participants were instructed to fully extend their knees in a controlled movement (without touching the bed) and then returning their legs back to the 90º hip flexion position (Phase 2). This entire phase was performed in four seconds in a controlled movement. Finally, the participants lowered their legs back to the starting position on the bed (Phase 3). The

entire TST 3 task was performed in six seconds which was recorded by a timer, and was monitored on the computer and a research assistant.

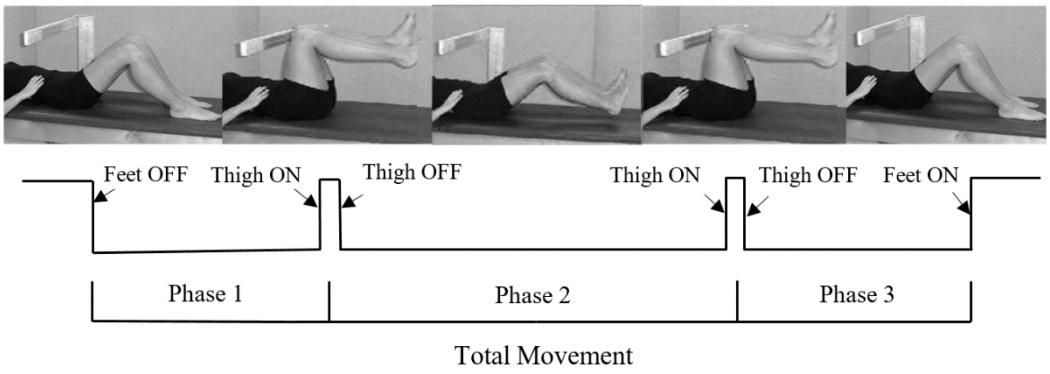

Figure 3-4: Modified TST level 3.

3.7. TST EVENT DETERMINATION

The signal from the foot switch trigger was used to determine the beginning and end of each trial in the TST exercises (i.e. feet off and feet on). Furthermore, to identify when the participant was at the 90^{o} hip flexion position, his relative right hip flexion angle was analyzed to determine when the maximum relative hip flexion angle occurred (See Figs. 3-5 and 3-6). Since the participant was at 90^{o} hip flexion position twice in TST 3, an algorithm was developed to find the maximum relative hip joint angles in both the first and second half of each TST 3 trial (see Fig. 3-6).

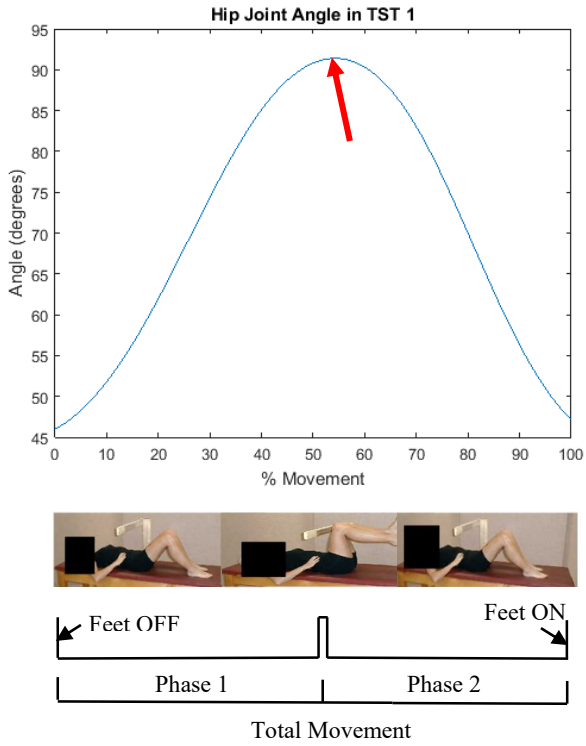

Figure 3-5: Sagittal plane relative right hip joint angle in TST 1. The arrow indicates when the participant was at the 90º hip flexion position.

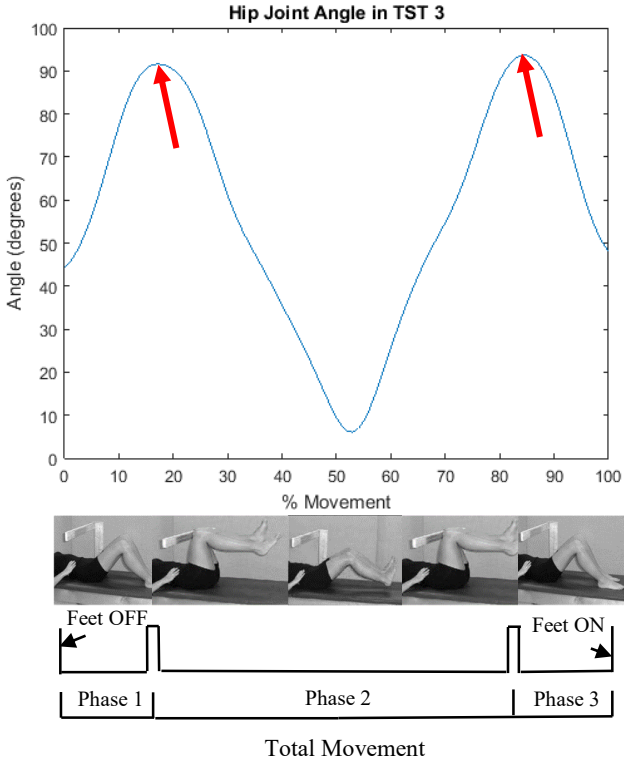

Figure 3-6: Sagittal plane relative right hip joint angle in TST 3. The arrows indicate when the participant was at the 90º hip flexion positions.

Lastly, to identify when the participant's knees were at full knee extension in TST 3, his relative right knee joint angle was analyzed to find when the relative knee joint angle is at minimum (see Fig. 3-7).

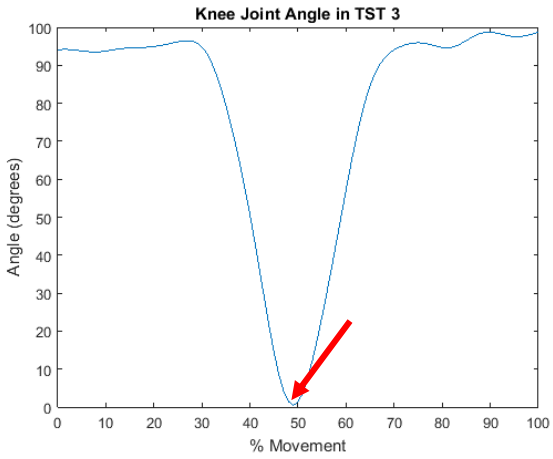

Figure 3-7: Sagittal plane relative knee joint angle in TST 3. The arrow indicates when the participant was at the full knee extension position.

3.8. General Data Acquisition

For this study, the electromyography (EMG) signals were pre-amplified (200X) and further amplified using an AMT8 EMG measurement system (Bortec Inc., Calgary, AB, Canada; band-pass 10-1000 Hz, CMRR = 115 dB at 60 Hz, input impedance = 10 GΩ). Raw EMG signals were sampled at 2000 Hz (16 bit, +/-5V) using an analog-to-digital (A/D) conversion board (Qualisys™, Gothenburg, Sweden) and QTM software (Version 2.7, Qualisys™, Gothenburg, Sweden).

Three dimensional ground reaction forces (GRFs) and moments of force from pelvis were collected by a force platform (R-Mill, Force Link™, Culemborg, Netherlands) and were

sampled at 2000 Hz (16 bit, +/-5V) using an A/D converter (Qualisys™, Gothenburg, Sweden). The force plate was aligned to the global coordinate system in the laboratory.

Three-dimensional motion data of the body segments (see Fig. 3-1) were recorded at 100 Hz by eight cameras using Qualisys™ motion capture system (Qualisys™, Gothenburg, Sweden). All data (i.e. EMG, force plate, and motion) were synchronized, and were stored for later processing using QTM software (Version 2.7, Qualisys™, Gothenburg, Sweden).

3.9. General Data Processing

All data processing was completed using custom programs written in MATLAB version 8.6 (Mathworks, Natick, MA, USA). The following sections describe the general data processing procedures that were used in this study.

3.9.1. Surface Electromyography

To minimize noise due to electrocardiographic artifact, the EMG signals were high-pass filtered at 30 Hz (Butler, Newell, Hubley-Kozey, & Kozey, 2009). The power spectrum for each EMG signal was calculated, and if there were any unwanted signals such as 60 Hz noise due to the power system, they were removed using an inverse Fast Fourier Transform (FFT) filter. The surface EMG data was corrected for gain and (participant and system) bias, converted to microvolts, full-wave rectified, and low-pass filtered at 6 Hz (Butterworth 4^{th} order recursive filter) to provide a linear envelope profile. The data were also time normalized from foot-off (when legs were lifted off the foot switch board) to foot-on (when the legs were placed back on the foot switch board) using a cubic spline interpolation algorithm. Finally, the EMG data was amplitude normalized to the 500 ms

peak amplitude from the normalization exercises (Hubley-Kozey & Vezina, 2002b). The EMG waveform in each trial was visually inspected for consistency, and then an ensemble average waveform was calculated for each participant.

3.9.2. Kinematics

In this study, the motion markers' position data were low-pass filtered at 6 Hz using a Butterworth 4^{th} order recursive filter (Wells & Winter, 1980).

From the one-second static standing calibration trial, invariant pose matrices from the local coordinate system (LCS) and anatomical coordinate system (ACS) of the body segments (i.e. trunk, pelvis, thighs, and shanks) to the global coordinate system (GCS) were calculated. Then using these matrices, the pose matrices from the LCS to ACS for each segment were computed. In the motion trials, the motion of the triads was tracked in the GCS. Hence by using the LCS to ACS matrices calculated above, the motion of each segment in its ACS was obtained.

The axes of the L4/L5 joint was defined by the Joint Coordinate System which uses a Cardan rotation sequence of first about the Z axis (medial-lateral) for flexion/extension, second about the X axis (anterior-posterior) for abduction/adduction, and finally the Y axis (proximal-distal) for internal/external rotation (Grood & Suntay, 1983). The L4/L5 joint motion was described as movement of the pelvis (distal segment) about the trunk (the proximal segment) (Robertson et al., 2013; Winter, 2009).

Appendix A explains in detail the calculation procedure for the LCS and ACS of body segments, rotational and translational pose matrices, linear and angular velocity and acceleration, and the relative L4/L5 joint angle. In this thesis, the relative L4/L5 joint

angle was calculated by measuring the angular motion of pelvis relative to trunk around the L4/L5 joint axis.

3.9.3. Kinetics

First, using the data from the one-second force plate calibration trial, the force plate offset during the motion trials was removed. This was done by calculating the mean of the raw data in the calibration trial (i.e. Fx, Fy, Fz, Mx, My, Mz), and then subtracting the results from the force plate's data during the motion trials. Next, using the force plate's calibration matrix given by the manufacturer (R-Mill, Force Link™, Culemborg, Netherlands), the raw force plate data in the motion trials was processed (i.e. Fx, Fy, Fz, and center of pressure (COPx and COPy) data were calculated in SI units). The resulting data were low-pass filtered at 30 Hz using a Butterworth 4^{th} order recursive filter. The COP data was further filtered using a low-pass filter at 6 Hz (Butterworth 4^{th} order recursive).

Net external L4/L5 joint moment was calculated using a standard bottom-up inverse dynamics approach, projected on to the L4/L5 joint coordinate system. Inverse dynamics technique is a linked segment model that combines body segment motion data, ground reaction forces, and body segment inertial properties (BSIPs), and by starting at the distal segment and working proximally to calculate net external forces and moments acting on joints (Robertson et al., 2013). One major assumption in this study is that the trunk, pelvis, thighs, and shanks are rigid bodies and act independently. Figure 3-8 illustrates the pelvis free body diagram (FBD) (Please refer to section A.5 of Appendix A for the full FBD of the linked segment model used in this thesis). Equation 3-1 below shows the equation which calculates net joint forces at the L4/L5 joint by combining pelvis's mass,

pelvis's gravitational and linear accelerations, and the reactive forces from the distal segments (i.e. thighs) and the ground reaction forces (GRF).

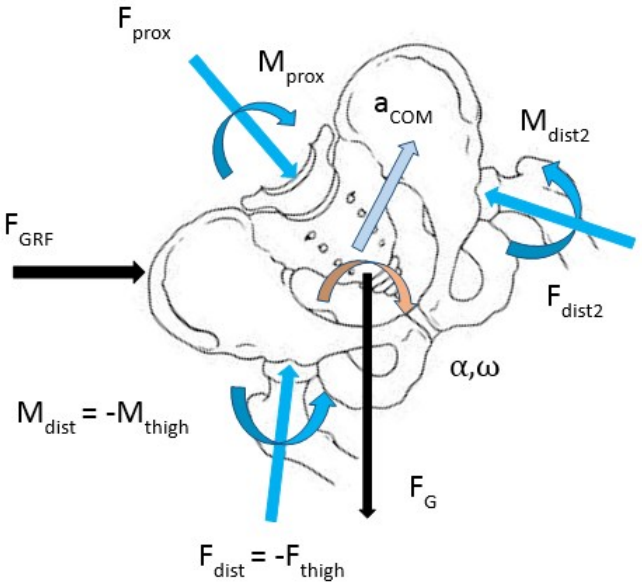

Figure 3-8: Pelvis free body diagram.

$$F_{prox} + F_{dist1} + F_{dist2} + mg + F_{GRF} = m\alpha \;\rightarrow\; F_{prox} = m\alpha - F_{dist1} - F_{dist2} - mg - F_{GRF}$$

(Eq. 3-1)

In the above equation, "F_{prox}" is the net proximal force acting on the L4/L5 joint, "mg" is the weight of the pelvis, "F_{dist1}" and "F_{dist2}" are the forces that act on the L4/L5 joint from the thighs, "m" is the mass of the pelvis, "α" is the linear acceleration of the pelvis, and "F_{GRF}" is the ground reaction forces acting on the pelvis.

Equation 3-2 below shows the formula which computes the net L4/L5 joint moment by combining the time rate of change of pelvis's angular momentum (calculated using pelvis's moment of inertia, angular velocity and acceleration), the L4/L5 joint's contact moment (calculated by cross product of moment arm (from pelvis's center of mass to the

L4/L5 joint center) and the pelvis's net force), the hip joints' contact moments (calculated by cross product of moment arms (from pelvis's center of mass to hip joints centers) and the thighs' net force), and the net hip joints moment.

$$M_{prox} + (PJC - COM) \times F_{prox} + (HJC1 - COM) \times F_{dist1} + (HJC2 - COM) \times F_{dist2} + (-M_{dist1}) + (-M_{dist2}) + (COP - COM) \times F_{GRF} = H_{dot}$$

$$\rightarrow M_{prox} = H_{dot} - (PJC - COM) \times F_{prox} - (HJC1 - COM) \times F_{dist1} - (HJC2 - COM) \times F_{dist2} - (-M_{dist1}) - (-M_{dist2}) - (COP - COM) \times F_{GRF} \quad \text{(Eq. 3-2)}$$

In the equation above, "H_{dot}" is the time rate of change of the pelvis's angular momentum, "M_{prox}" is the L4/L5 joint's contact moment, "M_{dist1}" and "M_{dist2}" are the hip joints' contact moments, "PJC" is the proximal (i.e. L4/L5) joint center, "COM" is the pelvis's center of mass, "F_{prox}" is the pelvis's net force, "HJC1" and "HJC2" are the hip joints' centers, "F_{dist1}" and "F_{dist2}" are the thighs' net forces, "M_{dist1}" and "M_{dist2}" are the net hip joints moments, "COP" is the ground reaction force's center of pressure, and "F_{GRF}" is the ground reaction force acting on the pelvis. The pelvis's masse, center of mass location, and moment of inertia were calculated using regression equations and tables presented by Dumas et al. in 2007. These anthropometric data were originally presented by McConville et al. who studied 31 men (mean age 27.5 years old, mean weight 80.5 kg, mean stature 1.77 m) using stereo-photogrammetric technique (McConville, Churchill, Kaleps, Clauser, & Cuzzi, 1980). However, since McConville et al. calculated the segment axes based on the bony anatomical landmarks, Dumas et al. adjusted the original data so that the segment axes would be based on joint centers instead of bony anatomical landmarks.

Appendix A (section A.5) presents more detailed information on how the net joint forces and net external joint moments were calculated in this thesis.

3.10. OBJECTIVE 1 METHODOLOGY

Due to the developmental nature of this study, the following section describes the methodology (i.e. the data collection procedure and processing, and the experimental trials) that were specific only to Objectives 1b, 1c, and 1d of this thesis.

3.10.1. Absolute & Relative Angle Calculations (Objective 1-b)

Data Collection & Processing: Using the marker placements described in section 3.3, a one second static standing trial was collected from a participant. Then, using the marker locations data from the standing trial and the anthropometric model described by Dumas et al, an anatomical coordinate system was established for each segment (i.e. trunk, pelvis, thighs, and shanks) with x axis directed anteriorly, y axis directed vertically from distal to proximal, and z axis directed from left side to the right side of body segment (Dumas et al., 2007). Using the triads on each segment, the technical coordinate systems were formed for each segment of the body. The technical and anatomical coordinate systems allowed us to establish a technical to anatomical rotation matrix for each segment. By using a zxy rotation sequence (flexion/ extension then abduction/ adduction, and then internal/ external rotation) and the technical to anatomical matrices obtained from the standing trial, the L4/L5 joint angle was calculated (i.e. relative angle). Using the same procedure and as described in Appendix A, the angular displacement of the shanks, thighs, and pelvis were calculated (i.e. absolute angle). For detailed methodology including the equations used to calculate relative and absolute angles, please see Appendix A.

An electrogoniometer (Biometrics Ltd., Newport, UK) was calibrated before use, and its accuracy was found to be ±2 degrees. The electrogoniometer was used to measure the relative L4/L5 joint angle, and then to compare the results with the ones calculated from the motion capture system in order to check the agreement between the two methods. Since the electrogoniometer generates voltage at each specific angle instead of degrees, the electrogoniometer's output was calibrated by placing the sensors at specific angles measured by a standard goniometer (i.e. -120º, -90º, -60º, -30º, 0º, 30º, 60º, 90º, 120º). Figure 3-9 shows the result of this calibration in which the output voltages were plotted against the known angles in order to obtain the calibration equation.

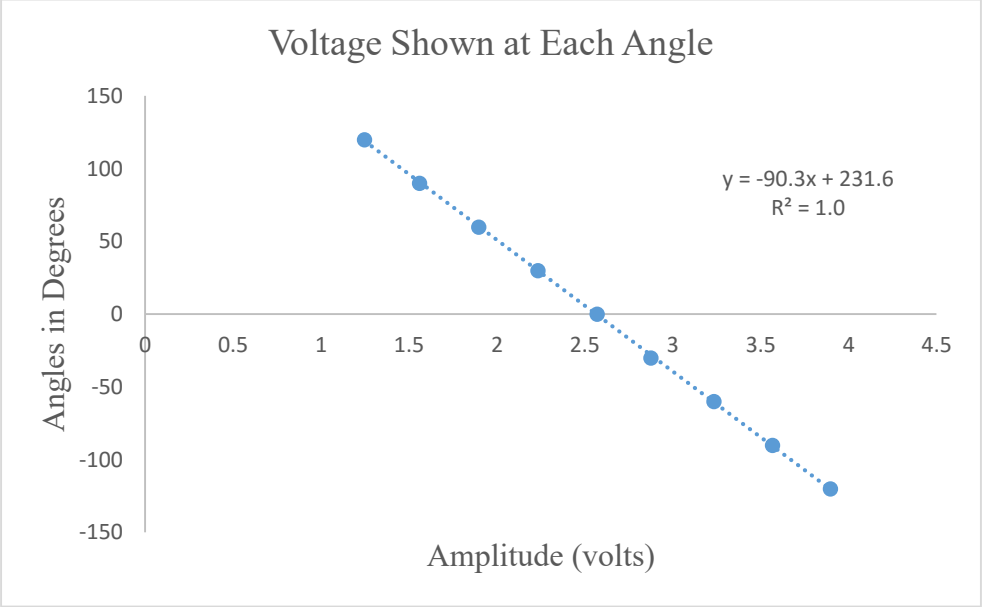

Figure 3-9: The electrogoniometer calibration equation obtained by plotting the angles versus the output voltages.

An inclinometer (STP Electronic Inclinometer, Saunders Therapy Products, Bloomington, MN, USA) was also calibrated, and its accuracy was found to be ±1 degrees. The inclinometer was used to measure the absolute angles of thighs and shanks, and then to compare the results with the ones estimated by the thesis's kinematic model.

Experimental Trials: All the experimental trials were performed in the sagittal plane, and hence all the results represent sagittal plane angles. The test trials for the validation of absolute angles included a single participant lying in the supine position. Next, an inclinometer was placed on the desired shank or thigh, and then the participant was instructed to lift that body segment in 10° intervals starting from 0° and finishing at 60° from the floor resulting in seven data points for each shank and thigh. This was repeated for the shank and thigh on the other side of the body. Simultaneously, the motion camera system captured the 3D positions of the markers on the body.

For the relative angles comparison, a flexible electrogoniometer was placed on the long axis of the participant's back such that one endblock was on the lower lumbar spine, and the other endblock was on the lower thoracic spine (See Fig. 3-10). Then, the participant was instructed to perform a set of trunk flexion and extension in the sagittal plane while standing.

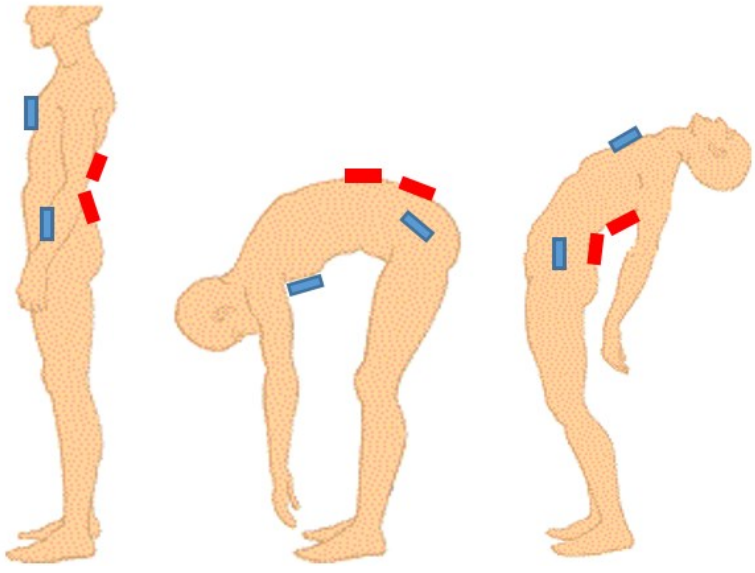

Figure 3-10: Location of the motion capture system triads (blue rectangles) and the sensors of the electrogoniometer (red rectangles).

3.10.2. Dynamic vs. Quasi-Static Analysis (Objective 1-c)

After the motion markers were placed on participants' body landmarks (see section 3.3), the participants were instructed to lie on a force platform in supine position with their ASIS aligned with the proximal edge of the force plate, and his feet on a foot switch trigger (see Fig. 3-2). They were then instructed to perform TST levels 1 and 3 as described in section 3.6.

Section 3.9 and Appendix A describe a kinematic and kinetic model which was designed to calculate the sagittal plane L4/L5 joint moment dynamically. To compute the sagittal plane L4/L5 joint moment quasi-statically, the inertial and acceleration terms were removed from the dynamic equations of motion (equations 3-1 and 3-2) which resulted in Eq. 3-3 and 3-4 below. For more information, please refer to section 3.9.3.

$$F_{prox} + F_{dist1} + F_{dist2} + mg + F_{GRF} = 0 \quad \rightarrow \quad F_{prox} = - F_{dist1} - F_{dist2} - mg - F_{GRF} \qquad \text{(Eq. 3-3)}$$

$$M_{prox} + (PJC - COM) \times F_{prox} + (HJC1 - COM) \times F_{dist1} + (HJC2 - COM) \times F_{dist2} + (-M_{dist1}) + (-M_{dist2}) + (COP - COM) \times F_{GRF} = 0$$

$$\rightarrow M_{prox} = - (PJC - COM) \times F_{prox} - (HJC1 - COM) \times F_{dist1} - (HJC2 - COM) \times F_{dist2} - (-M_{dist1}) - (-M_{dist2}) - (COP - COM) \times F_{GRF} \qquad \text{(Eq. 3-4)}$$

3.10.3. Dynamic Analysis w/ and wo/ GRFs (Objective 1-d)

Similar to section 3.10.2, after the motion markers were placed on participants' body segments, the participants lay on a force platform in supine position with their ASIS aligned with the proximal edge of the force plate, and their feet on a foot switch trigger

(see Fig. 3-2). The participants were then instructed to perform the TST levels 1 and 3 as described in section 3.6.

To examine the effect of the GRF data on the sagittal plane L4/L5 dynamic joint moment, the GRFs data were removed from the dynamic equations of motion (equations 3-1 and 3-2) which resulted in Eq. 3-5 and 3-6 below. For more information, please refer to section 3.9.3.

$$F_{prox} + F_{dist1} + F_{dist2} + mg + 0 = m\alpha \;\rightarrow\; F_{prox} = m\alpha - F_{dist1} - F_{dist2} - mg \qquad \text{(Eq. 3-5)}$$

$$M_{prox} + (PJC - COM) \times F_{prox} + (HJC1 - COM) \times F_{dist1} + (HJC2 - COM) \times F_{dist2} + (-M_{dist1}) + (-M_{dist2}) + 0 = H_{dot}$$

$$\rightarrow M_{prox} = H_{dot} - (PJC - COM) \times F_{prox} - (HJC1 - COM) \times F_{dist1} - (HJC2 - COM) \times F_{dist2} - (-M_{dist1}) - (-M_{dist2}) \qquad \text{(Eq. 3-6)}$$

3.11. OBJECTIVE 2 METHODOLOGY

This section describes the detailed methodology (i.e. the data collection procedure and processing, and the experimental trials) that were specific only to Objective 2 of this thesis.

An overview of the experimental protocol for Objective 2 is depicted in Fig. 3-11. The following sections provide detailed information on each component of the protocol.

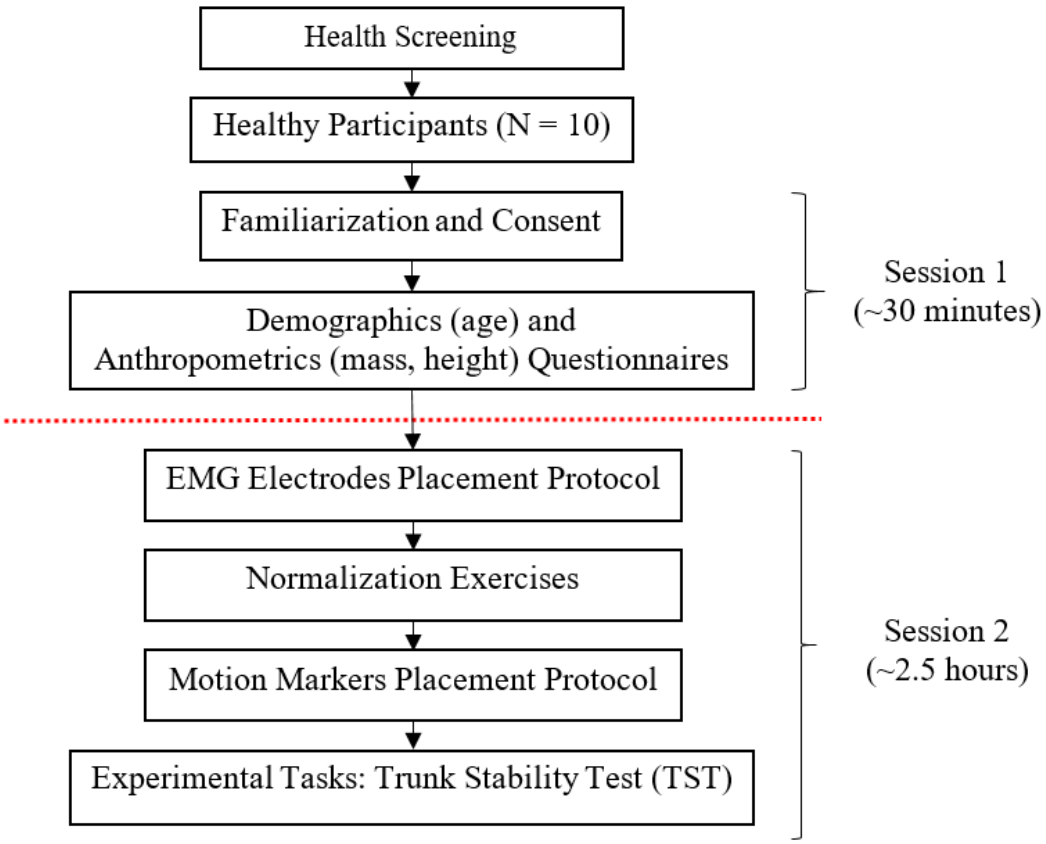

Figure 3-11: Flowchart of the experimental procedure. Total participation time for each individual was approximately three hours.

3.11.1. Session I

After participants were recruited, each individual was invited to attend session 1. During this session, the participant received and signed consent forms approved by Dalhousie University Health Sciences Research Ethics Board. Moreover, standard demographic information such as age, mass (using a scale), and height (using a stadiometer) were recorded. Lastly, the participants were instructed on how to perform experimental tasks, and were given handouts so that they could practice the exercises five times on at least three days prior to the second session. The entire session 1 took approximately 30 minutes for each participant.

3.11.2. Session II

The second session took place within two weeks after the first one. In this session, the participants wore gym t-shirts and shorts to allow for unobstructed placement of surface EMG electrodes and motion capture system markers. Session two took approximately 2.5 hours, and its components are described in the following sections.

3.11.2.1. Experimental Tasks

The experimental tasks included two levels of a modified trunk stability test (TST) protocol which have been described in section 3.6. For the Objective 2 of this thesis, each TST task was done in two conditions: i) with abdominal hollowing (i.e. pull your abdomen up and in toward your chest as if to tuck your stomach under your ribcage) prior to lifting or extending their legs while trying to minimize their pelvic and lower back motion during the task (AH). ii) without abdominal hollowing prior to or during the exercise (NAH) and no instruction to minimize pelvis motion. For the AH tasks, it was crucial that the participants were instructed to minimize their pelvic and lower back motion since the L4/L5 joint angle is one of the main components of dynamic joint stiffness equation and would be used to calculate sagittal plane dynamic L4/L5 joint stiffness in this study. Figure 3-12 illustrates the order in which the experimental tasks were performed. As shown in this figure, the participants performed the NAH tasks first and in random order, then, they did the AH tasks (also in random order).

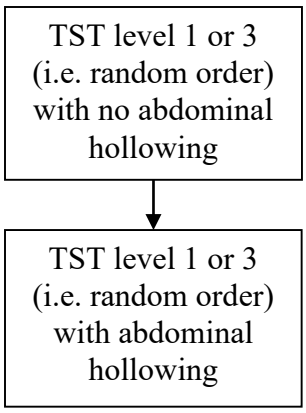

Figure 3-12: Flowchart illustrating the order in which the participants performed the experimental tasks.

3.11.3. Data Processing

All data processing was completed using custom programs written in MATLAB version 8.6 (Mathworks, Natick, MA, USA). The following sections describe the data processing procedures that were used for the Objective 2 of this thesis. The data processing procedure for surface electromyography, kinematics, and kinetics have already been described in section 3.9.

3.11.3.1. Dynamic L4/L5 Joint Stiffness Calculation

The sagittal plane dynamic L4/L5 joint stiffness was calculated using the slope (derivative) of joint moment versus joint angle data (Beach et al., 2005; Green et al., 2002; McGill et al., 1994; Parkinson et al., 2004; Zatsiorsky, 2002). To calculate the slope of sagittal plane L4/L5 joint moment versus sagittal plane L4/L5 joint angle, the finite difference equation (Eq. 3-7) below was used:

$$K(i) = \left|\frac{M(i+1)-M(i-1)}{\theta(i+1)-\theta(i-1)}\right| \quad \text{(Eq. 3-7)}$$

Where “K” is sagittal plane L4/L5 dynamic joint stiffness, M is sagittal plane L4/L5 joint moment, θ is sagittal plane L4/L5 joint angle, and i is the sample or instant at which dynamic L4/L5 joint stiffness is being calculated.

To calculate L4/L5 dynamic joint stiffness for each task and condition, the following steps were taken:

1. Examining Eq. 3-7, it is clear that if the change in sagittal plane L4/L5 joint angle is minimal (i.e. very small denominator), the L4/L5 dynamic joint stiffness becomes very large. Similarly, if the change in L4/L5 joint moment is minimal (i.e. very small numerator), we would have instances during the TST tasks when the dynamic joint stiffness would approach zero. Therefore, to minimize the instability in the numeric calculation of dynamic joint stiffness, it was necessary to low-pass filter both L4/L5 joint moment and joint angle to obtain smooth joint moment and angle waveforms. For each participant, L4/L5 joint moments and angles curves data were low-pass filtered using a Butterworth 4^{th} order recursive filter. For each individual, an iteration of different filtering frequencies from 2.5 Hz to 1 Hz was applied to the L4/L5 joint moment and angle curve data, and the highest filtering frequency that would minimize the number of local minima and maxima in the joint moment and angle waveforms was selected (Olney & Winter, 1985). Figure 3-13 illustrates the sagittal plane L4/L5 joint angle waveform in TST 1 before and after applying a 1.5 Hz low-pass filter.

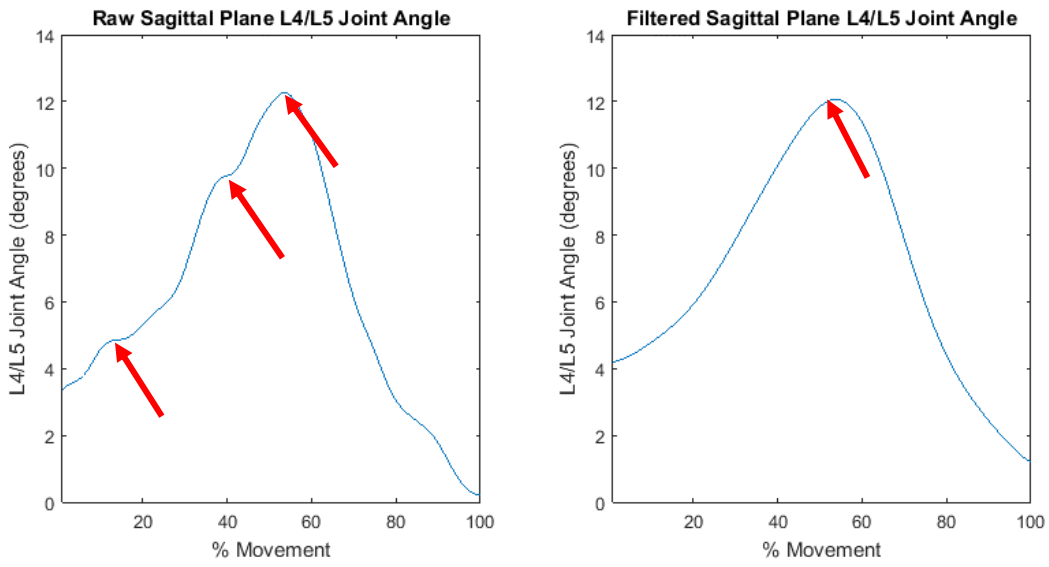

Figure 3-13: Comparison of ensemble averaged sagittal plane L4/L5 joint angle waveform in TST level 1, before (left picture) and after (right picture) low-pass filtering at 1.5 Hz using a Butterworth 4th order recursive filter. The red arrows indicate the areas where the change in joint angle (denominator of Eq. 3-7) is minimal.

2. For each individual and for each trial, the sagittal plane L4/L5 dynamic joint stiffness was calculated using Eq. 3-7.
3. To avoid abnormally large joint stiffness values (i.e. outside the expected physiological range) during the instances (for example at the 90^{o} hip flexion position, and also during the full knee extension in TST 3) where the change in L4/L5 joint angle were minimal or in other words, the L4/L5 joint angle velocity approaches zero and stiffness would no longer be dynamic, two methods were used. One method was to choose an L4/L5 joint angle velocity ($\dot{\theta}$) that is a percentage of the maximum $\dot{\theta}$, at which point in time the joint stiffness values start to become very high and exceed the physiological limits of lumbar spine as reported in the literature (Bazrgari et al., 2012; Liebenson, Karpowicz, Brown, Howarth, & McGill, 2009). Then, the L4/L5 joint stiffness at the instances during

which the $\dot{\theta}$ is below the selected value would not be calculated. A second approach was to choose a single discrete value for $\dot{\theta}$, below which the joint stiffness would not be calculated. Hence, the large spikes of stiffness values that occurred as a results of $\dot{\theta} \approx 0$ degree/second, would be removed from the stiffness data. These methods were compared, and the results are shown in section 5.2.7. Equation 3.8 illustrates how $\dot{\theta}$ was calculated.

$$\dot{\theta}(i) = \frac{\theta(i+1)-\theta(i-1)}{2h} \qquad \text{(Eq. 3-8)}$$

In equation above, $\dot{\theta}$ is the L4/L5 joint angle velocity, θ is the L4/L5 joint angle, and h is the inverse of motion markers' data frequency (i.e. 100 Hz in this study).

3.11.4. Dependent Variables

Table 3-1 shows the main dependent variables in this study. As shown in Fig. 3-14, the mean EMG amplitude was calculated over one second prior to the start of each task. The window during which the mean EMG amplitude was calculated is shown by * in Fig. 3-14.

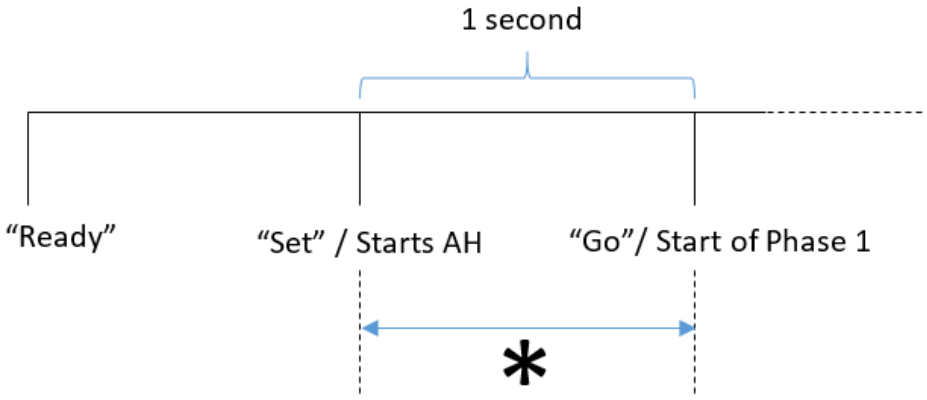

Figure 3-14: Diagram showing the area where the mean EMG amplitude was calculated.

The sagittal plane L4/L5 joint angle range of motion (ROM) was calculated by subtracting the minimum joint angle value from the maximum value. This is shown in Figs. 3-15 and 3-16. Comparison of the ROM values between the AH and NAH tasks determined whether AH helped the participants minimize their pelvic and lumbar spine motion during the exercises. Furthermore, comparison of the ROM values between the TST 1 and 3 tasks determined whether the leg extension phase in TST 3 resulted in higher ROM compared to TST 1.

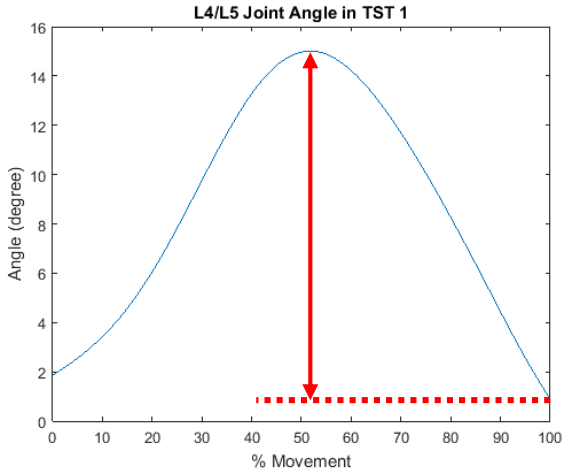

Figure 3-15: Sagittal plane L4/L5 joint angle range of motion (ROM) calculation in TST1.

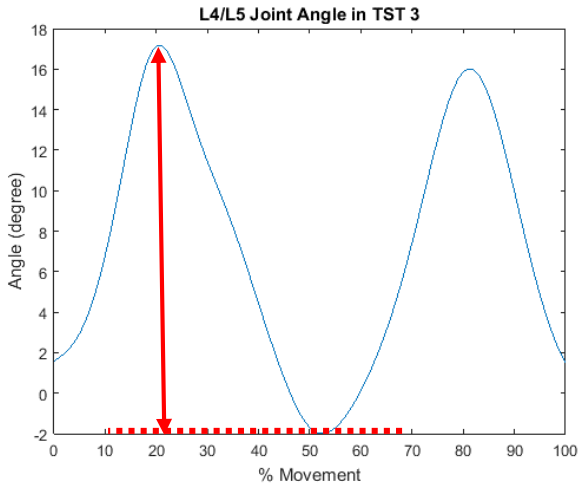

Figure 3-16: Sagittal plane L4/L5 joint angle range of motion (ROM) calculation in TST3.

To compare the sagittal plane L4/L5 joint moment waveforms between the AH and NAH tasks, the joint moments at the minima and maxima in each task were calculated as illustrated in Figs 3-17 and 3-18. Furthermore, to compare the L4/L5 joint moments between TST 1 and 3, the following comparisons were made:

- m1 in TST 1 versus m1 in TST 3.
- m2 in TST 1 versus m2 in TST 3.
- m3 in TST 1 versus m5 in TST 3.

Lastly, to investigate the demand required by the tasks, the absolute maximum of joint moment in TST 3 (i.e. at m3) and TST 1 (i.e. m1 or m3 depending on where the joint moment magnitude is higher) were compared (Juker et al., 1998). These locations are where the trunk muscles produce the highest amount of torque around the L4/L5 joint of spine to counteract the moment created by the leg movements.

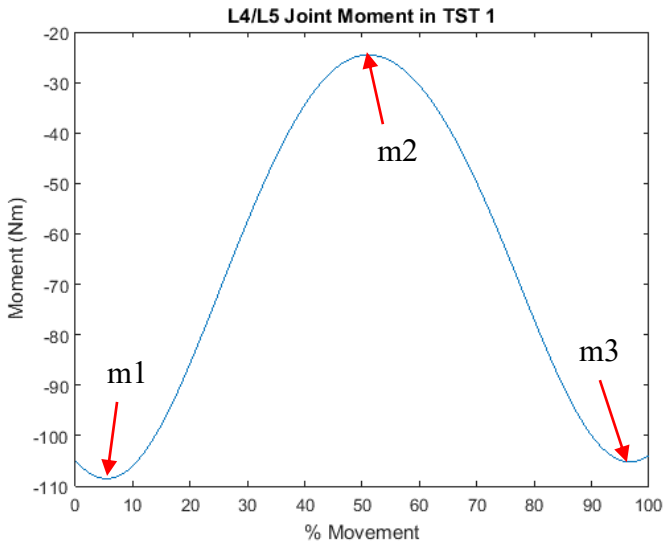

Figure 3-17: Calculation of the L4/L5 joint moments at the minima and maxima in TST level 1.

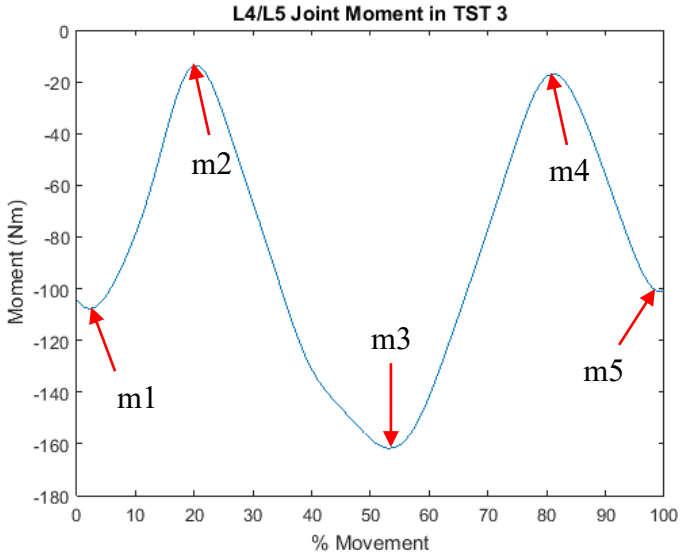

Figure 3-18: Calculation of the L4/L5 joint moments at the minima and maxima in TST level 3.

Average joint stiffness in each phase and the entire task were obtained by calculating the average of L4/L5 dynamic joint stiffness values during each phase and the entire task respectively. In this study, the dynamic L4/L5 joint stiffness was calculated using the finite difference equation as described in section 3.11.3.1.

Table 3-1: Dependent variables

Category	Variables
Internal oblique EMG data	1. Mean EMG amplitude one second prior to start of the task
Sagittal plane L4/L5 joint angle	2. Range of motion (ROM)
Sagittal plane L4/L5 joint moment	3. L4/L5 joint moments at the minima and maxima.
Sagittal plane L4/L5 dynamic joint stiffness	4. Average joint stiffness during each phase. 5. Average joint stiffness during entire task

3.11.5. Statistical Analysis

The main objective of this study was to develop a dynamic measure of L4/L5 joint stiffness, and then compare the results between two standardized tasks (i.e. TST levels 1 and 3) and conditions (i.e. with abdominal hollowing while minimizing pelvic and lower back motion, and without abdominal hollowing). The following sections describe statistical analysis procedures that were used to analyze the dependent variables in Table 3-1. All the statistical procedures were performed in Minitab™, Ver. 17 (Minitab Inc. State College, PA, USA). For each dependent variable for Objective 2, the Anderson-Darling normality test in Minitab™, Ver. 17 (Minitab Inc. State College, PA, USA) was used, and for non-normally distributed variables, a Johnson transformation was utilized.

1. **Mean EMG amplitude one second prior to start of the task:** For each task and muscle group (i.e. right and left IO muscles), 1-tailed Student's t-test ($p<0.05$) was used to test for significant difference between the mean of ten AH tasks (i.e.

ten participants) and NAH tasks. A significant difference result ($p<0.05$) would indicate significantly higher IO activity in the AH tasks compared to the NAH tasks.

2. **Sagittal plane L4/L5 joint angle range of motion (ROM):** A two-way (factors: tasks and conditions) repeated measure ANOVA ($\alpha = 0.05$) was used to test for significant task and condition main effects and interactions. The null hypothesis was that the participants' L4/L5 joint ROM were not significantly different under different tasks, conditions, and their respective interaction. Post hoc Tukey test were applied to the significant differences.

3. **Sagittal plane L4/L5 joint moment at the minima and maxima:** To compare the joint moments between the AH and NAH tasks, separate two-way (factors: condition and locations (i.e. m1, m2, etc.)) repeated measures ANOVA for each task were used to test for significant condition and location main effects and interactions at the minima and maxima identified in the previous section. The null hypothesis is that there was no significant difference in L4/L5 joint moments between conditions, locations, or interaction. Post hoc Tukey test were applied to the significant differences.

   To compare the joint moments between TST 1 and 3, two-way (factors: tasks and locations (i.e. m1, m2, etc.)) repeated measures ANOVA were used to test for significant task and location main effects and interactions at the minima and maxima identified in the previous section. The null hypothesis is that there was no

significant difference in L4/L5 joint moments between tasks, locations, or interactions. Post hoc Tukey test were applied to the significant findings.

Finally, to compare the demand of the TST tasks, a 1-tailed Student's t-test ($p<0.05$) was used to test for significant difference of absolute maximum in L4/L5 joint moments between TST 3 and TST 1. A significant difference result ($p<0.05$) would indicate significantly higher demand in TST 3 compared to TST 1.

4. **Average joint stiffness during each phase:** For each of TST level 1 and 3 tasks, a two-way (factors: condition and phases) repeated measures Analysis of Variance (ANOVA) were used to test for significant differences in L4/L5 dynamic joint stiffness phase by phase. The null hypothesis is that in each task, there would be no significant difference in L4/L5 joint stiffness between phases, conditions, and their respective interaction. Post hoc Tukey test were applied to the significant differences.
5. **Average joint stiffness during entire task:** A two-way (factors: tasks and conditions) repeated measures ANOVA were used to test for significant task and condition main effects and interactions. The null hypothesis is that there was no significant difference in L4/L5 joint stiffness between tasks, conditions, and their respective interaction. Post hoc Tukey test were applied to the significant differences.

   Note: In part 4 and 5, in total three ANOVA tests were applied to the joint stiffness data. Therefore, alpha was set at 0.050 divided by 3 (i.e. $\alpha = 0.017$).

CHAPTER 4 OBJECTIVE 1 RESULTS

4.1. INTRODUCTION

Since the absolute angles of the shanks, thighs, and pelvis would be used to estimate the body segments' angular velocities and acceleration, a digital inclinometer was utilized to compare the measured angular displacements of the shanks and thighs with the values calculated from the kinematic model (the model is fully described in Appendix A). The absolute angle of pelvis was not compared between the two methods because it is not feasible to measure angular displacement of the pelvis by an inclinometer. Furthermore, since the L4/L5 joint angle (relative angle) was used to estimate the L4/L5 dynamic joint stiffness, it was of an interest to compare the relative L4/L5 joint angle as well by estimating it using the thesis's kinematic model and then comparing the values with an electrogoniometer. Overall, the purpose of Objective 1-b was to check the agreement between the angles (i.e. absolute and relative) measured by the thesis's kinematic model, and the ones estimated by other measurement systems (i.e. inclinometer for absolute angles, and electrogoniometer for relative angles) to gain confidence about the designed kinematic model.

The kinematic and kinetic model described in Section 3.9 and Appendix A was designed to calculate kinematic and kinetic data dynamically. Hence, it was of interest to investigate whether simplifying the dynamic model by removing the inertial and acceleration terms (i.e. quasi-static analysis) resulted in similar values as those from the dynamic analysis. Therefore, the acceleration and inertial terms were removed from the dynamic equations of motion (see section 3.10.2), and the results were compared with the dynamic L4/L5 joint moments.

Additionally, this thesis attempted to investigate the effect of excluding the ground reaction forces (GRFs) from the dynamic equations of motion (see section 3.10.3). Again, the motivation was to determine whether a simplified kinetic model without the GRFs would result in similar values for the sagittal plane L4/L5 joint moments. For the two joint moment comparisons an estimate of the error between the full model and the reduced model was performed.

4.2. RESULTS

4.2.1. Absolute and Relative Angles Calculations (Objective 1-b)

Figures 4-1 to 4-4 illustrate the absolute angles measured by both the digital inclinometer and the motion capture system for shanks and thighs. As can be seen in these graphs, the absolute angles measured by the two methods were similar with root mean squared errors (RMSE) that ranged from 0.7 to 2.4 degrees for the shanks, and from 2.0 to 2.2 degrees for the thighs.

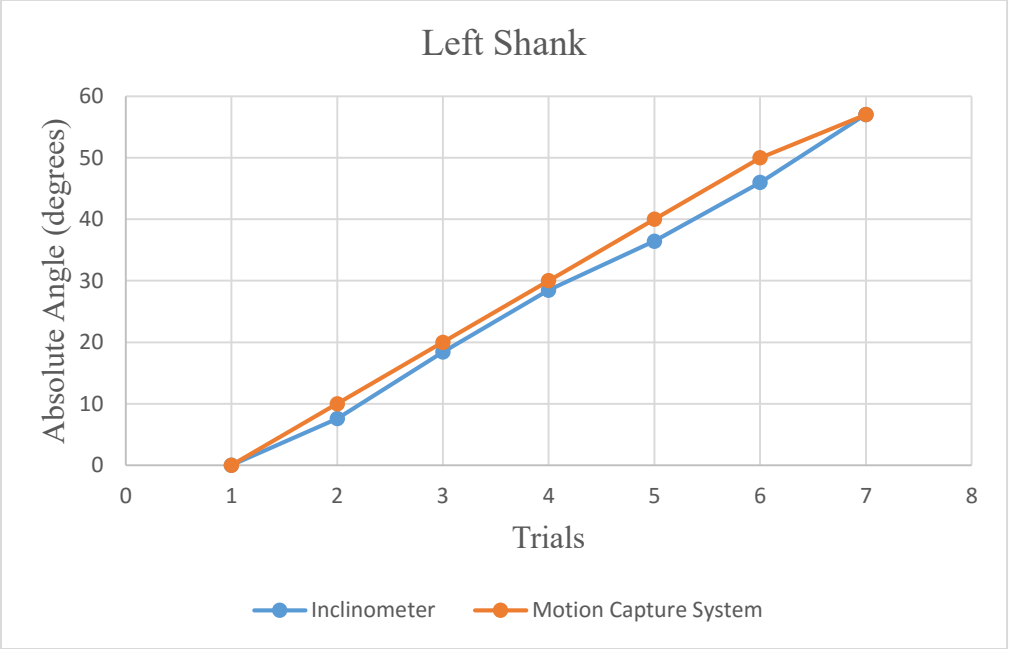

Figure 4-1: Comparison of absolute angle measurements between the motion camera system and inclinometer for the left shank. RMSE = 2.4 degrees.

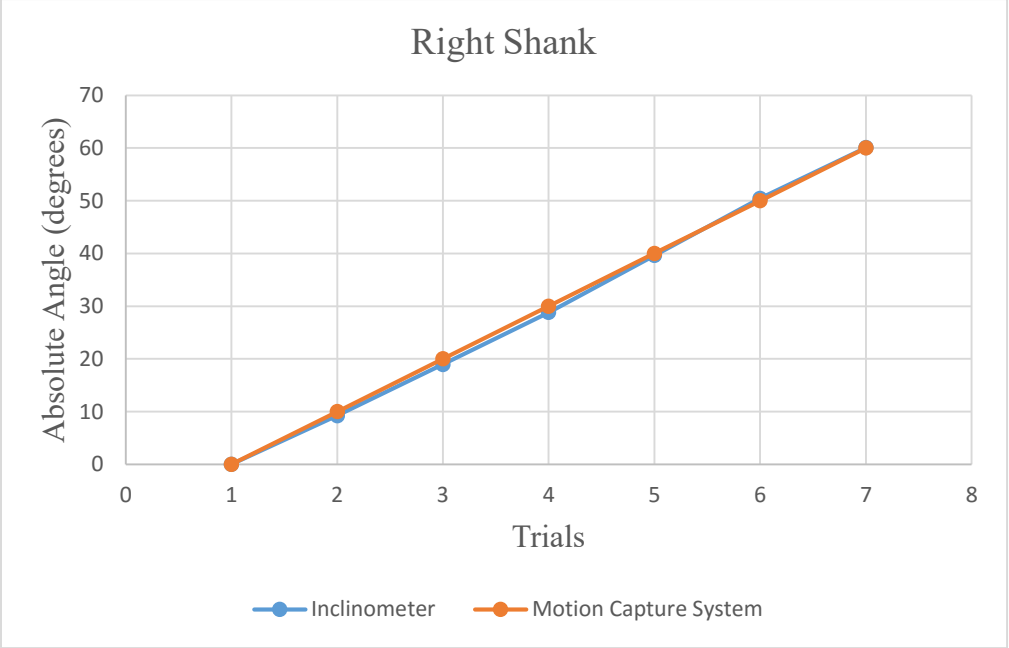

Figure 4-2: Comparison of absolute angle measurements between the motion camera system and inclinometer for the right shank. RMSE = 0.7 degrees.

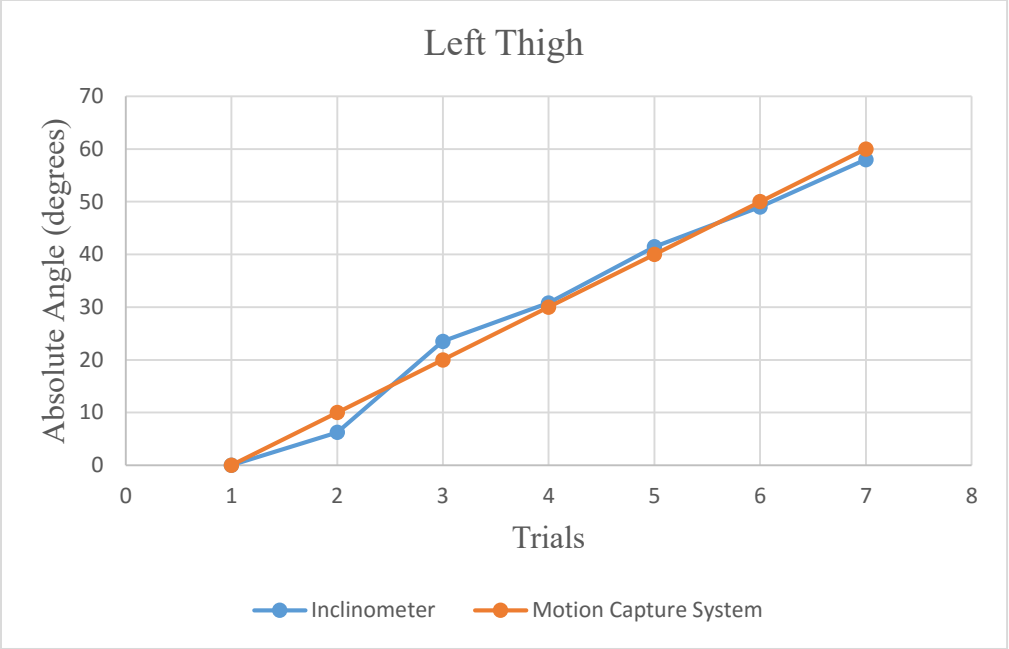

Figure 4-3: Comparison of absolute angle measurements between the motion camera system and inclinometer for the left thigh. RMSE = 2.2 degrees.

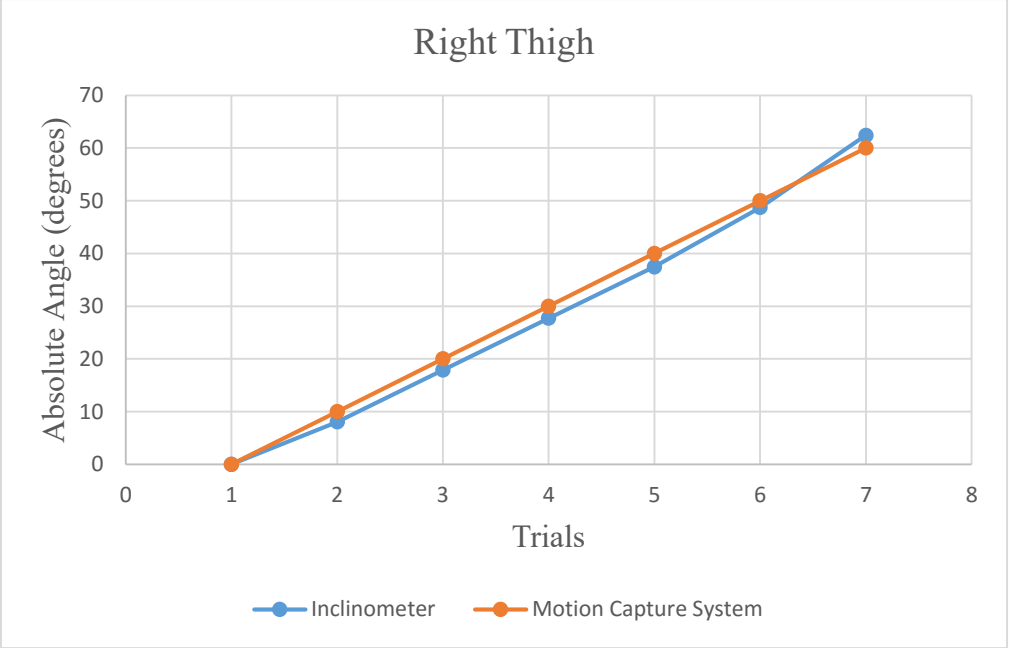

Figure 4-4: Comparison of absolute angle measurements between the motion camera system and inclinometer for the right thigh. RMSE = 2.0 degrees.

Figure 4-5 illustrates the trunk flexion/extension angles measured by the electrogoniometer and the thesis's kinematic model. For each of the trials shown in Fig. 4-5, Table 4-1 depicts the corresponding RMSE and difference in ROM between the two methods. As shown in Fig. 4-5, the general shape and pattern of the relative L4/L5 joint angle measured by electrogoniometer and the developed kinematic model are similar. However, since the electrogoniometer sensors were placed on the lower lumbar and upper lumbar/lower thoracic spine, it was expected that the electrogoniometer and the developed kinematic model would not measure the sagittal plane angles around the exact same joint (i.e. kinematic crosstalk). This is better illustrated in Table 4-1 as the two methods did not produce similar ROM. Furthermore, it appears that the angles were most similar in the first trial of the experiment. This was perhaps because the participant's spinal column slightly bent inward or outward during trunk flexion and extension which was not visually visible during the experiment. Moreover, the slight over-flexion or extension of the cable in the electrogoniometer would lead to measurement errors.

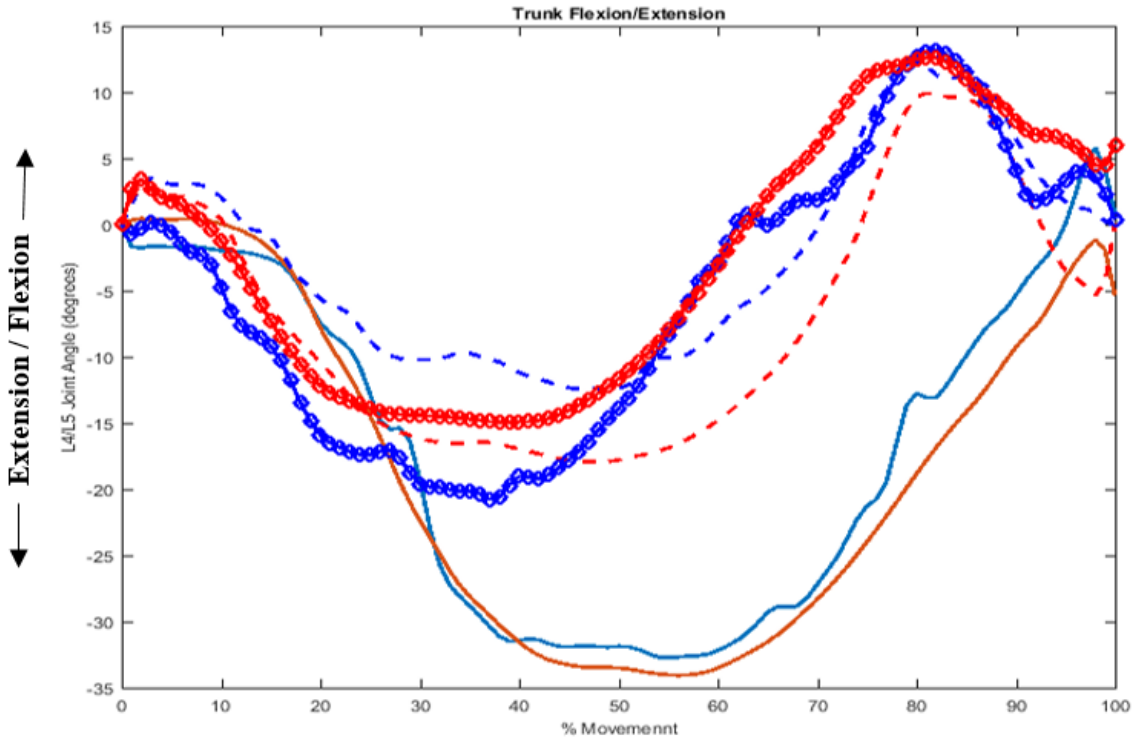

Figure 4-5: Three trials of trunk flexion/extension. The blue and red lines correspond to the angles estimated by the thesis's kinematic model and electrogoniometer respectively. Trial 1: Solid line, Trial 2: Dashed line, Trial 3: dotted line

Table 4-1: Root mean squared error (RMSE) and the range of motion (ROM) difference between the angles estimated by the thesis's kinematic model and electrogoniometer. Percent ROM error was calculated by dividing the ROM difference by the ROM that was estimated by the developed kinematic model. The result was then multiplied by 100.

	RMSE (degrees)	*ROM difference (degrees)*	*% ROM Error*
Trial 1	2.8	4.0	10.5 %
Trial 2	5.1	2.7	10.9 %
Trial 3	3.3	6.3	18.6 %
Mean (SD)	3.7 (1.2)	4.4 (1.8)	13.3 (4.6)

4.2.2. Dynamic vs. Quasi-Static Analysis (Objective 1-c)

Figures 4-6 shows the ensemble L4/L5 joint moments in the sagittal plane calculated both dynamically and quasi-statically. As shown in this figure, although the general shape and pattern of the L4/L5 joint moment is maintained in the quasi-static analysis, the joint moment amplitudes appear to be different between the dynamic and quasi-static moments at the minima and maxima.

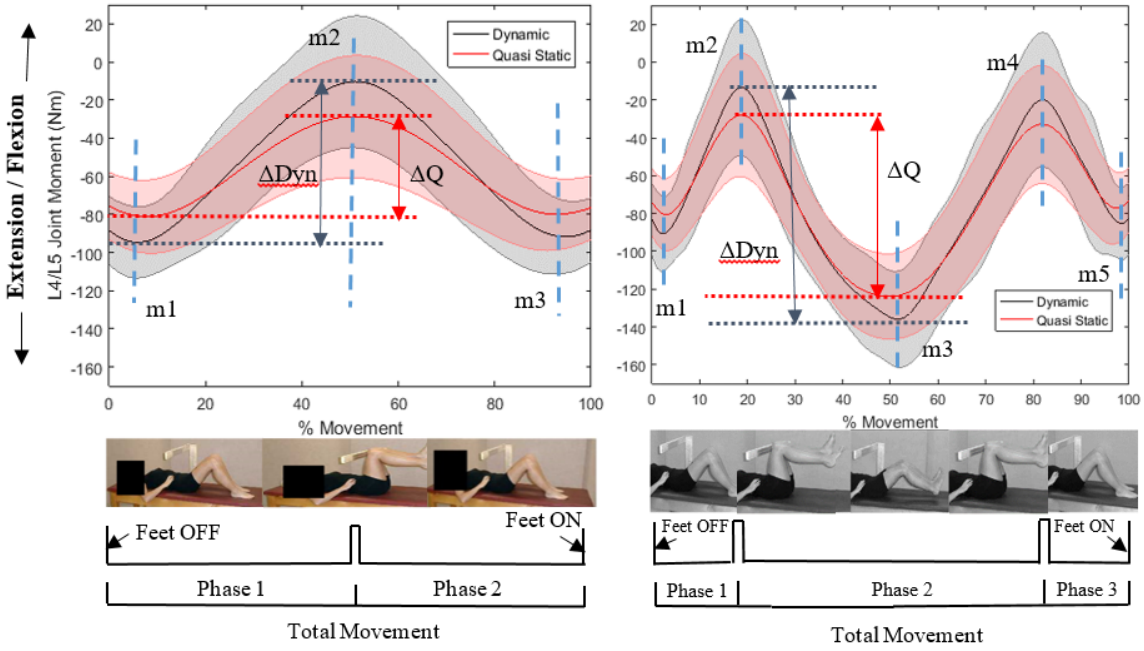

Figure 4-6: Ensemble averaged dynamic and quasi-static L4/L5 joint moments in the sagittal plane in TST 1 (left) and TST 3 (right). The shaded areas show one standard deviation. ΔDyn and ΔQ represent peak to peak dynamic and quasi-static L4/L5 joint moments respectively. The vertical lines indicate the minima and maxima where the difference between dynamic and quasi-static moments are at the greatest.

The dynamic and quasi-static L4/L5 joint moments for all participants were analyzed and compared, and the results are shown in Table 4-2. In these tables, the %Error was calculated by dividing the RMSE (i.e. the RMS of the difference between the dynamically and quasi-statically determined joint moments) by the RMS of the dynamic

L4/L5 joint moment. As depicted in Table 4-2, the mean %Error 18.1% for TST 1, and 9.5% for TST 3. For a full comparison of dynamic and quasi-static L4/L5 joint moments across all participants, please refer to Appendix C.

Table 4-2: Comparison of dynamic and quasi-static sagittal plane L4/L5 net external joint moments in TST 1 and 3. Values show the mean and standard deviation across all participants. For a description of |ΔDyn| and |ΔQ|, please refer to Fig. 4-6.

Task	*|ΔDyn| (Nm)*	*|ΔQ| (Nm)*	*|ΔDyn-ΔQ | (Nm)*	*RMSE (Nm)*	*RMS Dyn (Nm)*	*%Error*
TST 1	86.2 (32.9)	54.5 (24.4)	31.7 (9.0)	11.3 (3.3)	67.2 (14.0)	18.1 (8.7)
TST 3	127.1 (49.2)	98.6 (42.5)	28.5 (8.4)	7.9 (3.2)	84.8 (15.9)	9.5 (3.5)

To obtain a better understanding of how quasi-static analysis affects the joint moment magnitude at the minima and maxima (see Fig. 4-6), the difference between the dynamic and quasi-static joint moments at the minima and maxima were calculated. Moreover, the difference between the moments as a percentage of peak to peak dynamic moment (i.e. ΔDyn in Fig. 4-6) were also computed, and the results are shown in Table 4-3.

As depicted in Table 4-3, on average the difference between the dynamic and quasi-static L4/L5 joint moments at the minima and maxima were 14.3 Nm (16.4%) at m1, 18.7 Nm (23.1%) at m2, and 13.2 Nm (15.1%) at m3. These results indicate that at the maxima (i.e. m2) where both deceleration and acceleration of the body segments occur, the exclusion of the acceleration and inertial terms had the largest effect on the joint moment during TST 1.

As shown in Table 4-3, on average the difference between the dynamic and quasi-static L4/L5 joint moments for TST 3 at the minima and maxima were 11.2 Nm (8.8%) at m1,

15.2 Nm (12.6%) at m2, 14.0 Nm (11.4%) at m3, 14.4 Nm (11.2%) at m4, and 10.8 Nm (7.5%) at m5. Based on these results, it appears that the exclusion of the acceleration and inertial terms resulted in higher difference in joint moments (i.e. Δmi) at the maxima compared to the minima. Moreover, the quasi-static analysis led to less Δmi at the maxima in TST 3 compared to the maxima in TST 1 (i.e. 15.2 Nm and 14.4 Nm versus 18.7 Nm). Additionally, Δmi at the initial and last minima in TST 3 was smaller compared to the ones reported at the minima in TST 1 (i.e. 11.2 Nm and 10.8 Nm versus 14.3 Nm and 13.2 Nm).

Table 4-3: Difference between dynamic and quasi-static L4/L5 net external joint moments at the minima and maxima (Δmi) in TST 1 and 3. Values show the mean and standard deviation across all participants. %Δmi was calculated by dividing Δmi by the peak to peak dynamic moment (Δdyn), and then multiplying the result by 100.

Tasks	***Δm1 (Nm)***	***% Δm1***	***Δm2 (Nm)***	***% Δm2***	***Δm3 (Nm)***	***% Δm3***	***Δm4 (Nm)***	***% Δm4***	***Δm5 (Nm)***	***% Δm5***
TST 1	14.3 (6.8)	16.4 (2.7)	18.7 (3.3)	23.1 (5.0)	13.2 (5.7)	15.1 (1.5)	-	-	-	-
TST 3	11.2 (5.5)	8.8 (2.1)	15.2 (4.3)	12.6 (2.9)	14.0 (4.4)	11.4 (3.1)	14.4 (6.2)	11.2 (2.3)	10.8 (8.9)	7.5 (3.4)

4.2.3. Dynamic Analysis w/ and wo/ GRF (Objective 1-d)

Figures 4-7 illustrates the ensemble dynamic L4/L5 joint moment in sagittal plane during TST 1 and 3, with and without GRF data. As shown in this figure, although the general shape of the waveforms looks similar between the two methods, the exclusion of the GRF data resulted in a systematic bias in joint moment magnitude during both TST 1 and 3.

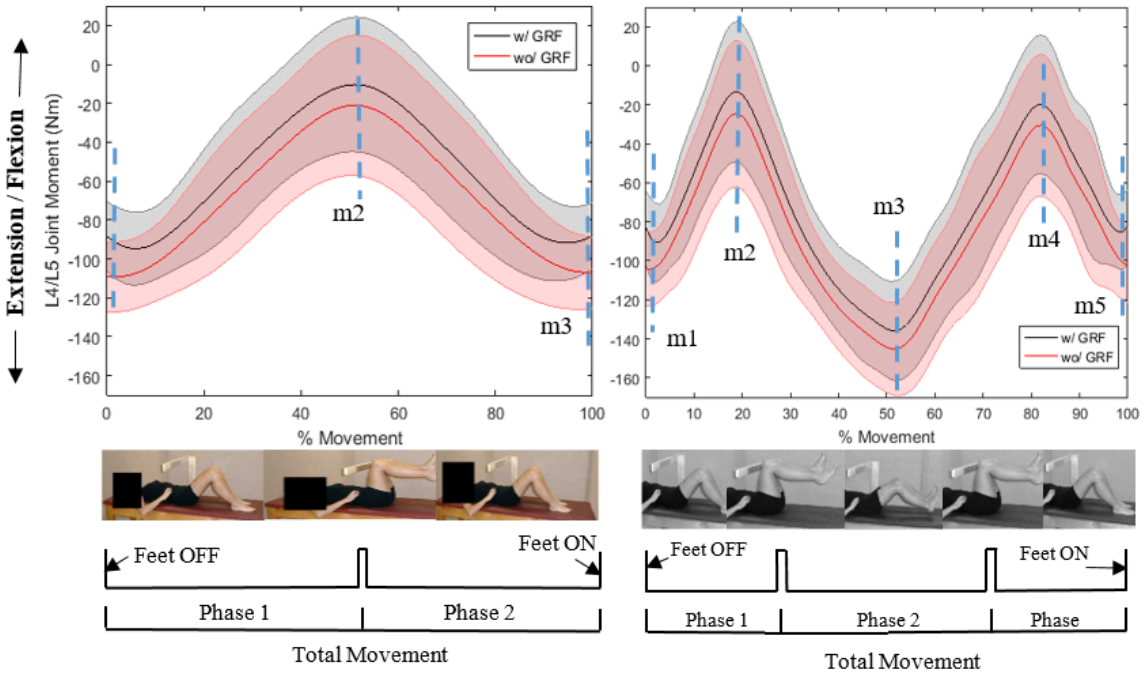

Figure 4-7: Comparison of ensemble dynamic sagittal plane L4/L5 joint moment with and without GRF in TST 1 (left) and TST 3 (right). The shaded areas show one standard deviation. The vertical lines indicate the locations where the difference in moments between those with and without GRF is at the greatest (i.e. at the maxima, and during the start and end of the tasks).

The dynamic L4/L5 joint moments with and without GRF data for all participants were analyzed and compared, and the results are shown in Table 4-4. As shown in Table 4-4, the mean %Error was 18.0% for TST 1, and 13.4% for TST 3. Moreover, the mean peak to peak difference between the two types of moment calculation was 4.2 Nm for TST 1 and 2.6 Nm for TST 3. Thus, although the mean %Error between the two methods was above 10% for both TST 1 and 3, the exclusion of the GRF data from the moment calculation had very small effect on the peak to peak joint moment during the exercises as compared to the quasi-static moments.

Table 4-4: Comparison of dynamic sagittal plane L4/L5 net external joint moments with and without GRF in TST 1 and 3. Values show the mean and standard deviation across all participants.

Task	*|ΔDyn| (Nm)*	*|ΔQ| (Nm)*	*|ΔDyn-ΔQ | (Nm)*	*RMSE (Nm)*	*RMS Dyn (Nm)*	*%Error*
TST 1	86.2 (32.9)	89.0 (33.5)	4.2 (4.0)	11.8 (3.6)	67.2 (14.0)	18.0 (5.9)
TST 3	127.1 (49.2)	125.1 (48.1)	2.6 (1.3)	10.9 (3.4)	84.8 (15.9)	13.4 (5.2)

To understand how the exclusion of the GRF data from the dynamic joint moments affects the joint moment magnitude at the locations specified in Fig. 4-7, the difference between the moments with and without GRF at the maxima, and the start and end of the tasks were calculated. The reason that the difference in moments at the minima was not investigated was the fact that the exclusion of GRF had resulted in higher errors at the start and end of the tasks compared to the minima (see Fig. 4-7). The difference between the moments as a percentage of peak to peak dynamic moment (i.e. ΔDyn) were also computed, and the results are shown in Table 4-5.

As depicted in Table 4-5, on average the difference between the moments with and without GRF were 20.8 Nm (27.8%) at m1, 12.1 Nm (16.3%) at m2, and 18.9 Nm (25.3%) at m3. These results indicate that at the initiation and end of the tasks, the exclusion of the GRF data had the largest effect on the joint moment during TST 1.

Furthermore, as illustrated in Table 4-5, on average the difference between the moments with and without GRF were 20.8 Nm (19.0%) at m1, 12.2 Nm (11.2%) at m2, 11.0 Nm (10.1%) at m3, 11.9 Nm (10.7%) at m4, and 19.4 Nm (17.8%) at m5. Similar to TST 1, these results indicate that at the initiation and end of the tasks, the exclusion of the GRF

data had the largest effect on the joint moment during TST 3. Moreover, as can be seen from Table 4-5, the effect of the exclusion of the GRF data is relatively consistent across the tasks at the maxima (i.e. 12.1 Nm in TST 1 vs. 12.2 Nm and 11.9 Nm in TST 3), and during the initiation (i.e. 20.8 Nm in TST 1 vs. 20.8 Nm in TST 3) and end (i.e. 18.9 Nm in TST 1 vs. 19.4 Nm in TST 3) of the tasks.

Table 4-5: Difference between dynamic L4/L5 net external joint moments with and without GRF at the locations shown in Fig. 4-7 in TST 3 (Δmi). Values show the mean and standard deviation across all participants. %Δmi was calculated by dividing Δmi by the peak to peak dynamic moment (Δdyn), and then multiplying the result by 100.

	Δm1 (Nm)	***%Δm1***	***Δm2 (Nm)***	***%Δm2***	***Δm3 (Nm)***	***%Δm3***	***Δm4 (Nm)***	***%Δm4***	***Δm5 (Nm)***	***%Δm5***
TST 1	20.8 (5.8)	27.8 (13.8)	12.1 (3.5)	16.3 (7.8)	18.9 (5.0)	25.3 (11.0)	N/A	N/A	N/A	N/A
TST 3	20.8 (5.6)	19.0 (9.5)	12.2 (3.5)	11.2 (5.3)	11.0 (4.0)	10.1 (5.5)	11.9 (3.8)	10.7 (4.8)	19.4 (5.2)	17.8 (7.9)

In an attempt to determine if there was a systematic offset between the L4/L5 joint moments with and without GRFs data associated with body mass, the participants' mass was plotted against RMSE obtained in Table 4-4. Then, a linear regression line was fitted to the data to obtain the R-squared value. The R-squared value is a statistical measure of how close the data are to the statistical model (i.e. the fitted regression line). In other words, it provides a measure of how well the observed outcomes are estimated by the model (Coolidge & Coolidge, 2012). The mass and RMSE data for all the participants are shown in Table 4-6.

Figure 4-8 illustrates the results of the fitted regression lines to the RMSE versus participants' mass data. The results show an R-squared value of 0.09 for TST 1 and 0.06 for TST 3 indicating no relationship between the participants' mass and the RMSE (i.e. offset between the moments as shown in Fig. 4-7). This indicates that there is no systematic increase in offset related to the participants' mass.

Table 4-6: Participants' mass, and their associated RMSE in TST 1 and 3.

Participant #	***Mass (kg)***	***RMSE in TST 1 (Nm)***	***RMSE in TST 3 (Nm)***
1	91.7	14.3	13.2
2	60.2	8.9	9.8
3	69.6	6.8	4.8
4	84.2	8.8	8.4
5	87.0	14.6	13.4
6	66.7	16.0	14.7
7	66.4	9.7	9.6
8	72.3	17.4	16.1
9	72.6	11.7	10.4
10	69.0	9.7	8.7
Mean (SD)	**74.0 (10.2)**	**11.8 (3.6)**	**10.9 (3.4)**

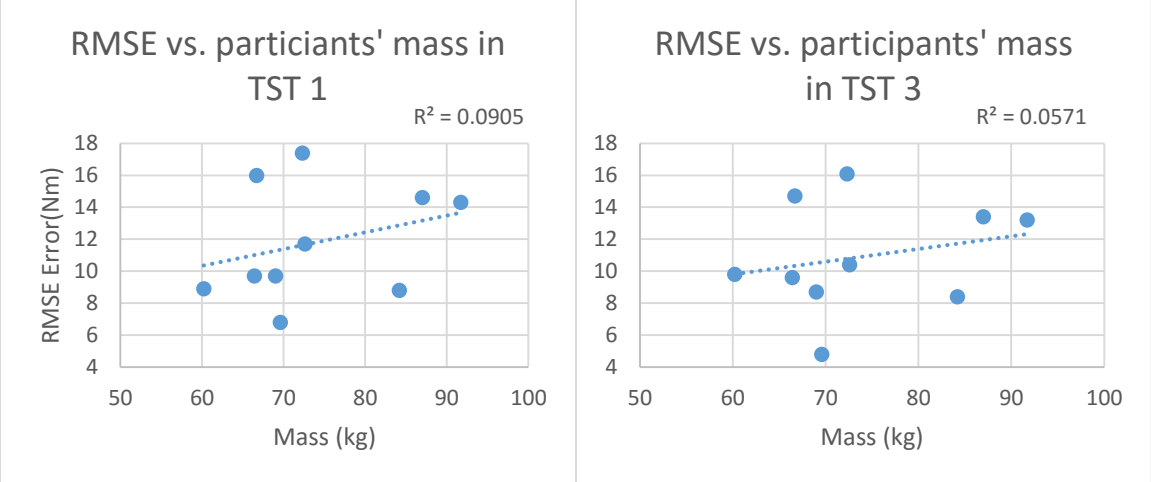

Figure 4-8: Plots of RMSE versus participants' mass in TST 1 (left) and TST 3 (right).

CHAPTER 5 OBJECTIVE 2 RESULTS

INTRODUCTION

The main objective (i.e. objective 2) of this thesis was to compare the dynamic L4/L5 joint stiffness between two different controlled dynamic tasks (TST 1 and 3) with each task performed under two different conditions (with and without abdominal hollowing). This chapter will present the results of this objective which include the participants' demographics, the exercise timing, internal oblique muscles' mean EMG amplitudes, sagittal plane L4/L5 range of motion (ROM), sagittal plane L4/L5 joint moments, and sagittal plane L4/L5 dynamic joint stiffness.

5.2. RESULTS

5.2.1. Normality Test Results

Using the Anderson-Darling normality test in Minitab™, Ver. 17 (Minitab Inc. State College, PA, USA), the normality of Objective 2 discrete variables was examined. In total, 13 out of 44 variables were not normally distributed. Johnson transformation in Minitab™, Ver. 17 was utilized to transform the non-normal variables prior to the statistical analyses. This transformation in Minitab™, Ver. 17 examines the data and chooses the best transformation to meet the assumptions of the ANOVA model. For a complete list of Objective 2 discrete variables and the results of the Anderson-Darling normality test, please see Appendix B.

5.2.2. Participants' Demographics

For this study, ten healthy men between the age of 20 and 30 years old, and with no history of LBP were recruited through posters and emails. Table 5-1 shows the mean age, mass, and height of the participants.

Table 5-1: Participants information.

Participants	*Age*	*Mass (kg)*	*Height (cm)*
Mean (SD)	25.1 (2.2)	74.0 (10.2)	179.4 (6.2)

5.2.3. Exercise Timing

Table 5-2 illustrates the average time that took the participants to finish TST 1 and 3. The table also depicts the timing for each phase as well.

Table 5-2: Exercise timing for TST levels 1 and 3.

Exercise	*Start to End (s)*	*Phase 1 (s)*	*Phase 2 (s)*	*Phase 3 (s)*
TST 1_NAH	1.9 (0.1)	0.9 (0.1)	0.9 (0.1)	N/A
TST 1_AH	2.0 (0.2)	1.0 (0.1)	1.0 (0.1)	N/A
TST 3_NAH	5.9 (0.3)	1.1 (0.1)	3.7 (0.3)	1.1 (0.2)
TST 3_AH	5.8 (0.3)	1.0 (0.1)	3.7 (0.2)	1.2 (0.2)

As shown in Table 5-2, for each of TST 1 and TST 3 tasks, there is minimal difference in timing between the AH and NAH conditions. Furthermore, there is minimal variability (i.e. very small standard deviation as shown inside the parentheses in Table 5-2) in each task and condition. These results illustrate that this study was successful in controlling the exercise timing across all participants and for all the exercises.

5.2.4. Internal Oblique Muscles' Mean EMG Amplitude

Table 5-3 shows the IO muscles' mean EMG amplitude–averaged over one second prior to the leg movement–in TST levels 1 and 3 in %MVIC. Using Anderson-Darling normality test, it was determined that two out of eight discrete variables were not normally distributed (see Appendix B). Johnson transformation was utilized to transform the non-normal variables prior to the statistical analysis. Statistical analysis indicated that in both tasks and in both right and left IO, AH led to significantly ($p < 0.05$) higher muscle activity (i.e. from 25.5 to 31.6 %MVIC) compared to NAH tasks (i.e. from 4.5 to 5.6 %MVIC).

Table 5-3: IO muscles mean EMG amplitude in TST levels 1 and 3.

		Right IO (%MVIC)		***Left IO (%MVIC)***	
Task		NAH	AH	NAH	AH
TST 1	**Mean (SD)**	4.7 (2.1)	29.6 (20.1)	5.6 (3.7)	31.6 (22.1)
	p Value	0.003		0.003	
TST 3	**Mean (SD)**	4.5 (3.3)	25.5 (18.9)	5.1 (4.3)	27.8 (19.9)
	p Value	0.007		0.005	

5.2.5. Sagittal Plane L4/L5 Range of Motion

Table 5-4 illustrates the mean and standard deviation for the sagittal plane L4/L5 range of motion (ROM) patterns for TST levels 1 and 3. Using Anderson-Darling normality test, it was determined that all 14 discrete variables were normally distributed. Hence, no transformation was needed prior to the statistical analysis (see Appendix B). Statistical

analyses of the foot-off to foot-on L4/L5 joint ROM revealed significant main effects for task ($p = 0.000$) and condition ($p = 0.005$) but no significant task and condition interaction effect ($p = 0.819$). Post-hoc analysis showed that the sagittal plane L4/L5 joint ROM was significantly higher in TST 3 (i.e. 12.7 (3.2) degrees) compared to TST 1 (i.e. 9.4 (3.2) degrees), as well as in NAH tasks (i.e. 11.7 (3.6) degrees) compared to AH tasks (i.e. 10.4 (3.6) degrees).

Statistical analysis was also performed for each task separately to examine differences among phases. For TST 1, the results indicated significant main effects for condition ($p = 0.000$) and phase ($p = 0.021$) but no significant condition and phase interaction ($p = 0.771$). Post-hoc analysis revealed that TST 1 NAH (i.e. 9.3 (3.2) degrees) resulted in higher L4/L5 joint ROM compared to TST 1 AH (7.6 (3.4) degrees). Furthermore, the L4/L5 joint ROM was significantly higher in phase 2 (i.e. 8.9 (3.5) degrees) compared to phase 1 (i.e. 7.9 (3.2) degrees). For TST 3, ANOVA revealed significant main effects for condition ($p = 0.000$) and phase ($p = 0.000$) but again no significant condition and phase interaction ($p = 0.572$). Post-hoc analyses showed that TST 3 NAH (i.e. 10.4 (3.7) degrees) led to higher L4/L5 ROM compared to TST 3 AH (i.e. 8.6 (3.8) degrees). Moreover, the L4/L5 joint ROM was significantly higher in phase 2 (i.e. 12.1 (3.6) degrees) compared to both phase 1 (i.e. 7.7 (3.3) degrees) and 3 (i.e. 8.6 (3.2) degrees).

Table 5-4: Sagittal plane relative L4/L5 joint range of motion (ROM) in TST levels 1 and 3.

		Foot-off to foot-on (deg)		***Phase 1 (deg)***		***Phase 2 (deg)***		***Phase 3 (deg)***	
Task		**NAH**	**AH**	**NAH**	**AH**	**NAH**	**AH**	**NAH**	**AH**
TST 1	**Mean (SD)**	10.1 (3.1)	8.6 (3.4)	8.9 (3.1)	7.0 (3.2)	9.7 (3.4)	8.2 (3.7)	N/A	N/A
TST 3	**Mean (SD)**	13.4 (3.3)	12.1 (3.2)	8.6 (2.6)	6.8 (3.8)	13.3 (3.3)	11.0 (3.7)	9.1 (3.5)	8.0 (3.0)
TST 1	**Mean (SD)**	9.4 (3.2)		7.9 (3.2)		8.9 (3.5)		N/A	
TST 3	**Mean (SD)**	12.7 (3.2)		7.7 (3.3)		12.1 (3.6)		8.6 (3.2)	
Cond.	**AH**	**Mean (SD)**	10.4 (3.6)						
	NAH	**Mean (SD)**	11.7 (3.6)						

Figure 5-1 illustrates the ensemble average of sagittal plane L4/L5 joint angle for all ten participants in TST 1 and 3. As shown in the figure, AH leads to less sagittal plane L4/L5 joint angle ROM as found from the statistical results for the ROM. Furthermore, the difference in L4/L5 joint angle between the AH and NAH tasks is greater at the initiation and end of the tasks, and also during full knee extension in TST 3.

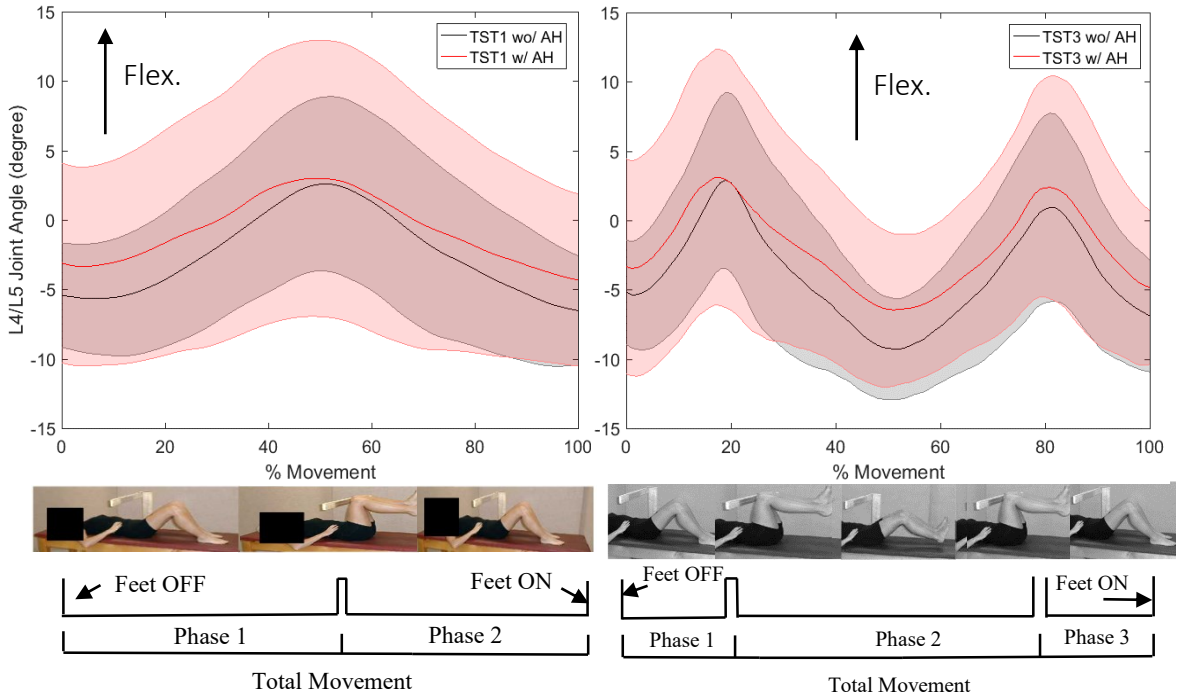

Figure 5-1: Ensemble averaged sagittal plane L4/L5 joint angle for all the participants in TST 1 (left) and TST 3 (right).

5.2.6. Sagittal Plane L4/L5 Joint Moment

Table 5-5 below depicts the mean and standard deviation of the L4/L5 joint moments at the minima and maxima in TST 1 and 3. Using Anderson-Darling normality test, it was determined that 6 out of 16 discrete variables were not normally distributed. Hence, using the Johnson transformation, the non-normal variables were transformed prior to the statistical analysis (see Appendix B). Statistical analyses revealed that for each task, there were no significant differences ($p > 0.05$) in joint moments at the minima and maxima between AH and NAH tasks. In other words, AH had no significant effect on the joint moment magnitude at the minima and maxima during the exercises as compared to the NAH tasks. Furthermore, statistical analysis determined that the joint moment magnitudes at the minima and maxima across the tasks (i.e. TST 1 at m1 versus TST 3 at

m1; TST 1 at m2 versus TST 3 at m2; TST 1 at m3 versus TST 3 at m5) were similar ($p>0.05$). Lastly, it was shown that the moment required in TST 3 was significantly higher ($p<0.05$) compared to TST 1 (i.e. the absolute maximum joint moment in TST 3 was higher than in TST 1) suggesting a greater external demand.

Table 5-5: Sagittal plane L4/L5 joint moments at the minima and maxima in TST levels 1 and 3.

	m1 (Nm)	***m2 (Nm)***	***m3 (Nm)***	***m4 (Nm)***	***m5 (Nm)***
TST 1 NAH	-95.6 (19.1)	-9.9 (35.2)	-93.7 (17.8)		
TST 1 AH	-90.6 (22.7)	-12.4 (32.6)	-90.4 (19.7)		
TST 3 NAH	-91.7 (20.4)	-12.4 (35.9)	-137.3 (24.9)	-16.3 (33.6)	-87.7 (18.4)
TST 3 AH	-90.5 (23.2)	-13.4 (42.5)	-136.9 (26.6)	-21.0 (30.7)	-86.5 (23.7)

Figure 5-2 illustrates the ensemble averaged sagittal plane L4/L5 external joint moment for all ten participants in TST levels 1 and 3. As shown in the figure, visually it can be seen that there are minimal differences between AH and NAH tasks.

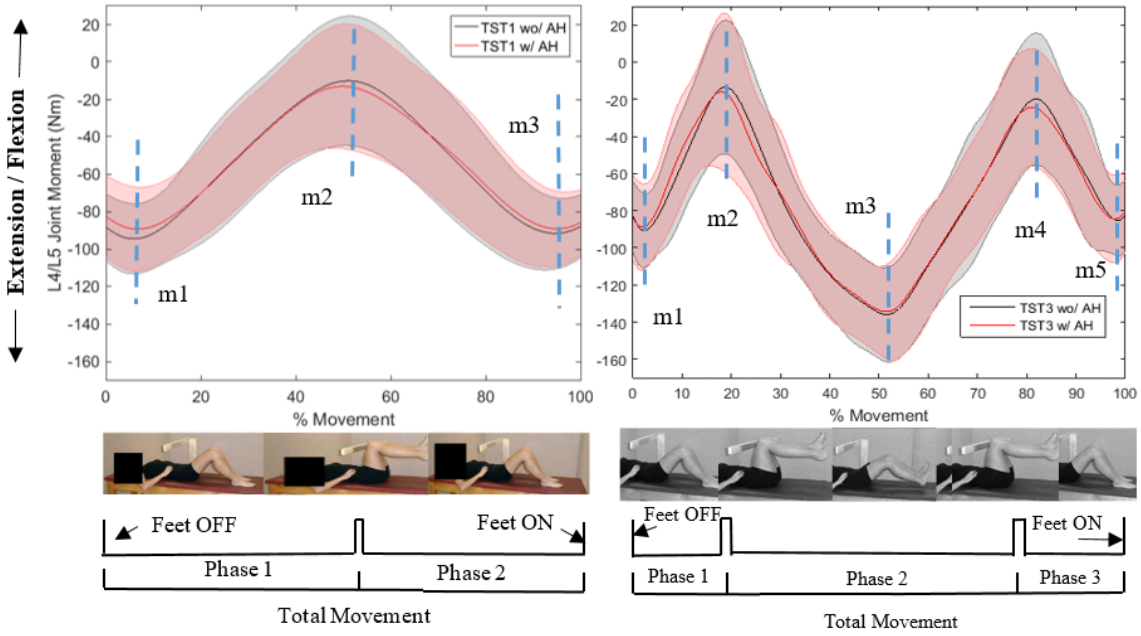

Figure 5-2: Ensemble averaged sagittal plane L4/L5 external joint moment for all the participants in TST 1 (left) and TST 3 (right).

5.2.7. Sagittal Plane L4/L5 Dynamic Joint Stiffness

The analysis of the L4/L5 joint stiffness waveforms revealed that the stiffness values at the instances where the change in L4/L5 joint angle (i.e. the denominator of Eq. 3-7) approached zero resulted in large spikes in the stiffness waveform which were outside the physiological range based on the literature (Bazrgari et al., 2012; Liebenson et al., 2009). In some cases, there was more than one region in a trial where these high values occurred. Therefore, there was a need to develop a procedure that does not include calculations of stiffness in these regions (non-dynamic) so that only the values that were representative of L4/L5 dynamic joint stiffness (dynamic motion occurred) and were within physiological limits remained in the waveforms.

To delete the values in these regions of the stiffness waveforms, the dynamic L4/L5 joint stiffness waveforms in the TST1 NAH task were visually inspected for all trials and for all participants (i.e. 30 trials in total), and a joint angle velocity that was reasonably representative of the $\dot{\theta}_{\text{critical}}$ was selected. The $\dot{\theta}_{\text{critical}}$ was the velocity at which the stiffness values increased above a physiological value resulting in large spike in the stiffness waveforms. Furthermore, the reason that only the TST 1 NAH task was investigated was to develop a criterion measure as a proof in principle which could be applied across all conditions for all participants.

As mentioned earlier, in some cases, there was more than one region in the stiffness waveform of a trial, and hence, more than one $\dot{\theta}_{\text{critical}}$ value had to be determined for a single trial. Hence, for each trial, the largest $\dot{\theta}_{\text{critical}}$ value was selected to ensure that the stiffness values associated with these regions would be deleted from the stiffness waveforms. Table 5-6 presents the $\dot{\theta}_{\text{critical}}$ value for each trial. In the next step, the maximum absolute joint angle velocity ($\dot{\theta}_{\text{max}}$) in the acceptable regions of each trail was calculated and shown in Table 5-6. Finally, for each trial, the $\dot{\theta}_{\text{critical}}$ value was divided by the $\dot{\theta}_{\text{max}}$ value, and then the result was multiplied by 100 to obtain $\%\dot{\theta}_{\text{critical}}$ value (see last column in Table 5-6).

As mentioned previously in section 3.11.3.1., two methods were used in order to identify these regions where the L4/L5 joint stiffness values changed to non-physiological spikes as the task was no longer dynamic. The methods were to select either a $\%\dot{\theta}_{\text{critical}}$ value or a $\dot{\theta}_{\text{critical}}$ value which would identify these regions in the stiffness waveforms. As illustrated in Table 5-6, the $\%\dot{\theta}_{\text{critical}}$ values ranged from 0.5 to 28.4% whereas the $\dot{\theta}_{\text{critical}}$

values ranged from 0.3 to 3.3 degree/second. Therefore, the $\dot{\theta}_{\text{critical}}$ values produced a lower range of scores than the $\%\dot{\theta}_{\text{critical}}$ values, and as a result, it was decided to select a single discrete $\dot{\theta}_{\text{critical}}$ that would reasonably delete the spikes in stiffness values from the waveforms.

For this study, it was decided that at the instances when the $\dot{\theta}$ values reached a value between -1 and +1 degree/second, the joint stiffness values at those instances were deleted. The selection of ±1 degree/second as the criterion measure is arbitrary and less than the mean of the $\dot{\theta}_{\text{critical}}$ which potentially results in including unacceptable stiffness values in the final stiffness waveforms. However, selecting a low criterion measure would most likely ensure that the correct stiffness values would not be discarded from data which would otherwise occur if a higher criterion measure was selected.

Table 5-6: The maximum ($\dot{\theta}$ max) and critical ($\dot{\theta}$ critical) L4/L5 joint angle velocities during TST 1 NAH.

Participant	**Trial #**	**$\dot{\theta}$ max (deg/sec)**	**$\dot{\theta}$ critical (deg/sec)**	**($\dot{\theta}$critical/ $\dot{\theta}$max) *100**
A	1	8.1	0.4	4.9
	2	11.2	0.8	7.1
	3	11.9	1.2	10.1
B	1	27.5	1.6	5.8
	2	23.4	2.7	11.5
	3	30.2	1.0	3.3
C	1	12.2	0.8	6.6
	2	7.4	0.7	9.5
	3	9.6	0.3	3.1
D	1	21.8	1.0	4.6
	2	24.2	1.8	7.4
	3	20.9	1.8	8.6
E	1	14.4	2.8	19.4
	2	9.9	1.5	15.2
	3	14.1	3.3	23.4
F	1	13.3	0.4	3.0
	2	19.2	0.4	2.1
	3	23.3	0.9	3.9
G	1	13.2	1.0	7.6
	2	11.1	2.6	23.4
	3	19.0	1.2	6.3
H	1	19.5	0.1	0.5
	2	21.2	0.7	3.3
	3	21.7	1.3	6.0
I	1	9.9	2.1	21.2
	2	9.5	2.7	28.4
	3	6.7	0.4	6.0
J	1	13.3	1.6	12.0
	2	15.2	2.1	13.8
	3	11.1	0.8	7.2
Mean (SD)		15.8 (6.3)	1.3 (0.9)	9.5 (7.2)

Table 5-7 depicts the sagittal plane L4/L5 joint stiffness in TST 1 and 3. Anderson-Darling normality test revealed that five out of 14 discrete variables were not normally distributed. Johnston transformation was used to transform the non-normally distributed variables prior to the statistical analysis. Statistical analysis of the foot-off to foot-on L4/L5 joint stiffness revealed significant main effect for condition ($p = 0.000$) but no significant main effect for task ($p = 0.452$) nor significant task and condition interaction effect ($p = 0.971$). Post-hoc analysis showed that AH led to significantly higher L4/L5 joint stiffness (16.5 (8.3) Nm/degree) compared to NAH tasks (13.3 (6.8) Nm/degree). Statistical analysis was also performed on each task separately. For TST 1, it was revealed that there are significant main effects for condition ($p = 0.000$) and phase ($p = 0.043$) but no significant condition and phase interaction effect ($p = 0.284$). Post-hoc analysis showed that AH led to higher L4/L5 joint stiffness in TST 1 (16.2 (7.9) Nm/degree versus 13.0 (6.5) Nm/degree). Also, the joint stiffness was higher in phase 1 compared to phase 2 (15.4 (7.3) Nm/degree versus 13.8 (7.5) Nm/degree). For TST 3, the statistical analysis determined significant main effects for condition ($p = 0.000$) and phase ($p = 0.006$) but no significant condition and phase interaction effect ($p = 0.203$). Post-hoc analysis showed that in TST 3, again AH resulted in higher L4/L5 joint stiffness compared to TST 3 NAH (16.4 (8.5) Nm/degree versus 13.3 (7.1) Nm/degree). Moreover, the L4/L5 joint stiffness was significantly higher in both phase 1 (15.5 (8.2) Nm/degree) and 2 (16.0 (8.6) Nm/degree) compared to phase 3 (12.9 (7.2) Nm/degree).

Table 5-7: Sagittal plane L4/L5 joint stiffness in TST levels 1 and 3.

		Foot-off to foot-on (Nm/deg)		***Phase 1 (Nm/deg)***		***Phase 2 (Nm/deg)***		***Phase 3 (Nm/deg)***	
Task		**NAH**	**AH**	**NAH**	**AH**	**NAH**	**AH**	**NAH**	**AH**
TST 1	**Mean (SD)**	13.0 (6.8)	16.2 (8.2)	13.4 (6.3)	17.4 (8.1)	12.6 (7.1)	15.0 (8.2)	N/A	N/A
TST 3	**Mean (SD)**	13.7 (7.1)	16.8 (8.9)	13.2 (7.0)	17.8 (9.0)	14.2 (7.2)	17.7 (9.9)	12.3 (8.1)	13.4 (6.5)
TST 1	**Mean (SD)**	14.6 (7.5)		15.4 (7.3)		13.8 (7.5)		N/A	
TST 3	**Mean (SD)**	15.2 (8.0)		15.5 (8.2)		16.0 (8.6)		12.9 (7.2)	
Cond.	**AH**	**Mean (SD)**	16.5 (8.3)						
	NAH	**Mean (SD)**	13.3 (6.8)						

Figures 5-3 and 5-4 illustrate the sagittal plane dynamic L4/L5 joint stiffness during TST 1 and 3 respectively. As shown in these figures, the major challenge in this study was the discontinuities in the dynamic L4/L5 joint stiffness due to the mathematical instability of Equation 3.7 (i.e. finite difference equation used to calculate dynamic L4/L5 joint stiffness). Using this equation, during the instances when the sagittal plane L4/L5 joint angle remained constant (e.g. during the beginning and end of each phase, and also during the full knee extension in phase 2 of TST 3), the change in L4/L5 joint angle (i.e. the denominator of Equation 3.7) approached zero. This led to abnormally high dynamic L4/L5 joint stiffness at those instances which was outside the physiological range and where the task was no longer dynamic. In other words, due to minimal change in L4/L5 joint angle at some instances during the tasks, there were situations where a non-zero denominator was being divided by a near zero numerator resulting in a stiffness value reaching infinity. This issue was dealt with by ignoring the dynamic L4/L5 joint stiffness

during the instances when the L4/L5 joint angle velocity reached a value of between -1 and +1 degree/second. The result of this process is depicted in Figs. 5-3 and 5-4.

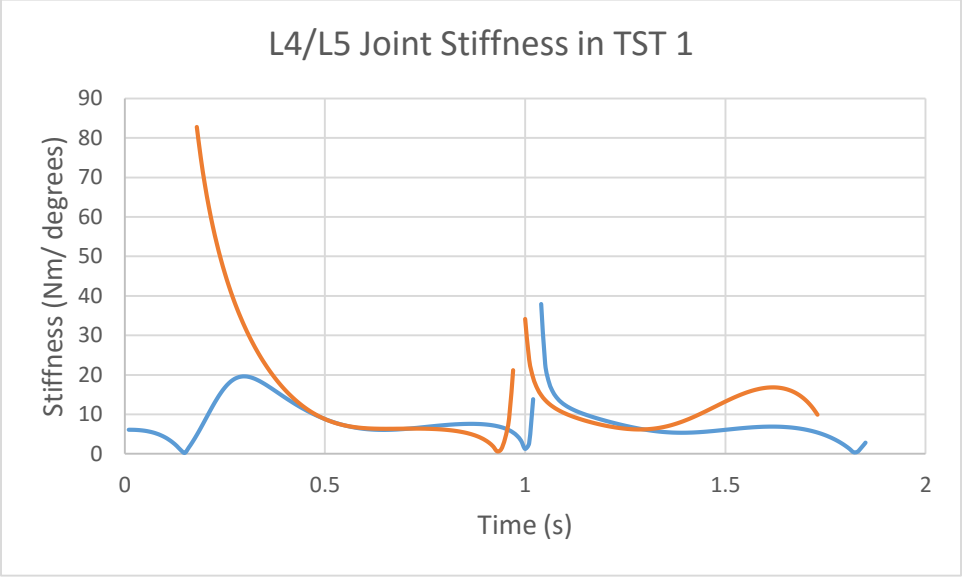

Figure 5-3: A representative (i.e. one individual and during one trial) sagittal plane dynamic L4/L5 joint stiffness in TST 1. Blue: NAH, orange: AH.

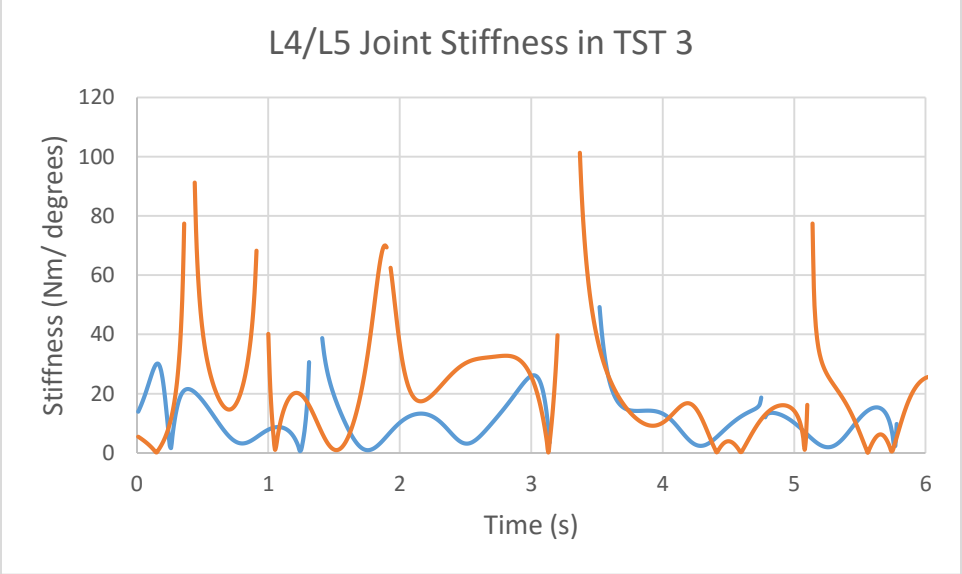

Figure 5-4: A representative (i.e. one individual and during one trial) sagittal plane dynamic L4/L5 joint stiffness in TST 3. Blue: NAH, orange: AH.

CHAPTER 6 DISCUSSION

6.1. OBJECTIVE 1

6.1.1. Objective 1.a

Given the importance of lumbar joint stiffness for maintaining dynamic stability, the first objective of this thesis was to develop equations to estimate dynamic L4/L5 joint stiffness in sagittal plane. In essence, this study attempted to explore the joint moment versus joint angle approach, which up until now, has only been used to study trunk passive stiffness and to calculate stiffness as a discrete measure (Beach et al., 2005; McGill et al., 1994; Parkinson et al., 2004). Hence in this study, three dimensional segment motion was captured using a passive marker motion capture system, inertial properties were determined from body segment markers locations and Dumas et al.'s anthropometric model (Dumas et al., 2007), and ground reaction forces were captured using a force platform from ten young and healthy male participants with no history of low back pain (LBP). Then, using these data, and linked segment model and inverse dynamics techniques, kinematic and kinetic models were developed to calculate sagittal plane joint angles and dynamic joint moments during controlled dynamic tasks (Robertson et al., 2013; Winter, 2009). One of the main reasons that the kinematic and kinetic model in this thesis was novel is that while the participants performed the leg movements in the TST tasks bilaterally, joint kinematics and kinetics were calculated bilaterally at both left and right knees and hips. This was done to account for the asymmetries in lower limbs segment mass and length between the right and left sides. Furthermore, while the majority of motion in the TST tasks were done by the lower

limbs, the bottom-up inverse dynamics model in this study incorporated the GRF acting on pelvis into the model by combining the GRF with the forces and moments at the hips.

6.1.2. Objective 1.b

One of the sub-objectives of Objective 1 of this thesis was to calculate body segment absolute angle and the relative L4/L5 joint angle, and then check their agreements with the values estimated by other angle measurement systems. The assessment of this sub-objective was important because the body segment absolute angles were used to compute the segments angular velocities and accelerations which were then utilized to calculate time rate of change of the body segments' angular momentum (Robertson et al., 2013). Similarly, since the relative L4/L5 joint angle was used to estimate the dynamic L4/L5 joint stiffness, it was crucial to make sure that the model in this study measured the L4/L5 joint angle correctly.

To check the agreement of the absolute angle measurements between a digital inclinometer and the developed kinematic model, a participant lay supine on a bed. Then, he was instructed to raise his lower limbs (i.e. shanks and thighs) in 10^{o} interval from 0^{o} to 60^{o}. The comparison of the limb segments' absolute angles between the inclinometer and the developed kinematic model revealed minimal root mean squared error (RMSE) between the two methods which ranged from 0.7 to 2.4 degrees. In other words, this study confirmed that there is a good agreement between the output of the inclinometer and the angle data of the developed kinematic model. Previous studies in the literature have compared inclinometers to other angle measurement systems during various movements. Overall, while the inclinometers have not been compared to motion capture systems, their output were shown to be correlated with other measurement tools, and are

highly reliable even during complex motions such as during cervical ROM (Malmstrom et al., 2003) and shoulder motion (Kolber et al., 2012; Kolber et al., 2011) measurements. Hence, the use of inclinometer to check the agreement of lower limbs absolute angle measurements between the inclinometer and the developed kinematic model was justified.

Objective 1-b of this thesis also checked the agreement of the L4/L5 joint angle measurements between an electrogoniometer and the developed kinematic model. In the Objective 1-b of this thesis, the participant was asked to perform a set of pure trunk flexion/extension movements with minimum movement in other planes. Hence, since the trunk's movement in other planes (i.e. internal/external rotation and abduction/adduction movements) were not present, error due to crosstalk from movement in other planes was negligible in this study. However, the biggest source of error in this study was the "kinematic crosstalk" phenomenon which is defined and caused by variability in the experimental determination of the joint axis (e.g. L4/L5 joint flexion axis). (Baudet et al., 2014; Böhm & Krämer, 2008; Piazza & Cavanagh, 2000). The developed kinematic model in this study defined the trunk and pelvis anatomical coordinate systems such that the lumbar spine flexion/extension axis would be located at the L4/L5 joint of spine (i.e. the lumbar spine flexion angle was calculated around the L4/L5 joint flexion axis). On the other hand, since the electrogoniometer's endblocks were placed on the lower lumbar spine and upper lumbar/lower thoracic spine, effectively the electrogoniometer was measuring the lumbar flexion angle around a different flexion axis (i.e. at a level above L4/L5 joint axis). It has been already shown that due to the inherent curvatures of the spinal column, different joint angles would be observed at different levels of the spinal

column during flexion/extension movement, hence non-rigidity of the spine represents one source of error. Furthermore, the "kinematic crosstalk" phenomenon due to axis misalignment represents another potential source of error. However, since the temporal patterns of the lumbar spine's relative joint angle were similar between the electrogoniometer and the developed kinematic model, and that the RMSE and difference in range of motion were relatively low (mean RMSE = 3.7^{o}, and mean difference in ROM = 4.4^{o}), it can be concluded that the joint angles measured by the two methods were in agreement. The variability in RMSE and "ROM difference" results (See Table 4-1) across the trials could be explained by potential over-flexion or extension of the strain gauge inside the connecting cable of the electrogoniometer during the flexion/extension movements. Another explanation could be the fact that the flexion/extension movement was not standardized between the experimental trials (i.e. the participant did not perform the experimental trials within a fixed ROM, and the movement varied in each trial) which also resulted in different joint angle temporal patterns between the trials.

6.1.3. Objective 1.c

In Objective 1-c of this thesis, this study attempted to investigate whether similar results would be obtained when calculating the L4/L5 joint moments using a quasi-static analysis instead of dynamic analysis during two different controlled dynamic tasks (i.e. TST levels 1 and 3). In quasi-static analysis, the inertial and acceleration terms were excluded from the dynamic equations of motion, and hence, the researchers' work would be simplified by not having to calculate inertial and acceleration terms. The results of this study revealed that the dynamic and quasi-static analyses yield sagittal plane L4/L5 joint moments with similar shape and pattern, but with different amplitudes. From the

temporal pattern of L4/L5 joint moments (see Fig. 4.6) it can be seen that at the initiation and end of each task, and also when the direction of motion changes (i.e. during 90^{o} hip flexion position in TST 1 and 3, and also at the full knee extension in TST 3), quasi-static analysis underestimates the moment magnitude. This is expected because during the initiation and end of the tasks, the increase and decrease in velocity creates acceleration and deceleration respectively. Furthermore, when the direction of the motion changes during the 90^{o} hip flexion position in TST 1 and 3 or at the full knee extension in TST 3, the decrease and then increase in velocity creates deceleration and acceleration. Thus, removing the acceleration and inertial terms in quasi-static analysis, leads to underestimation of the moment magnitude during the instances described above. These findings are in agreement with previous studies which found similar results (McGill & Norman, 1985; Wood & Hayes, 1974).

The comparison of dynamically and quasi-statically determined L4/L5 joint moments revealed that for TST 1 and 3, the error ranged from 10.8 to 34.6% with a mean of 18.1% for TST 1, and from 6.1 to 16.5% with a mean of 9.5% for TST 3. One reason that the %error was smaller in TST 3 was because of the added leg extension phase in TST 3 which made the RMS of the dynamic moment in TST 3 larger compared to TST 1. In other words, the denominator in the error calculation was larger for TST 3 which resulted in smaller %error values in TST 3 compared to TST 1. The second reason was the fact that the phase 2 of TST 3 was performed in four seconds whereas in TST 1, each phase was done in only one second. In other words, when a participant is required to complete a phase in only one second compared to four seconds, the amount of angular displacement in a given time frame will have to be greater for the shorter phase. This can also be seen

in Fig. 4.6 where the dynamically and quasi-statically determined joint moments during phase 2 of TST 3 almost lie on each other most of the time during this phase except at the full knee extension. As a result, the RMSE for TST 3 was found to be lower compared to TST 1 (see Table 4-2), and hence, the %error was smaller in TST 3 compared to TST 1.

This study also examined the difference in moment magnitude between the dynamically and quasi-statically determined joint moments around the minima and maxima (see Fig.4-6) where the difference between the moments is the greatest. For both TST 1 and 3, it was shown that the effect of quasi-static analysis was greater at the instances when change in motion direction occurred (see Table 4-3). This could be explained by the fact that at these instances, deceleration and then immediately after that, acceleration took place as a result of decrease and then increase in velocity. On the other hand, during the initiation and end of the tasks, only acceleration and deceleration existed respectively. Therefore, removing the acceleration and inertial terms at the instances when change in motion direction occurred, had greater effects on the moment magnitude.

Other studies in the literature similarly found significant differences between the dynamically and quasi-statically determined lumbar joint moments during various tasks such as in lifting (Freivalds et al., 1984; McGill & Norman, 1985; Wood & Hayes, 1974) and rising from chair (Hutchinson et al., 1994). The results of Objective 1-c and the studies in the literature showed that the quasi-static analysis underestimates joint moment magnitude during the maxima (i.e. during 90^{o} hip flexion position), and minima (i.e. at the start and end of the task, and also at the full knee extension in TST 3) as shown in Fig. 4-6.

Overall, it was shown that during the shorter duration task (i.e. TST 1) in which each phase was performed in only one second, the amount of error was higher compared to the longer task (i.e. TST 3). Therefore, to simplify data processing, researchers may use quasi-static analysis during the tasks in which the movements are done in a slow movement which would minimize acceleration or deceleration during the movement. Furthermore, the tasks should not include change in motion direction as in TST 1 and 3. As an example, it was shown that during the phase 2 of TST 3, since this phase was performed in four seconds in a slow movement rather than in just one second, the dynamically and quasi-statically determined moments were almost identical except during the full knee extension when the change in motion direction took place (i.e. knee was fully extended and came to a stop (deceleration), and then immediately after, the legs were brought toward 90^{o} hip flexion position (acceleration)).

6.1.4. Objective 1.d

Similar type of analysis was performed for the last sub-objective of Objective 1. In Objective 1-d, this thesis attempted to understand whether excluding the GRFs data from the dynamic equations of motion would still result in similar L4/L5 joint moments during two different controlled dynamic tasks (i.e. TST levels 1 and 3). In other words, this study aimed to investigate whether the effect of GRFs on the pelvis during TST levels 1 and 3 are negligible, and hence whether in future studies, the participants could simply lie on a patient bed instead of a force platform.

The results of this analysis revealed that the dynamic analysis of the L4/L5 joint moment both with and without GRFs resulted in moments with similar shape and pattern but with different amplitudes. As shown in Fig. 4-7, the joint moment magnitude became

overestimated at all instances during the tasks. The effect of GRF on the net joint moment was that when the legs were moved up toward 90^{o} hip flexion position, a flexion moment around the L4/L5 joint was created while the GRF produced an opposing extension moment around the same joint. Similarly, lowering the legs from the 90^{o} hip flexion position created an extension moment around the L4/L5 joint while the GRF generated an opposing flexion moment around the joint. In other words, the role of the GRF during the TST tasks was to produce an opposing torque to the one created by the leg movement around the L4/L5 joint. Hence, excluding the GRF data from the dynamic equations of motion would create an offset in joint moment amplitude as shown in Fig. 4-7.

One of the findings of Objective 1-d was that the GRF data had the highest effect during the initiation and end of the tasks as shown in Fig. 4-7. This finding was also depicted in Table 4-5 where the highest difference between the moments were during the beginning and end of the tasks. This was due to the fact that the participants exerted an extra force on the force plate during the initiation and end of the tasks by pushing on the force plate with their pelvis (i.e. anterior pelvic tilt). Furthermore, while the peak to peak moment difference (i.e. $|\Delta Dyn - \Delta Q|$) was smaller compared to the results of Objective 1-c, the errors ranged from 11.8 to 27.9% with a mean of 18.0% for TST 1, and from 5.2 to 22.1% with a mean of 13.4% for TST 3 (see Tables 4-4). To try and determine whether the error was systematic related to mass, a correlational analysis was performed. These results showed that for TST 1 and 3, there was no correlation between the participants' mass and their corresponding RMSE values which means that the offset (i.e. RMSE) between the two types of moment calculations (i.e. dynamic moment w/ and wo/ GRF) was not directly dependent on the participants' masses. In other words, the systematic

offset between the moments was potentially due to more than one factor, with one be possibly the fact that the body segments acceleration during the tasks were different across the participants.

Based on the preceding paragraph, for both TST 1 and 3, if a force plate is available, it is not suggested to neglect the GRF data in the joint moment calculations as the amount of error can reach up to 27.9% and 22.1% for TST 1 and 3 respectively. However, if a force plate is not readily available in the laboratory, the researchers can exclude the GRF data from the dynamic equations of motion to examine the general shape of the joint moment's temporal patterns. Moreover, since it was shown that exclusion of the GRF data overestimates the joint moment magnitude, the researchers may be able to approximate the true amplitudes of dynamic joint moments (i.e. moments with GRF). Nevertheless, the researchers need to be cautious about drawing any conclusions about the joint moment amplitudes.

6.2. OBJECTIVE 2

In Objective 2 which was the main objective of this study, ten healthy men with no history of LBP were recruited and instructed to perform two controlled dynamic tasks (i.e. TST levels 1 and 3) under two different conditions of with and without abdominal hollowing (AH). The two levels of TST exercises were performed to provide a dynamic challenge to lumbar spine so that the trunk musculature had to respond to constant changes in load (i.e. leg lifting, lowering, and extension) moments (Hanada et al., 2008; Hubley-Kozey & Vezina, 2002b; Moreside et al., 2014). Moreover, the AH was performed to change the active stiffness of the internal oblique muscles as per previous research (Davidson & Hubley-Kozey, 2005).

A key in this study was to ensure that the exercises for each condition were performed with a standardized timing (Moreside et al., 2014). Hence, the exercise timing for each of the modified TST 1 and 3 tasks were calculated and were compared between the conditions. In TST 1, the AH and NAH tasks produced almost identical timing with minimal variability (see Table 5-2). Similar findings were obtained for TST 3. These results indicate that AH had no effect on the timing of the exercises. Furthermore, it showed that this study did an excellent job of standardizing the timing for all exercises across all participants.

Furthermore, for each task, the EMG amplitudes of the IO muscles were compared between the conditions to determine whether participants performed the AH which would be reflected by an increase the IO muscles activation amplitudes prior to the initiation of the task. The results illustrated that in each task, and for both the right and left IO muscles, AH significantly increased the mean EMG amplitude. One of the interesting finding was the high variability in IO EMG amplitude during AH for all the participants which is in agreement with findings of other studies (Kim & Oh, 2015; Maeo, Takahashi, Takai, & Kanehisa, 2013; Tahan, Arab, Vaseghi, & Khademi, 2013; Urquhart et al., 2005). Furthermore, the mean EMG amplitudes for both the right and left IO muscles were in agreement with the findings of previous studies which analyzed similar tasks. (Hanada et al., 2008; Hubley-Kozey et al., 2009; Moreside et al., 2014). In these studies, the activation amplitude of the IO muscles at the foot-off ranged between 20 and 35 %MVIC which is comparable to the results obtained in this study (i.e. 25.5 to 31.6 % MVIC; see Table 5-3) considering different demographics of the study population and different exercise protocol.

This study also calculated the sagittal plane L4/L5 joint angle ROM, and then compared the results between the tasks and conditions. The findings of this study indicated that the AH condition significantly reduced the L4/L5 joint angle ROM. These differences were all less than two degrees except during the leg extension phase of TST 3 in which the difference was slightly higher at 2.3°. While the differences were small, in some cases the ROM was reduced by about 21% (e.g. in phase 1 of the TST tasks). In the literature, AH has been shown to reduce the anterior pelvic tilt by 7° (i.e. statistically significant) during prone hip extension (Oh et al., 2007), and by 1.8° (i.e. statistically significant) during controlled lifting task (Butler et al., 2007) with the latter being similar to the findings mentioned above. In contrast to these studies, Vera-Garcia et al. showed that AH is not an effective muscle activation technique in reducing the lumbar spine displacement (i.e. the lumbar spine displacement was reduced by less than 1°) during rapid perturbation of the trunk (Vera-Garcia et al., 2007). Hence, it appears that in some exercises, AH may not be an effective technique to minimize pelvic motion. In this thesis, as mentioned earlier, AH and the instruction to minimize pelvic motion resulted in significantly smaller L4/L5 joint angle ROM.

The sagittal plane L4/L5 joint angle ROM was also compared between the TST exercises. The results indicated that the ROM was about 3.3° higher in TST 3 compared to TST 1. This was expected as there was an added leg extension phase during TST 3, and hence, causing a larger ROM compared to TST 1 (see Table 5-4). In the literature, the difference in sagittal plane pelvic motion during exercises similar to the ones in this thesis was about 1.1° (Hanada et al., 2008) which was 2.2° lower compared to the findings of this thesis. The difference between the findings of Hanada et al. and this thesis could be due

to several reasons such as the use of different angle measurement systems. Hanada et al. recorded the pelvic angular motion with respect to a global reference (and not an anatomical reference system) by a Flock of Birds Motion Capture™ system. Furthermore, while the population of this thesis were between 20 and 30 years old, the participants in Hanada et al.'s study ranged from 65 to 75 years old. Lastly, the exercises in Hanada et al. included single leg lifting (and not bilateral leg lifting as in this thesis) tasks which might have resulted in the lower pelvic motion compared to this thesis.

Additionally, a separate statistical analysis on the sagittal plane L4/L5 joint angle ROM for TST 1 revealed that the ROM was significantly smaller in phase 1 compared to phase 2. This finding perhaps indicates that the effect of AH condition diminishes as the task progresses to phase 2, and hence, the L4/L5 joint angle ROM increases in the second phase of TST 1. For TST 3, it was shown that the ROM was significantly higher in phase 2 (i.e. leg extension phase) compared to both phase 1 and 3, but the difference in ROM between phase 1 and 3 was not statistically significant.

Using a linked segment model and inverse dynamics technique, the sagittal plane L4/L5 joint moments during TST 1 and 3 were calculated. In the literature, the sagittal plane L4/L5 joint moment magnitude during bent-leg raise, a task similar to TST 1 NAH, has been reported to be 82 (36) Nm (Axler & McGill, 1997). This value is comparable to the L4/L5 joint moment magnitude calculated in TST 1 NAH (i.e. 95.6 (19.1) Nm). Although Axler et al. used a similar population in their study (i.e. nine men with a mean age of 23.0 (4.8) years old), the bent-leg raise in Axler et al. was performed more slowly compared to the TST 1 in this thesis. Furthermore, Axel et al. estimated the L4/L5 joint moment around the hip joint, and not the L4/L5 joint of spine.

Comparison of the L4/L5 joint moments at the minima and maxim between the AH and NAH tasks revealed that AH had no effect on the joint moments during TST 1 and 3. This was expected as the participants performed each exercise under standardized timing and movement constraints resulting in similar body segments velocities and accelerations in both conditions. The comparison of the L4/L5 joint moments between the tasks showed no significant difference indicating that the participants were consistent in producing the same amount of moment across different tasks. Lastly, it was shown that the demand required in TST 3 was significantly higher compared to TST 1 indicating as expected that due to the added knee extension phase in TST 3, the trunk muscles were required to produce more torque around L4/L5 joint in TST 3 compared to TST 1.

Finally, the overall objective was to calculate the dynamic L4/L5 joint stiffness in the sagittal plane during TST 1 and 3. There were several challenges in this study regarding the calculation of a dynamic stiffness waveform and these will be discussed later. Despite these challenges, this study showed that the AH resulted in higher dynamic L4/L5 joint stiffness in the sagittal plane compared to the NAH tasks. These results indicate that in the AH tasks, the pelvic motion was minimized by providing higher active stiffness and hence, higher stability to the lumbar spine. Furthermore, while the difference in joint stiffness between the AH and NAH tasks was statistically significant, AH resulted in only 3.2 Nm higher stiffness as compared to the NAH tasks. This result could potentially be a clinically important finding as small increases in muscle activation and stiffness were associated with improved stability (Cholewicki & McGill, 1996; Cholewicki, Panjabi, & Khachatryan, 1997; McGill, Grenier, Kavcic, & Cholewicki,

2003) but this low level of stiffness may not increase lumbar compression, and hence would not be harmful for the lumbar spine of patients with LBP.

Separate statistical analyses were also performed on each of TST levels 1 and 3. The results revealed that the dynamic L4/L5 joint stiffness in the first phase of TST level 1 was significantly higher compared to the second phase. The higher stiffness in phase 1 of TST 1 resulted in less pelvic motion in this phase compared to phase 2. In TST level 3, it was shown that the dynamic L4/L5 joint stiffness was significantly higher in the first and second phase compared to the third phase. These results indicate that the trunk muscles provided higher active stiffness during the first and second phases of the task in order to minimize pelvic motion, and hence increase the lumbopelvic stability during motion. A possible explanation for the higher dynamic stiffness in the phase 1 of the TST tasks compared to the last phase could be the force of gravity which aided the movement during the last phase of the exercises whereas in phase 1, it had to be fought against in order to move the legs up toward the 90^{o} hip flexion position.

The major limitation of the stiffness model used in this thesis was the discontinuities in the stiffness values associated with the mathematical instability of the finite difference equation that was used to calculate joint stiffness. In other words, during the instances when the change in L4/L5 joint angle approached zero (i.e. the denominator of Eq. 3-7 became zero), the joint stiffness values became highly non-linear and very large which were not in agreement with the values reported in the literature. To tackle this issue, two different methods were proposed. The first method was to calculate the L4/L5 joint angle velocity (see Eq. 3-8), and then determine that at what percentage of maximum velocity the stiffness values start becoming non-linear and out of the expected physiological range

in each trial. The second method was to select a single discrete value of joint angle velocity and apply it to all the trials so that when the joint angle velocities reach a value lower than the specified number, the joint stiffness would not be calculated. This study investigated both methods and showed that the threshold determined using the first method is highly variable across the trials and participants. On the other hand, it was shown that a single discrete threshold of ±1 deg/second produces a more consistent result across the trials and participants (see Table 5-6). As a result, it was decided that for this study, at the instances where the L4/L5 joint angle velocity becomes a value in the range of ±1 deg/second, the joint stiffness at that instance was not calculated. Future research will need to be done to assess the accuracy of this method in addressing the discontinuities associated with the finite difference equation depicted in Eq. 3-7.

In the literature, researchers calculated the trunk stiffness during different exercises using different modeling techniques compared to this study. The stiffness values reported in the literature range from under 1.0 Nm/degree to about 420 Nm/degree (Bazrgari et al., 2012; Brown & McGill, 2009; Cholewicki et al., 1999; Cholewicki et al., 2010; Green et al., 2002; McGill et al., 1994; Muslim et al., 2013). One study in particular calculated the lumbar spine stiffness during a straight leg raise, a task similar to phase 1 of the TST exercises. The mean lumbar spine stiffness during straight leg raise while doing abdominal bracing was about 35 Nm/degree (Liebenson et al., 2009). Moreover, the abdominal bracing in this study produced mean EMG amplitudes of between 20 and 25 %MVIC for the IO muscles which are very close to the values reported in this thesis (see Table 5-3). The L4/L5 joint stiffness values reported in Table 5-7 are within the value

reported by Liebenson et al., hence providing confidence that the criterion used to remove the stiffness values outside the spine physiological range was reasonable.

CHAPTER 7 CONCLUSION

7.1. SUMMARY

This study developed equations to estimate sagittal plane dynamic L4/L5 joint stiffness. To do this, three dimensional segment motion was captured using a passive marker motion capture system, inertial properties were determined from body segment markers locations and Dumas et al.'s anthropometric model (Dumas et al., 2007), and ground reaction forces were captured using a force platform from ten young and healthy male participants with no history of low back pain (LBP). Using these data, and link segment model and inverse dynamic techniques, kinematic and kinematic models were developed to calculate dynamic L4/L5 joint angles and moments. Furthermore, by calculating the slope of L4/L5 dynamic joint moment versus joint angle using a finite difference equation, sagittal plane dynamic L4/L5 joint stiffness was determined. Due to the developmental nature of this study, and since the movements in the exercises were primarily done in the sagittal plane, this study only focused on motion in the sagittal plane.

In Objective 1-b of this thesis, limb segments absolute angles were calculated by an inclinometer and the thesis kinematic model, and their results were compared together. The findings of this study showed that due to very small RMSE values, the limb segments absolute angles calculated by the two methods were in a good agreement. Furthermore, the L4/L5 relative joint angle was calculated by an electrogoniometer and the thesis kinematic model, and their outputs were compared together. The two methods produced similar relative joint angle patterns with mean RMSE of 3.7^{o} and a mean difference in ROM of 4.4^{o}. The higher RMSE in the relative angle test compared to the

absolute angle test could be possibly because of slight over-flexion or extension and bending of the strain gauge during the exercises. Furthermore, the developed kinematic model in this study measured the relative L4/L5 joint angle around the flexion/extension L4/L5 joint axis whereas in the electrogoniometer the angles were measured around a higher lumbar spine joint axis.

In Objective 1-c, the sagittal plane L4/L5 joint moment was determined using a dynamic and quasi-static analyses during TST 1 and 3. While the general shape and pattern of the L4/L5 joint moment was similar between the dynamic and quasi-static moments, it was shown that the quasi-static analysis resulted in different joint moment magnitude at the minima and maxima. The results indicated that the quasi-static analysis resulted in mean error of 18.1% for TST 1, and 9.5% for TST 3. Furthermore, it was shown that at the minima and maxima of the joint moment waveforms, the quasi-static analysis underestimated the joint moment magnitude. Additionally, it was shown that quasi-static analysis had higher effect TST 1 (i.e. a task that was done in less amount of time compared to TST 3) in which the participants produced higher acceleration and deceleration in order to finish the movements during each phase in one second. Therefore, for the most accurate results, the researchers are suggested to use dynamic analysis instead of quasi-static analysis, for this high velocity dynamic task. However, if the goal is to simplify data processing by removing the inertial and acceleration terms from the equations of motion, the researchers should use exercises in which the motion is done slowly and over longer period of time to minimize the errors associated with the quasi-static analysis.

In Objective 1-d, the GRF data were excluded from the dynamic equations of motion, and its effect on the L4/L5 joint moment was examined. This analysis was done to understand whether it is necessary to utilize a force plate to accurately estimate the L4/L5 joint moments during the TST tasks. In this study, it was shown that the exclusion of the GRF data had minimal effect on the general shape and pattern of the L4/L5 joint moment waveform, but it overestimated the joint moment magnitude across the tasks. The results indicated that the exclusion of the GRF data from the dynamic joint moments resulted in mean error of 18.0% for TST 1, and 13.4% for TST 3. Moreover, it was shown that the exclusion of the GRF data had much less effect on the peak to peak moment range as compared to the quasi-static analysis. In other words, the results of Objective-1d illustrated a systematic offset in L4/L5 joint moments when the GRF data was excluded from the dynamic equations of motion. To see if there is a correlation between this systematic offset and the participants' mass, a correlation analysis was performed in which a linear regression line was fitted to the RMSE versus mass data. In both tasks, there was no correlation between the participants' masses and their corresponding RMSE indicating that the systematic offset caused by the exclusion of the GRF data is not directly dependent on the participants' mass. Overall, for the accurate estimates of the dynamic L4/L5 joint moments during the TST tasks, it is suggested to utilize a force plate to record the GRF acting on the pelvis. However, if a force plate is not readily available in the laboratory, the results of this sub-objective can be useful for the researchers by showing that the removal of the GRF data from the equations of motion, the L4/L5 joint moment magnitude is overestimated during the TST tasks.

In Objective 2, it was shown that AH had no effect on exercise timing (i.e. the time it took the participants to complete each phase and the entire tasks) in either of TST 1 and 3 tasks. Additionally, it was shown that this study did an excellent job of standardizing the exercise timing for all the participants as they finished each phase and the entire tasks according to instructions given by the researchers with minimal variation between the trials.

The findings of this objective indicated that AH resulted in significantly higher IO muscles activation amplitudes prior to the start of the TST tasks. Furthermore, it was shown that AH resulted in significantly less L4/L5 joint angle ROM compared to the NAH tasks. Additionally, due to the added knee extension phase in TST 3, the ROM was found to be larger in this task compared to TST 1.

Comparison of the L4/L5 joint moments at the minima and maxima revealed no significant differences between the AH and NAH tasks. Moreover, there was no difference in L4/L5 joint moments between TST 1 and 3 at the minima (i.e. at the initiation and end of the tasks) and maxima (i.e. at the 90^{o} hip flexion position). Also, by analyzing the highest L4/L5 joint moment magnitudes in each task, it was found that TST 3 is more demanding than TST 1.

Finally, while it was shown that the dynamic L4/L5 joint stiffness was not different between TST 1 and 3, it was found to be significantly different between the AH and NAH tasks. Additionally, it was found that the L4/L5 joint stiffness in TST 1 was higher in the first phase compared to the second phase. In TST 3, the stiffness was shown to be higher in first and second phases compared to the third phase.

7.2. IMPLICATIONS

Up until now in the literature, the researchers have estimated the spinal joint stiffness using discrete measures meaning that they have calculated stiffness over an entire dynamic task or at a specific instance of time, and then reported stiffness as a single discrete number.

This study attempted to address this gap in the literature by proposing a model that would produce dynamic profiles of L4/L5 joint stiffness. However, the discontinuities in the joint stiffness waveforms proved to be a major difficulty in calculating dynamic joint stiffness. Hence, to be able to compare joint stiffness between different tasks and conditions, this study developed a method to remove the discontinuities from the stiffness waveforms, and calculated the average stiffness across the tasks and phases.

A key finding of this study was that the L4/L5 joint moments were not altered by the AH condition. However, this study determined that the AH condition in which the IO muscles were selectively activated and participants were asked to minimize pelvic motion did indeed reduce pelvic motion and hence increase the dynamic L4/L5 joint stiffness during TST tasks. The specific role of the AH maneuver was in part supported by previous studies which showed that AH significantly reduced pelvic motion during different tasks (Butler et al., 2007; Oh et al., 2007) and that it increased lumbar spine stiffness and stability by reducing the sacroiliac joint laxity (Richardson et al., 2002).

7.3. LIMITATIONS

The limitations of this study are as follows:

- When developing the kinematic and kinetic model in this study, the body segments were assumed as rigid bodies. Biomechanists normally make this assumption when using the inverse dynamics approach to calculate joint forces and moments (Robertson et al., 2013).
- Due to the nature of the experimental tasks (i.e. TST levels 1 and 3) in this thesis, during the instances when the change in sagittal plane L4/L5 joint angle was minimal (i.e. at the beginning and end of each phase, and also during the full knee extension in TST level 3), the joint stiffness equation produced abnormally large stiffness values. To overcome this, an algorithm was developed to discard the L4/L5 joint stiffness values when change in L4/L5 joint angle was minimal (i.e. the L4/L5 joint angle velocity was between -1 and +1 degrees per second).
- Due to the developmental nature of this study, and since the movements in the exercises were primarily done in the sagittal plane, this study only focused on motion in the sagittal plane. In other words, the L4/L5 joint angle, moments and stiffness were not studied in the frontal and transverse planes.

7.4. FUTURE RESEARCH

This study attempted to develop equations to calculate dynamic joint stiffness profiles at the L4/L5 joint of spine. However, the discontinuities in the joint stiffness waveforms introduced difficulties in achieving this goal. Therefore, future studies need to be done to address this issue so that the researchers will be able to obtain dynamic joint stiffness profiles during dynamic tasks.

Furthermore, this study only focused on the L4/L5 joint biomechanics in the sagittal plane. Hence, future studies will need to be done to investigate the L4/L5 joint angle, moment, and stiffness in the frontal and transverse planes during the TST tasks.

7.5. CONCLUSION

In conclusion, the results of this study confirmed the first hypothesis by showing that the AH condition led to different sagittal plane dynamic L4/L5 joint stiffness in TST levels 1 and 3. The decrease in L4/L5 angle can explain this finding as there were no differences in joint moment measures between conditions. As for the second hypothesis, the findings of this study showed that the L4/L5 joint moments at the minima (i.e. at the initiation and end of the tasks) and maxima (i.e. at the 90^{o} hip flexion position) were not different between TST 1 and TST 3 however that the demand of the task in TST 3 was higher compared to TST 1. Furthermore, no significant difference in L4/L5 joint stiffness between TST 1 and 3 was found.

This is the first study that that the authors know of that attempted to estimate dynamic L4/L5 joint stiffness waveforms during controlled dynamic tasks. Hence, this thesis is hoping that it has provided the ground work for researchers to estimate the spinal joint stiffness over the dynamic portions of the task rather than just reporting discrete measures for the stiffness during dynamic tasks.

BIBLIOGRAPHY

Adams, P. S., & Keyserling, W. M. (1993). Three methods for measuring range of motion while wearing protective clothing: A comparative study. *International Journal of Industrial Ergonomics, 12*(3), 177-191. doi:http://dx.doi.org/10.1016/0169-8141(93)90024-8

Anders, C., Brose, G., Hofmann, G. O., & Scholle, H. C. (2007). Gender specific activation patterns of trunk muscles during whole body tilt. *Eur J Appl Physiol, 101*(2), 195-205. doi:10.1007/s00421-007-0490-z

Anders, C., Wagner, H., Puta, C., Grassme, R., & Scholle, H. C. (2009). Healthy humans use sex-specific co-ordination patterns of trunk muscles during gait. *Eur J Appl Physiol, 105*(4), 585-594. doi:10.1007/s00421-008-0938-9

APTA. (2012). Low Back Pain by the Numbers (Infographic). Retrieved from http://www.moveforwardpt.com/LowBackPain/Infographic/Default.aspx

ASDA. (2009). Back Pain Stats. Retrieved from http://www.americanspinal.com/back-pain-stats.html

Asher, A. (2013). Back Pain Prevalence and Statistics. Retrieved from http://backandneck.about.com/od/medication/a/Back-Pain-Prevalence-And-Statistics.htm

Axler, C. T., & McGill, S. M. (1997). Low back loads over a variety of abdominal exercises: searching for the safest abdominal challenge. *Med Sci Sports Exerc, 29*(6), 804-811.

Baudet, A., Morisset, C., d'Athis, P., Maillefert, J. F., Casillas, J. M., Ornetti, P., & Laroche, D. (2014). Cross-talk correction method for knee kinematics in gait analysis using principal component analysis (PCA): a new proposal. *PLoS One, 9*(7), e102098. doi:10.1371/journal.pone.0102098

Bazrgari, B., Nussbaum, M. A., & Madigan, M. L. (2012). Estimation of trunk mechanical properties using system identification: effects of experimental setup and modelling assumptions. *Comput Methods Biomech Biomed Engin, 15*(9), 1001-1009. doi:10.1080/10255842.2011.570340

Beach, T. A., Parkinson, R. J., Stothart, J. P., & Callaghan, J. P. (2005). Effects of prolonged sitting on the passive flexion stiffness of the in vivo lumbar spine. *Spine J, 5*(2), 145-154. doi:10.1016/j.spinee.2004.07.036

Bergmark, A. (1989). Stability of the lumbar spine. A study in mechanical engineering. *60*(230), 1-58.

Böhm, H., & Krämer, C. (2008). Optimization of Human Motion Exemplified with Handbiking by Means of Motion Analysis and Musculoskeletal Models. In B. Rosenhahn, R. Klette, & D. Metaxas (Eds.), *Human Motion: Understanding, Modelling, Capture, and Animation* (pp. 417-434). Dordrecht: Springer Netherlands.

Borenstein, D. G., & Callin, A. (2012). Low back pain. Retrieved from http://site.ebrary.com/id/10541135

Boyd, B. S. (2012). Measurement properties of a hand-held inclinometer during straight leg raise neurodynamic testing. *Physiotherapy, 98*(2), 174-179. doi:10.1016/j.physio.2011.04.352

Briggs, A., & Buchbinder, R. (2008). Back Pain: A National Health Priority Area in Australia? Retrieved from https://www.mja.com.au/journal/2009/190/9/back-pain-national-health-priority-area-australia#6

Bronner, S., Agraharasamakulam, S., & Ojofeitimi, S. (2010). Reliability and validity of electrogoniometry measurement of lower extremity movement. *J Med Eng Technol, 34*(3), 232-242. doi:10.3109/03091900903580512

Brown, S. H., & McGill, S. M. (2009). The intrinsic stiffness of the in vivo lumbar spine in response to quick releases: implications for reflexive requirements. *J Electromyogr Kinesiol, 19*(5), 727-736. doi:10.1016/j.jelekin.2008.04.009

Butler, H. L., Hubley-Kozey, C. L., & Kozey, J. W. (2007). Changes in trunk muscle activation and lumbar-pelvic position associated with abdominal hollowing and reach during a simulated manual material handling task. *Ergonomics, 50*(3), 410-425. doi:10.1080/00140130601128081

Butler, H. L., Hubley-Kozey, C. L., & Kozey, J. W. (2009). Electromyographic assessment of trunk muscle activation amplitudes during a simulated lifting task using pattern recognition techniques. *J Electromyogr Kinesiol, 19*(6), e505-512. doi:10.1016/j.jelekin.2008.09.010

Butler, H. L., Hubley-Kozey, C. L., & Kozey, J. W. (2013). Changes in electromyographic activity of trunk muscles within the sub-acute phase for individuals deemed recovered from a low back injury. *J Electromyogr Kinesiol, 23*(2), 369-377. doi:10.1016/j.jelekin.2012.10.012

Butler, H. L., Newell, R., Hubley-Kozey, C. L., & Kozey, J. W. (2009). The interpretation of abdominal wall muscle recruitment strategies change when the electrocardiogram (ECG) is removed from the electromyogram (EMG). *J Electromyogr Kinesiol, 19*(2), e102-113. doi:10.1016/j.jelekin.2007.10.004

Chang, K. C. (2008). A Physiatrist's Approach to Low Back Pain. Retrieved from http://www.sdapa.net/conferences/fall2008/presentations/chang-lowbackpain.pdf

Cholewicki, J., Juluru, K., Radebold, A., Panjabi, M. M., & McGill, S. M. (1999). Lumbar spine stability can be augmented with an abdominal belt and/or increased intra-abdominal pressure. *Eur Spine J, 8*(5), 388-395.

Cholewicki, J., Lee, A. S., Peter Reeves, N., & Morrisette, D. C. (2010). Comparison of trunk stiffness provided by different design characteristics of lumbosacral orthoses. *Clin Biomech (Bristol, Avon), 25*(2), 110-114. doi:10.1016/j.clinbiomech.2009.10.010

Cholewicki, J., & McGill, S. M. (1996). Mechanical stability of the in vivo lumbar spine: implications for injury and chronic low back pain. *Clinical biomechanics (Bristol, Avon), 11*(1), 1-15. Retrieved from http://www.ncbi.nlm.nih.gov/pubmed/11415593

Cholewicki, J., McGill, S. M., & Norman, R. W. (1991). Lumbar spine loads during the lifting of extremely heavy weights. *Med Sci Sports Exerc, 23*(10), 1179-1186.

Cholewicki, J., Panjabi, M. M., & Khachatryan, A. (1997). Stabilizing function of trunk flexor-extensor muscles around a neutral spine posture. *Spine (Phila Pa 1976), 22*(19), 2207-2212.

Clapis, P. A., Davis, S. M., & Davis, R. O. (2008). Reliability of inclinometer and goniometric measurements of hip extension flexibility using the modified Thomas test. *Physiother Theory Pract, 24*(2), 135-141. doi:10.1080/09593980701378256

Coolidge, F. L., & Coolidge, F. L. (2012). *Statistics: A Gentle Introduction: A Gentle Introduction*: SAGE Publications.

Crisco, J. J., Panjabi, M. M., Yamamoto, I., & Oxland, T. R. (1992). Euler stability of the human ligamentous lumbar spine. Part II: Experiment. *Clin Biomech (Bristol, Avon), 7*(1), 27-32. doi:10.1016/0268-0033(92)90004-n

Dahn, T. (2012). *The Effect of Sex and Menstrual Cycle Phase on Neuromuscular Control of Trunk Musculature.* (M.A.Sc.), Dalhousie University, Halifax, Nova Scotia, Canada.

Davidson, K. L., & Hubley-Kozey, C. L. (2005). Trunk muscle responses to demands of an exercise progression to improve dynamic spinal stability. *Arch Phys Med Rehabil, 86*(2), 216-223. doi:10.1016/j.apmr.2004.04.029

Dumas, R., Cheze, L., & Verriest, J. P. (2007). Adjustments to McConville et al. and Young et al. body segment inertial parameters. *J Biomech, 40*(3), 543-553. doi:10.1016/j.jbiomech.2006.02.013

Duthey, B. (2013). Priority Medicines for Europe and the World "A Public Health Approach to Innovation". Retrieved from www.who.int/medicines/areas/priority_medicines/BP6_24LBP.pdf

Freivalds, A., Chaffin, D. B., Garg, A., & Lee, K. S. (1984). A dynamic biomechanical evaluation of lifting maximum acceptable loads. *J Biomech, 17*(4), 251-262.

Granata, K. P., Orishimo, K. F., & Sanford, A. H. (2001). Trunk muscle coactivation in preparation for sudden load. *J Electromyogr Kinesiol, 11*(4), 247-254. doi:10.1016/S1050-6411(01)00003-7

Granata, K. P., & Rogers, E. (2007). Torso flexion modulates stiffness and reflex response. *J Electromyogr Kinesiol, 17*(4), 384-392. doi:10.1016/j.jelekin.2006.10.010

Green, J. P., Grenier, S. G., & McGill, S. M. (2002). Low-back stiffness is altered with warm-up and bench rest: implications for athletes. *Med Sci Sports Exerc, 34*(7), 1076-1081.

Grenier, S. G., & McGill, S. M. (2007). Quantification of lumbar stability by using 2 different abdominal activation strategies. *Arch Phys Med Rehabil, 88*(1), 54-62. doi:10.1016/j.apmr.2006.10.014

Grood, E. S., & Suntay, W. J. (1983). A joint coordinate system for the clinical description of three-dimensional motions: application to the knee. *J Biomech Eng, 105*(2), 136-144.

Hanada, E. Y., Hubley-Kozey, C. L., McKeon, M. D., & Gordon, S. A. (2008). The feasibility of measuring the activation of the trunk muscles in healthy older adults during trunk stability exercises. *BMC Geriatr, 8*, 33. doi:10.1186/1471-2318-8-33

Herrero, P., Carrera, P., Garcia, E., Gomez-Trullen, E. M., & Olivan-Blazquez, B. (2011). Reliability of goniometric measurements in children with cerebral palsy: a

comparative analysis of universal goniometer and electronic inclinometer. A pilot study. *BMC Musculoskelet Disord, 12*, 155. doi:10.1186/1471-2474-12-155

Hodges, P. W., & Richardson, C. A. (1999). Altered trunk muscle recruitment in people with low back pain with upper limb movement at different speeds. *Arch Phys Med Rehabil, 80*(9), 1005-1012.

Hubley-Kozey, C. L., Butler, H. L., & Kozey, J. W. (2012). Activation amplitude and temporal synchrony among back extensor and abdominal muscles during a controlled transfer task: comparison of men and women. *Hum Mov Sci, 31*(4), 863-879. doi:10.1016/j.humov.2011.08.010

Hubley-Kozey, C. L., Hanada, E. Y., Gordon, S., Kozey, J., & McKeon, M. (2009). Differences in abdominal muscle activation patterns of younger and older adults performing an asymmetric leg-loading task. *Pm r, 1*(11), 1004-1013. doi:10.1016/j.pmrj.2009.09.018

Hubley-Kozey, C. L., Moreside, J. M., & Quirk, D. A. (2014). Trunk neuromuscular pattern alterations during a controlled functional task in a low back injured group deemed ready to resume regular activities. *Work, 47*(1), 87-100. doi:10.3233/WOR-131689

Hubley-Kozey, C. L., & Vezina, M. J. (2002a). Differentiating temporal electromyographic waveforms between those with chronic low back pain and healthy controls. *Clin Biomech (Bristol, Avon), 17*(9-10), 621-629.

Hubley-Kozey, C. L., & Vezina, M. J. (2002b). Muscle activation during exercises to improve trunk stability in men with low back pain. *Arch Phys Med Rehabil, 83*(8), 1100-1108.

Hutchinson, E. B., Riley, P. O., & Krebs, D. E. (1994). A dynamic analysis of the joint forces and torques during rising from a chair. *IEEE Transactions on Rehabilitation Engineering, 2*(2), 49-56. doi:10.1109/86.313146

Izzo, R., Guarnieri, G., Guglielmi, G., & Muto, M. (2013). Biomechanics of the spine. Part I: spinal stability. *Eur J Radiol, 82*(1), 118-126. doi:10.1016/j.ejrad.2012.07.024

Juker, D., McGill, S. M., Kropf, P., & Steffen, T. (1998). Quantitative intramuscular myoelectric activity of lumbar portions of psoas and the abdominal wall during a wide variety of tasks. *Med Sci Sports Exerc, 30*(2), 301-310.

Kavcic, N., Grenier, S., & McGill, S. M. (2004). Quantifying tissue loads and spine stability while performing commonly prescribed low back stabilization exercises. *Spine (Phila Pa 1976), 29*(20), 2319-2329. Retrieved from http://www.ncbi.nlm.nih.gov/pubmed/15480148

Kim, M.-H., & Oh, J.-S. (2015). Effects of performing an abdominal hollowing exercise on trunk muscle activity during curl-up exercise on an unstable surface. *Journal of Physical Therapy Science, 27*(2), 501-503. doi:10.1589/jpts.27.501

Kolber, M. J., Fuller, C., Marshall, J., Wright, A., & Hanney, W. J. (2012). The reliability and concurrent validity of scapular plane shoulder elevation measurements using a digital inclinometer and goniometer. *Physiother Theory Pract, 28*(2), 161-168. doi:10.3109/09593985.2011.574203

Kolber, M. J., Vega, F., Widmayer, K., & Cheng, M. S. (2011). The reliability and minimal detectable change of shoulder mobility measurements using a digital

inclinometer. *Physiother Theory Pract, 27*(2), 176-184. doi:10.3109/09593985.2010.481011

Krabbe, B., Farkas, R., & Baumann, W. (1997). Influence of inertia on intersegment moments of the lower extremity joints. *J Biomech, 30*(5), 517-519.

Lamoth, C. J. C., Meijer, O. G., Daffertshofer, A., Wuisman, P. I. J. M., & Beek, P. J. (2006). Effects of chronic low back pain on trunk coordination and back muscle activity during walking: changes in motor control. *European Spine Journal, 15*(1), 23-40. doi:10.1007/s00586-004-0825-y

Lariviere, C., Gagnon, D., & Loisel, P. (2000). The comparison of trunk muscles EMG activation between subjects with and without chronic low back pain during flexion-extension and lateral bending tasks. *J Electromyogr Kinesiol, 10*(2), 79-91.

Liebenson, C., Karpowicz, A. M., Brown, S. H., Howarth, S. J., & McGill, S. M. (2009). The active straight leg raise test and lumbar spine stability. *Pm r, 1*(6), 530-535. doi:10.1016/j.pmrj.2009.03.007

Maeo, S., Takahashi, T., Takai, Y., & Kanehisa, H. (2013). Trunk Muscle Activities During Abdominal Bracing: Comparison Among Muscles and Exercises. *J Sports Sci Med, 12*(3), 467-474.

Malmstrom, E. M., Karlberg, M., Melander, A., & Magnusson, M. (2003). Zebris versus Myrin: a comparative study between a three-dimensional ultrasound movement analysis and an inclinometer/compass method: intradevice reliability, concurrent validity, intertester comparison, intratester reliability, and intraindividual variability. *Spine (Phila Pa 1976), 28*(21), E433-440. doi:10.1097/01.brs.0000090840.45802.d4

Marras, W. S., Davis, K. G., & Jorgensen, M. (2003). Gender influences on spine loads during complex lifting. *Spine J, 3*(2), 93-99. doi:10.1016/S1529-9430(02)00570-3

McConville, J. T., Churchill, T. D., Kaleps, I., Clauser, C. E., & Cuzzi, J. (1980). *Anthropometric relationships of body and body segment moments of inertia*. Retrieved from https://books.google.ca/books?id=ax_4y6y5_0YC

McGill, S. M. (2001). Low back stability: from formal description to issues for performance and rehabilitation. *Exerc Sport Sci Rev, 29*(1), 26-31.

McGill, S. M. (2004). Linking latest knowledge of injury mechanisms and spine function to the prevention of low back disorders. *J Electromyogr Kinesiol, 14*(1), 43-47. doi:10.1016/j.jelekin.2003.09.012

McGill, S. M. (2007). *Low Back Disorders: Evidence-based Prevention and Rehabilitation*: Human Kinetics.

McGill, S. M., Grenier, S., Kavcic, N., & Cholewicki, J. (2003). Coordination of muscle activity to assure stability of the lumbar spine. *J Electromyogr Kinesiol, 13*(4), 353-359.

McGill, S. M., & Norman, R. W. (1985). Dynamically and statically determined low back moments during lifting. *J Biomech, 18*(12), 877-885.

McGill, S. M., & Norman, R. W. (1986). Partitioning of the L4-L5 dynamic moment into disc, ligamentous, and muscular components during lifting. *Spine (Phila Pa 1976), 11*(7), 666-678.

McGill, S. M., Seguin, J., & Bennett, G. (1994). Passive stiffness of the lumbar torso in flexion, extension, lateral bending, and axial rotation. Effect of belt wearing and breath holding. *Spine (Phila Pa 1976), 19*(6), 696-704.

Moreside, J. M., Quirk, D. A., & Hubley-Kozey, C. L. (2014). Temporal patterns of the trunk muscles remain altered in a low back-injured population despite subjective reports of recovery. *Arch Phys Med Rehabil, 95*(4), 686-698. doi:10.1016/j.apmr.2013.10.003

Moriguchi, C., Sato, T., & Gil Coury, H. (2007). Ankle movements during normal gait evaluated by flexible electrogoniometer. *Brazilian Journal of Physical Therapy, 11*, 205-211. Retrieved from http://www.scielo.br/scielo.php?script=sci_arttext&pid=S1413-35552007000300006&nrm=iso

Moslehi, A. H., & Hubley-Kozey, C. L. (2014). *Developing Discrete Measures from Normalized EMG which Correlate with PC Scores.* Paper presented at the World Congress of Biomechanics, Boston, MA, USA.

Muslim, K., Bazrgari, B., Hendershot, B., Toosizadeh, N., Nussbaum, M. A., & Madigan, M. L. (2013). Disturbance and recovery of trunk mechanical and neuromuscular behaviors following repeated static trunk flexion: influences of duration and duty cycle on creep-induced effects. *Appl Ergon, 44*(4), 643-651. doi:10.1016/j.apergo.2012.12.004

Myer, K. (2009). BIOMECHANICS OF HUMAN MOVEMENTBiomedical Engineering and Design Handbook, Volume 1: McGraw Hill Professional, Access Engineering. Retrieved from http://accessengineeringlibrary.com/browse/biomedical-engineering-and-design-handbook-volume-1/p2001855b9970125001. Retrieved from

http://accessengineeringlibrary.com/browse/biomedical-engineering-and-design-handbook-volume-1/p2001855b9970125001

Ng, J. K., Kippers, V., & Richardson, C. A. (1998). Muscle fibre orientation of abdominal muscles and suggested surface EMG electrode positions. *Electromyogr Clin Neurophysiol, 38*(1), 51-58.

Ng, J. K., Parnianpour, M., Kippers, V., & Richardson, C. A. (2003). Reliability of electromyographic and torque measures during isometric axial rotation exertions of the trunk. *Clin Neurophysiol, 114*(12), 2355-2361.

Oh, J. S., Cynn, H. S., Won, J. H., Kwon, O. Y., & Yi, C. H. (2007). Effects of performing an abdominal drawing-in maneuver during prone hip extension exercises on hip and back extensor muscle activity and amount of anterior pelvic tilt. *J Orthop Sports Phys Ther, 37*(6), 320-324. doi:10.2519/jospt.2007.2435

Olney, S. J., & Winter, D. A. (1985). Predictions of knee and ankle moments of force in walking from EMG and kinematic data. *J Biomech, 18*(1), 9-20.

Panjabi, M. M. (1992). The stabilizing system of the spine. Part I. Function, dysfunction, adaptation, and enhancement. *Journal of spinal disorders, 5*(4), 383-389; discussion 397.

Panjabi, M. M. (2003). Clinical spinal instability and low back pain. *J Electromyogr Kinesiol, 13*(4), 371-379.

Panjabi, M. M. (2006). A hypothesis of chronic back pain: ligament subfailure injuries lead to muscle control dysfunction. *European spine journal : official publication of the European Spine Society, the European Spinal Deformity Society, and the European*

Section of the Cervical Spine Research Society, 15(5), 668-676. doi:10.1007/s00586-005-0925-3

Panjabi, M. M., Abumi, K., Duranceau, J., & Oxland, T. (1989). Spinal stability and intersegmental muscle forces. A biomechanical model. *Spine, 14*(2), 194-200.

Parkinson, R. J., Beach, T. A., & Callaghan, J. P. (2004). The time-varying response of the in vivo lumbar spine to dynamic repetitive flexion. *Clin Biomech (Bristol, Avon), 19*(4), 330-336. doi:10.1016/j.clinbiomech.2004.01.002

Piazza, S. J., & Cavanagh, P. R. (2000). Measurement of the screw-home motion of the knee is sensitive to errors in axis alignment. *J Biomech, 33*(8), 1029-1034.

Quirk, D. A., & Hubley-Kozey, C. L. (2014). Age-related changes in trunk neuromuscular activation patterns during a controlled functional transfer task include amplitude and temporal synergies. *Hum Mov Sci, 38*, 262-280. doi:10.1016/j.humov.2014.08.013

Reed, M., Manary, M. A., & Schneider, L. W. (1999). *Methods for measuring and representing automobile occupant posture* (0148-7191). Retrieved from

Reeves, N. P., Narendra, K. S., & Cholewicki, J. (2007). Spine stability: the six blind men and the elephant. *Clin Biomech (Bristol, Avon), 22*(3), 266-274. doi:10.1016/j.clinbiomech.2006.11.011

Richardson, C. A. (1999). *Therapeutic Exercise for Spinal Segmental Stabilization in Low Back Pain: Scientific Basis and Clinical Approach*: Churchill Livingstone.

Richardson, C. A., Snijders, C. J., Hides, J. A., Damen, L., Pas, M. S., & Storm, J. (2002). The relation between the transversus abdominis muscles, sacroiliac joint mechanics, and low back pain. *Spine (Phila Pa 1976), 27*(4), 399-405.

Robertson, G., Caldwell, G., Hamill, J., Kamen, G., & Whittlesey, S. (2013). *Research Methods in Biomechanics, 2E*: Human Kinetics.

Rowe, P. J., Myles, C. M., Hillmann, S. J., & Hazlewood, M. E. (2001). Validation of Flexible Electrogoniometry as a Measure of Joint Kinematics. *Physiotherapy, 87*(9), 479-488. doi:10.1016/S0031-9406(05)60695-5

Saur, P. M., Ensink, F. B., Frese, K., Seeger, D., & Hildebrandt, J. (1996). Lumbar range of motion: reliability and validity of the inclinometer technique in the clinical measurement of trunk flexibility. *Spine (Phila Pa 1976), 21*(11), 1332-1338.

Statistics Canada. (2006). Back Pain. Retrieved from http://www.statcan.gc.ca/pub/82-619-m/2006003/4053542-eng.htm

Tahan, N., Arab, A. M., Vaseghi, B., & Khademi, K. (2013). Electromyographic evaluation of abdominal-muscle function with and without concomitant pelvic-floor-muscle contraction. *J Sport Rehabil, 22*(2), 108-114.

Tesio, L., Monzani, M., Gatti, R., & Franchignoni, F. (1995). Flexible electrogoniometers: kinesiological advantages with respect to potentiometric goniometers. *Clin Biomech (Bristol, Avon), 10*(5), 275-277.

Urquhart, D. M., Hodges, P. W., Allen, T. J., & Story, I. H. (2005). Abdominal muscle recruitment during a range of voluntary exercises. *Man Ther, 10*(2), 144-153. doi:10.1016/j.math.2004.08.011

Vera-Garcia, F. J., Elvira, J. L., Brown, S. H., & McGill, S. M. (2007). Effects of abdominal stabilization maneuvers on the control of spine motion and stability against sudden trunk perturbations. *J Electromyogr Kinesiol, 17*(5), 556-567. doi:10.1016/j.jelekin.2006.07.004

Wells, R., & Winter, D. (1980). Assessment of signal and noise in the kinematics of normal, pathological and sporting gaits.

White, A. A., & Panjabi, M. M. (1978). *Clinical biomechanics of the spine*: Lippincott.

Winter, D. A. (2009). *Biomechanics and Motor Control of Human Movement*: Wiley.

Wood, G. A., & Hayes, K. C. (1974). A Kinetic Model of Intervertebral Stress During Lifting. *British Journal of Sports Medicine, 8*(2-3), 74-79. Retrieved from http://www.ncbi.nlm.nih.gov/pmc/articles/PMC1859485/

Wu, G., & Ladin, Z. (1996). Limitations of quasi-static estimation of human joint loading during locomotion. *Med Biol Eng Comput, 34*(6), 472-476.

Zatsiorsky, V. (2002). *Kinetics of Human Motion*: humankinetics.com.

APPENDIX A DETAILED KINEMATIC & KINETIC MODEL

A.1. SEGMENTS' ACS & LCS

After placing the motion markers on the participant's body according to the Fig. 3.2, a 1-second standing calibration trial was performed by instructing the participant to stand still for the duration of the trial. Then, using the three dimensional positions of the passive markers, and the guidelines below, anatomical and local (technical) coordinate systems (ACS and LCS respectively) were established for each segment of the body.

Legs ACS: The lateral and medial malleolus, and femoral epicondyles data are available from the standing calibration trial. For each leg, the ankle joint center (AJC) was calculated by estimating the midpoint between the lateral (LM) and medial (MM) malleolus:

$$AJC = \frac{LM + MM}{2}$$

Similarly, the knee joint center (KJC) was calculated by computing the midpoint between the lateral (LE) and medial (ME) femoral epicondyles:

$$KJC = \frac{LE + ME}{2}$$

For each leg, the anatomical Y-axis runs from the AJC to KJC. The X-axis is a vector normal to a plane containing the AJC, KJC and LE, and is calculated by the equations below:

v1 = LE – AJC

X-axis = Y-axis × v1

The Z-axis is the cross product of X-axis and Y-axis. Then, all the anatomical coordinate axes were converted to unit vectors by dividing each axis by its normal vector. This is shown below:

$$x = \frac{\vec{X}}{|x|}$$

$$y = \frac{\vec{Y}}{|y|}$$

$$z = \frac{\vec{Z}}{|z|}$$

The origin of the leg's coordinate system is KJC.

Thighs ACS: The hip joint center (HJC) was estimated based on equations from Reed et al. (Reed, Manary, & Schneider, 1999). Both left (LASIS) and right (RASIS) anterior superior iliac spine data are available from the standing calibration trial. First, flesh margin corrections were performed on both LASIS and RASIS to move these anatomical landmarks from surface to bone. This was done by subtracting 10mm AP vector (i.e. anterior to posterior or on the X-axis as shown in Fig. A.1.) from both LASIS and RASIS. Then the 3D position of HJC is scaled by the pelvis width (PW) which is defined as the distance between LASIS and RASIS. The scaling factors for the left HJC are -20.8%, -36.1%, and -27.8% of the pelvis width. For the right HJC, the scaling factors are equal to -20.8%, 36.1%, and -27.8% of the pelvis width. The pelvic width and the coordinate system used for scaling the HJCs are shown in Fig. A.1.

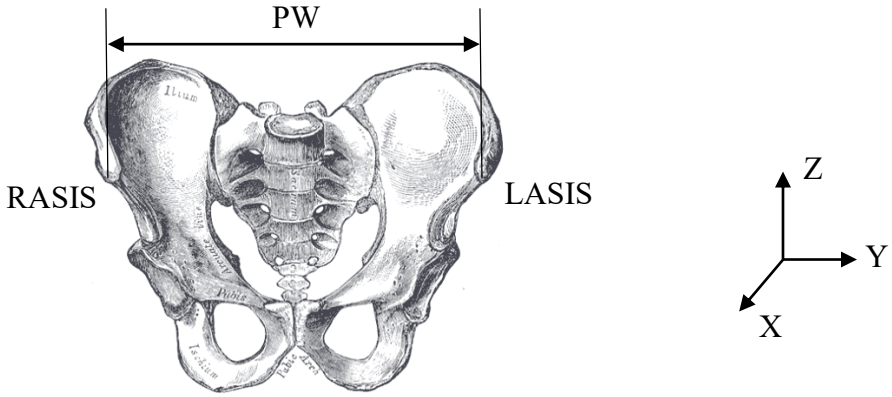

Figure A-1: Pelvis width, the locations of RASIS and LASIS, and the coordinate system used for estimating the HJCs. The coordinate system shown here is according to Reed et al. (1999) and was used for flesh margin adjustments of pelvis's anatomical landmarks, and calculation of hip joint centers and lumbar joint center. Henry Vandyke Carter [Public domain], via Wikimedia Commons.

The Y-axis of each thigh's anatomical coordinate system runs from KJC to HJC. The X-axis is normal to a plane containing HJC, LE and ME, and is calculated by the following equations:

$v2 = LE - ME$

$X\text{-axis} = Y\text{-axis} \times v2$

The Z-axis is simply the cross product of X-axis and Y-axis. Similar to the legs, the axes unit vectors were calculated from thighs' anatomical coordinate system vectors obtained above. The origin of the thigh's coordinate system is at HJC.

Pelvis ACS: First, the flesh margin adjustment was performed on the posterior superior iliac spines (PSISs) by a 10mm vector in the X-axis (the X-axis direction is shown in Fig. A.1.). The Z-axis of pelvis' anatomical coordinate system runs from LASIS to RASIS.

The Y-axis is normal to a plane containing LASIS, RASIS, and the midpoint between PSISs (MPSIS), and is calculated using the equations below:

$v3 = MPSIS - LASIS$

$Y\text{-axis} = v3 \times Y\text{-axis}$

The X-axis is the cross product of Y-axis and Z-axis. Then, the unit vectors of the pelvis' anatomical coordinate system were calculated. The origin of the pelvis's anatomical coordinate system is at lumbar joint center (LJC) or L5/S1 joint of spine which was calculated using the same procedure that estimates HJCs. For this study, it is assumed that the joint moments and stiffness calculated at L5/S1 are equal to the joint moments and stiffness at L4/L5. The scaling factors used to estimate LJC are -26.4%, 0%, and 12.6% of the pelvis width using the coordinate system directions shown in Fig. A.1.

Trunk ACS: The 3D positions of the suprasternale (SUP) and the 7th cervicale (C7) are available from the standing calibration trial. Using the 3D positions of SUP and C7, the cervical joint center (CJC) is estimated according to Reed et al. (1999). As illustrated in Fig. A.2, the location of the CJC is estimated based on a vector from C7 to SUP. The CJC is on a line forming an 8^{o} angle with the vector from C7 to SUP, and is located at 55% of the thorax width from C7.

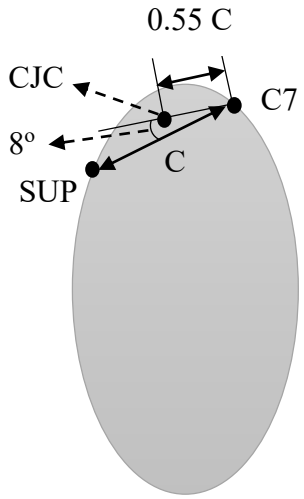

Figure A-2: The location of the cervical joint center as seen from the left side of the trunk. C is the thorax width which is defined as distance from C7 to SUP.

The equations that were used to calculate the CJC are as follows:

$$CJC\_tmp = 0.55 \times (SUP - C7)$$

$$CJC\_tmp2 = \begin{bmatrix} \cos(8°) & 0 & -\sin(8°) \\ 0 & 1 & 0 \\ \sin(8°) & 0 & \cos(8°) \end{bmatrix} \begin{bmatrix} CJC\_tmp \end{bmatrix}$$

$$CJC = C7 + CJC\_tmp2$$

The Y-axis of the trunk runs from the LJC to the CJC. The Z-axis is normal to a plane that contains LJC, SUP and CJC, and was calculated using the equations below:

$$v4 = SUP - LJC$$

$$Z\text{-axis} = v4 \times Y\text{-axis}$$

The X-axis is simply the cross product of Y-axis and Z-axis. Then, the unit vectors of the trunk's anatomical coordinate system were calculated. The origin of the trunk's anatomical coordinate system is located at the CJC.

Segment's LCS: As shown in Fig. 3-1, a triad was placed on each segment of the body including trunk, pelvis, thighs, and shanks. These triads were used to obtain the local/technical coordinate system (LCS) for each segment. For instance, the equations below were used to calculate the leg's LCS as shown in Fig. A.3.

v1 = P2 – P1 = Y

v2 = P3 – P1

v3 = v1 × v2 = X

v4 = v3 × v1 = Z

$$x = \frac{\vec{X}}{|x|}$$

$$y = \frac{\vec{Y}}{|y|}$$

$$z = \frac{\vec{Z}}{|z|}$$

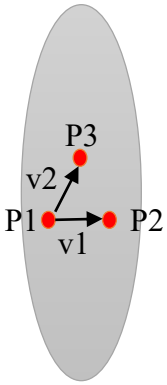

Figure A-3: Leg's triad.

Similarly, the LCS for other segments were calculated.

A.2. ROTATIONAL & TRANSLATIONAL MATRICES

After obtaining the LCS and ACS for the trunk, pelvis, thighs and legs from the standing calibration trial, the rotation and translation matrices were calculated for each segment. For instance, to obtain the rotation matrix (R) of the leg's LCS to the global coordinate system (GCS) set in the laboratory, the leg's LCS calculated above was used as shown below:

$$R\_leg = \begin{bmatrix} x\_i & y\_i & z\_i \\ x\_j & y\_j & z\_j \\ x\_k & y\_k & z\_k \end{bmatrix}$$

The translation matrix (T) moving the leg's LCS to the GCS was calculated as shown below:

First, an origin (O) was chosen for the leg's LCS. The location of the origin is arbitrary and it can be chosen anywhere (i.e. P1, P2, etc.). For this study, the location of the segment's LCS origin was calculated by taking mean of all points' locations on the triad:

$$O\_leg = \frac{P1 + P2 + P3}{3}$$

The leg's translation matrix (T) from the leg's LCS to the GCS is shown below:

$$\text{T\_leg} = \begin{bmatrix} 1 & 0 & 0 & 0 \\ O\_leg\_i & x\_i & y\_i & z\_i \\ O\_leg\_j & x\_j & y\_j & z\_j \\ O\_leg\_k & x\_k & y\_k & z\_k \end{bmatrix}$$

Similarly, the segment's rotation and translation matrices from the ACS to the GCS were calculated, except that the matrices included the segment's ACS unit vectors. Moreover, the origin of the segment's ACS to GCS translation matrix is pre-determined as described in section A.1. For instance, the origin of the leg's ACS to GCS translation matrix was located at the KJC.

After calculating each segment's ACS to GCS and LCS to GCS rotation and translation matrices from the standing calibration trial, we were now able to obtain each segment's ACS to LCS rotation and translation matrices as shown below (T represents the transpose of the matrix):

$R_{L/A} = [R_{G/L}]^T [R_{G/A}]$

$T_{L/A} = [T_{G/L}]^T [T_{G/A}]$

A.3. VELOCITY & ACCELERATION

In order to calculate the joint moments at the L4/L5 joint of spine, the linear and angular accelerations of the legs, thighs, and pelvis must be computed first.

Linear Velocity: First from the standing calibration data, the center of mass (COM) of each segment including the feet, legs, thighs, and pelvis were calculated using the scaling

equations provided by Dumas et al. (2007). Then, using the transpose of each segment's LCS to GCS translation matrix, each segment's COM was moved to the segment's LCS (i.e. $COM\_local = [T_{G/L}]^T\ COM\_global$). Since it is assumed that the ankle's angle was constant during the entire exercises, COM of the foot and the leg were added together (i.e. $COM_{foot\&leg} = (m_{foot} \times COM_{foot} + m_{leg} \times COM_{leg})/ (m_{foot} + m_{leg})$), and then the resulting COM was moved to the leg's LCS using the transpose of the leg's LCS to GCS translation matrix. For the motion trials, the segment's COM at each point in time was calculated by multiplying the segment's LCS to GCS transformation matrix at that point in time by the segment's COM_local obtained from the standing calibration trial as described above (i.e. $COM\_global_i = [T_{G/L}]_i\ COM\_local$; where i is the point in time or the sample under investigation).

The COM data were padded at both ends using the first and last two samples of the data. The linear velocity was calculated using the finite difference approach as shown below (Winter, 2009):

$$v_i = \frac{COM(i+1) - COM(i-1)}{2 \times h}$$

Where v is the linear velocity of the segment being analyzed, i is the sample number, and h is inverse of frequency (i.e. freq. = 100Hz). After calculating the linear velocity, the padding was removed by deleting the first and last samples from the data.

Linear Acceleration: The finite difference approach was used again to estimate the segment's linear acceleration:

$$a_i = \frac{v(i+1) - v(i-1)}{2 \times h}$$

The linear velocity used in the equation above was the padded version before removing its first and last samples.

Angular Velocity: To find the angular velocity of the body's segments, first the angular displacement of each segment was calculated. To do this, the ACS to GCS rotation matrix of each segment was computed at each point in time for the motion trials. Based on how the ACS was defined for the body's segments in section A.1, the rotations around the X-, Y-, and Z-axes are abduction/adduction, flexion/extension, and internal/external rotations respectively. Therefore, the Cardan angle sequence that was used to calculate each segment's angular displacement was a ZXY sequence (i.e. first flexion/extension, then abduction/adduction, and finally internal/external rotation as recommended by the Canadian Society of Biomechanics (CSB)).

$$[R] = [R]_Y[R]_X[R]_Z$$

$$= \begin{bmatrix} c\theta_y c\theta_z - s\theta_x s\theta_y s\theta_z & c\theta_y s\theta_z + s\theta_x s\theta_y c\theta_z & -c\theta_x s\theta_y \\ -c\theta_x s\theta_z & c\theta_x c\theta_z & s\theta_x \\ s\theta_y c\theta_z + s\theta_x c\theta_y s\theta_z & s\theta_y s\theta_z - s\theta_x c\theta_y c\theta_z & c\theta_x c\theta_y \end{bmatrix}$$

Where c and s stand for cos and sin respectively. The next step includes simply comparing the expanded matrix above to the already calculated rotation matrix.

$$\theta_x = \text{asin}(R_{2,3}) \qquad \theta_y = \text{atan}(\frac{-R_{1,3}}{R_{3,3}}) \qquad \theta_z = \text{atan}(\frac{-R_{2,1}}{R_{2,2}})$$

The formula to calculate angular velocity is as follows:

$$\omega = M_\omega + d\varphi \rightarrow \begin{bmatrix} \omega_x \\ \omega_y \\ \omega_z \end{bmatrix} = \begin{bmatrix} c\emptyset_y & 0 & -s\emptyset_y c\emptyset_x \\ 0 & 1 & 0 \\ s\emptyset_y & 0 & c\emptyset_x c\emptyset_y \end{bmatrix} \begin{bmatrix} \dot{\emptyset}_x \\ \dot{\emptyset}_y \\ \dot{\emptyset}_z \end{bmatrix}$$

To find dφ, the filtered angular displacement data was padded, and then using the finite difference approach, dφ was calculated. Assuming a ZXY rotation sequence, M_ω was calculated as follows:

$$\omega' = \begin{bmatrix} 0 \\ 0 \\ \dot{\emptyset}_z \end{bmatrix}$$

$$\omega'' = \begin{bmatrix} \dot{\emptyset}_x \\ 0 \\ 0 \end{bmatrix} + \begin{bmatrix} 1 & 0 & 0 \\ 0 & c\emptyset_x & s\emptyset_x \\ 0 & -s\emptyset_x & c\emptyset_x \end{bmatrix} \begin{bmatrix} 0 \\ 0 \\ \dot{\emptyset}_z \end{bmatrix} = \begin{bmatrix} \dot{\emptyset}_x \\ s\emptyset_x \dot{\emptyset}_z \\ c\emptyset_x \dot{\emptyset}_z \end{bmatrix}$$

$$\omega''' = \begin{bmatrix} 0 \\ \dot{\emptyset}_y \\ 0 \end{bmatrix} + \begin{bmatrix} c\emptyset_y & 0 & -s\emptyset_y \\ 0 & 1 & 0 \\ s\emptyset_y & 0 & c\emptyset_y \end{bmatrix} \begin{bmatrix} \dot{\emptyset}_x \\ s\emptyset_x \dot{\emptyset}_z \\ c\emptyset_x \dot{\emptyset}_z \end{bmatrix} = \begin{bmatrix} c\emptyset_y \dot{\emptyset}_x - s\emptyset_y c\emptyset_x \dot{\emptyset}_z \\ s\emptyset_x \dot{\emptyset}_z + \dot{\emptyset}_y \\ s\emptyset_y \dot{\emptyset}_x + c\emptyset_y c\emptyset_x \dot{\emptyset}_z \end{bmatrix} = M\omega + d\varphi$$

$$\rightarrow M_\omega = \begin{bmatrix} c\emptyset_y & 0 & -s\emptyset_y c\emptyset_x \\ 0 & 1 & s\emptyset_x \\ s\emptyset_y & 0 & c\emptyset_x c\emptyset_y \end{bmatrix}$$

Angular Acceleration: To find the angular acceleration of pelvis, thighs and legs, the finite difference approach was utilized:

$$\alpha_i = \frac{\omega(i+1) - \omega(i-1)}{2 \times h}$$

Before using the equation above, the angular velocity was padded. Then, after the calculation of the angular acceleration, the padding was removed from the data.

A.4. L4/L5 JOINT ANGLE

To calculate L4/L5 joint angle, first, the LCS to ACS matrices of the pelvis and trunk obtained during the static standing trial (see section A.2) along with the LCS to GCS

matrices computed in the motion trials were used to find the relationship between the pelvis's and trunk's ACS. This is shown below:

$$[R]_{TrkACS/PelACS} = [R]_{TrkACS/TrkLCS}[R]_{TrkLCS/GCS}[R]_{GCS/PelLCS}[R]_{PelLCS/PelACS}$$

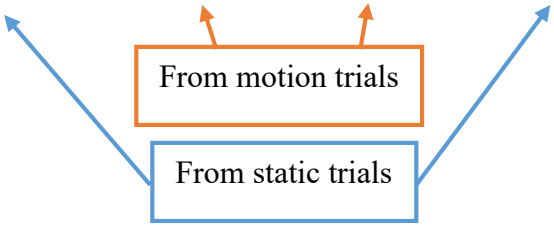

Where Trk and Pel stand for trunk and pelvis respectively, and also:

$$[R]_{PelLCS/PelACS} = [R]^{T}_{PelACS/PelLCS}$$

$$[R]_{TrkLCS/GCS} = [R]^{T}_{GCS/TrkLCS}$$

Now, the ZXY rotation sequence was calculated from the distal (i.e. pelvis) to proximal (i.e. trunk) which is negative (counter-clockwise) rotation about Y, then X, and then Z:

$$[R] = [R]_{Z}^{-1}[R]_{X}^{-1}[R]_{Y}^{-1}$$

$$= \begin{bmatrix} c\theta_y c\theta_z - s\theta_x s\theta_y s\theta_z & -c\theta_x s\theta_z & s\theta_y c\theta_z + s\theta_x c\theta_y s\theta_z \\ c\theta_y s\theta_z + s\theta_x s\theta_y c\theta_z & c\theta_x c\theta_z & s\theta_y s\theta_z - s\theta_x c\theta_y c\theta_z \\ -c\theta_x s\theta_y & s\theta_x & c\theta_x c\theta_y \end{bmatrix}$$

Where c and s stand for cos and sin respectively. The next step included simply comparing the expanded matrix above to the already calculated rotation matrix. Equation below shows the L4/L5 joint angle in the sagittal plane:

$$\theta_z = \text{atan}\left(\frac{-R_{1,2}}{R_{2,2}}\right)$$

A.5. INVERSE DYNAMICS

The L4/L5 joint moment was calculated using a standard bottom-up inverse dynamics technique. By using this technique, and by already having the linear and angular velocities and accelerations, ground reaction forces, and body segment inertial properties (BSIPs) (i.e. mass, COM, and moments of inertia), the net joint forces and moments were computed starting from the knees, then hips, and then the L4/L5 joint of spine. Figure A-4 illustrates a free body diagram (FBD) of a person at the starting position of the Trunk Stability Test protocol exercises (i.e. tasks used in this study).

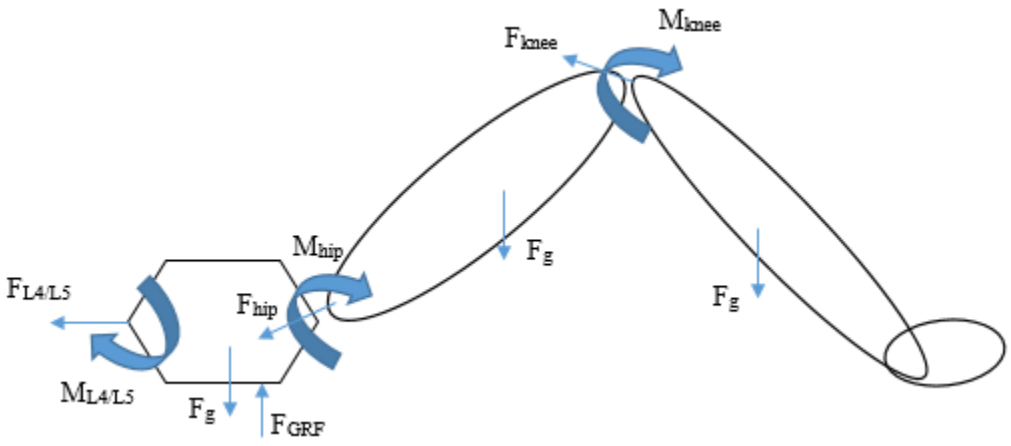

Figure A-4: Free body diagram of a person at the starting position of the Trunk Stability Test protocol exercises. For detailed free body diagrams of each body segment, please refer to Figs. A-5 to A-7.

The moments of inertia of the feet, legs, thighs, and pelvis were calculated using the equations provided by Dumas et al. (2007). In the joint moment's equations, the time rate of change of the body segments' angular momentum (H_{dot}) were calculated beforehand. This was done by first transforming the angular velocities and accelerations to the segments' ACS by means of the transpose of the ACS to the GCS rotation matrices of the

body segments in the motion trials. Then, by using the new angular velocities and accelerations and the previously calculated segments' moments of inertia, the H_{dot} in the sagittal plane was calculated:

$$H_{dot\_ACS} = I_{yy}\,\alpha_y + (I_{xx} - I_{zz})\,\omega_{xx}\,\omega_{zz}$$

Finally, the H_{dot} calculated above was transformed to the GCS using the body segments' ACS to the GCS rotation matrices. The values for H_{dot} was kept to be used in the joint moments equations described below.

Knee Joint Forces & Moments:

Figure A.5 depicts the FBD of foot and leg. Based on this figure, the force and moment equations at the knee joint were developed.

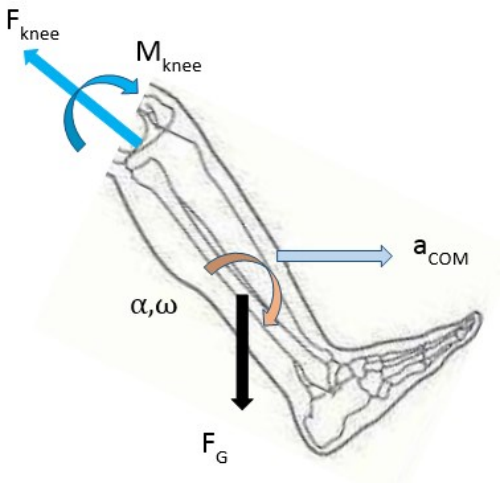

Figure A-5: Free body diagram of foot and shank.

$F_{KNEE} = m_1\ a_{com} - F_g$

Where F_{KNEE} = reaction force at the knee

m_1 = combined mass of foot and leg

a_{com} = linear acceleration of the combined center of mass of foot and leg

F_g = weight of combined foot and leg

Combined COM of foot and leg = $(m_{foot}\ COM_{foot} + m_{leg}\ COM_{leg})/ (m_{foot} + m_{leg})$

Where m_{foot} = mass of foot

COM_{foot} = location of foot's COM

m_{leg} = mass of leg

COM_{leg} = location of leg's COM

The knee moments equations are as follows:

$M_{knee} = H_{dot} - F_{KNEE} \times r$

$M_{kneey} = I_{yy}\ \alpha_y + (I_{xx} - I_{zz})\ \omega_{xx}\ \omega_{zz} - F_{KNEE}y \times r_y$

Where M_{kneey} = knee joint moment in the sagittal plane

r = vector pointing from segment's COM to knee joint center

I = combined foot's and leg's moments of inertia

ω = angular velocity of segment's COM

α = angular acceleration of segment's COM

Hip Joint Forces & Moments:

Figure A.5 illustrates the FBD of thigh. From this figure, the following equations were obtained:

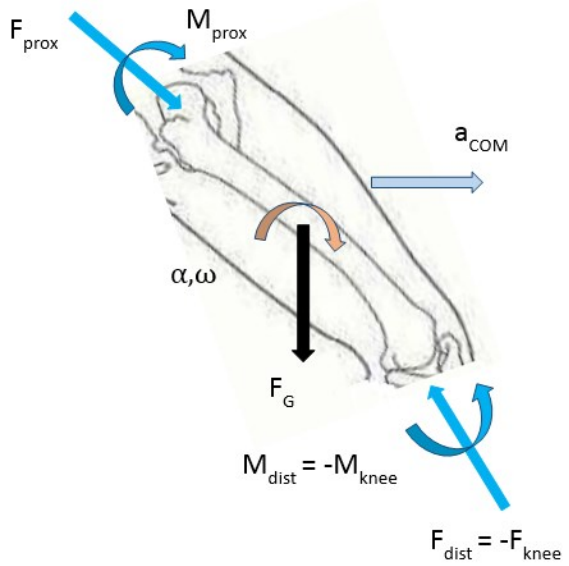

Figure A-6: Free body diagram of the thigh.

$F_{hip} = m_2\, a_{com} - F_g - F_{dist}$

Where F_{hip} = reaction force at the hip joint

m_2 = mass of thigh

a_{com} = linear acceleration of the thigh's COM

F_g = weight of thigh

$F_{dist} = - F_{knee}$

$M_{hip} = H_{dot} - F_{hip} \times r_1 - F_{dist} \times r_2 - M_{dist}$

Where M_{hip} = hip joint moment in the sagittal plane

H_{dot} = derivative of angular momentum of thigh about its 3D axes

F_{hip} = reaction force at the hip joint

r_1 = vector pointing from thigh's COM to hip joint center

$F_{dist} = - F_{knee}$

r_2 = vector pointing from thigh's COM to knee joint center

$M_{dist} = - M_{knee}$

L4/L5 Joint Forces & Moments:

Figure A.7 illustrates the FBD of pelvis. From this figure, the following equations were obtained:

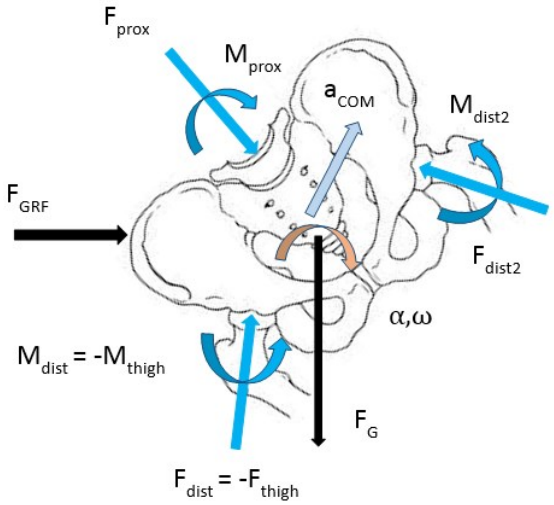

Figure A-7: Free body diagram of pelvis.

$F_{prox} = m_3\ a_{com} - F_g - F_{dist} - F_{GRF} - F_{dist2}$

Where F_{prox} = reaction force at the L4 / L5 joint in the sagittal plane

m_3 = mass of pelvis

a_{com} = linear acceleration of the pelvis's COM

F_g = weight of pelvis

F_{dist} and F_{dist2} = negative hip joint reaction forces.

F_{GRF} = ground reaction forces

$M_{prox} = H_{dot} - r_{prox} \times F_{prox} - r_{dist} \times F_{dist} - M_{dist} - M_{GRF} - r_{dist2} \times F_{dist2} - M_{dist2}$

Where M_{prox} = moment at the L4/L5 joint

H_{dot} = derivative of angular momentum of pelvis about its 3D axes

r_{prox} = vector pointing from pelvis's COM to L4/L5 joint

F_{dist} and F_{dist2} = negative reaction forces at the hip joints

r_{dist} and r_{dist2} = vector pointing from pelvis's COM to hip joint centers

M_{GRF} = ground reaction moments of force

The ground reaction forces and the center of pressure had a sampling rate of 2000Hz whereas the kinematic data captured by Qualisys™ were sampled at 100Hz. Therefore, prior to using the L4/L5 joint force and moments equations, the ground reaction force and center of pressure were down-sampled to 100Hz.

The L4/L5 joint moments calculated above were multiplied by (-1) to obtain the external joint moments. Moreover, since the moments were represented in the GCS, the L4/L5 joint moments were dotted with the joint coordinate system (JCS) axes of the joint. To do this, first the "floating axis" was calculated by the cross product of the medial-lateral axis of the trunk's ACS (Z-axis) and the long axis of the pelvis's ACS (Y-axis). The axes of the L4/L5 JCS included the floating axis pointing anteriorly (X-axis), the long axis of the pelvis (Y-axis), and the medial-lateral axis of the trunk (Z-axis).

APPENDIX B NORMALITY TEST RESULTS

Table below illustrates the normality test results of Objective 2 discrete variables using the Anderson-Darling technique. P-values under 0.05 indicate discrete variables that were not normally distributed (shown in bold font).

Discrete Variable	*p-Value*
Mean EMG amplitude of right IO in TST 1 NAH	0.343
Mean EMG amplitude of left IO in TST 1 NAH	0.339
Mean EMG amplitude of right IO in TST 1 AH	0.216
Mean EMG amplitude of left IO in TST 1 AH	0.646
Mean EMG amplitude of right IO in TST 3 NAH	**0.049**
Mean EMG amplitude of left IO in TST 3 NAH	**0.046**
Mean EMG amplitude of right IO in TST 3 AH	0.607
Mean EMG amplitude of left IO in TST 3 AH	0.492
L4/L5 joint angle ROM in TST 1 NAH from foot-off to foot-on	0.547
L4/L5 joint angle ROM in TST 1 NAH in phase 1	0.532
L4/L5 joint angle ROM in TST 1 NAH in phase 2	0.151
L4/L5 joint angle ROM in TST 1 AH from foot-off to foot-on	0.919
L4/L5 joint angle ROM in TST 1 AH in phase 1	0.626
L4/L5 joint angle ROM in TST 1 AH in phase 2	0.935
L4/L5 joint angle ROM in TST 3 NAH from foot-off to foot-on	0.822
L4/L5 joint angle ROM in TST 3 NAH in phase 1	0.810
L4/L5 joint angle ROM in TST 3 NAH in phase 2	0.852
L4/L5 joint angle ROM in TST 3 NAH in phase 3	0.731

L4/L5 joint angle ROM in TST 3 AH from foot-off to foot-on	0.087
L4/L5 joint angle ROM in TST 3 AH in phase 1	0.699
L4/L5 joint angle ROM in TST 3 AH in phase 2	0.325
L4/L5 joint angle ROM in TST 3 AH in phase 3	0.318
L4/L5 joint moment at m1 in TST 1 NAH	0.678
L4/L5 joint moment at m2 in TST 1 NAH	**<0.005**
L4/L5 joint moment at m3 in TST 1 NAH	0.655
L4/L5 joint moment at m1 in TST 1 AH	0.927
L4/L5 joint moment at m2 in TST 1 AH	**0.005**
L4/L5 joint moment at m3 in TST 1 AH	0.804
L4/L5 joint moment at m1 in TST 3 NAH	0.675
L4/L5 joint moment at m2 in TST 3 NAH	**<0.005**
L4/L5 joint moment at m3 in TST 3 NAH	0.234
L4/L5 joint moment at m4 in TST 3 NAH	**<0.005**
L4/L5 joint moment at m5 in TST 3 NAH	0.594
L4/L5 joint moment at m1 in TST 3 AH	0.965
L4/L5 joint moment at m2 in TST 3 AH	**0.008**
L4/L5 joint moment at m3 in TST 3 AH	0.336
L4/L5 joint moment at m4 in TST 3 AH	**0.036**
L4/L5 joint moment at m5 in TST 3 AH	0.826
L4/L5 joint stiffness in TST 1 NAH from foot-off to foot-on	**0.048**
L4/L5 joint stiffness in TST 1 NAH in phase 1	0.056
L4/L5 joint stiffness in TST 1 NAH in phase 2	0.089

L4/L5 joint stiffness in TST 1 AH from foot-off to foot-on	0.373
L4/L5 joint stiffness in TST 1 AH in phase 1	0.436
L4/L5 joint stiffness in TST 1 AH in phase 2	0.446
L4/L5 joint stiffness in TST 3 NAH from foot-off to foot-on	**0.036**
L4/L5 joint stiffness in TST 3 NAH in phase 1	**0.046**
L4/L5 joint stiffness in TST 3 NAH in phase 2	0.073
L4/L5 joint stiffness in TST 3 NAH in phase 3	**0.016**
L4/L5 joint stiffness in TST 3 AH from foot-off to foot-on	0.058
L4/L5 joint stiffness in TST 3 AH in phase 1	0.226
L4/L5 joint stiffness in TST 3 AH in phase 2	**0.047**
L4/L5 joint stiffness in TST 3 AH in phase 3	0.161

APPENDIX C DYNAMIC VS. QUASI-STATIC ANALYSIS

Tables below illustrate the results of comparison of dynamic and quasi-static L4/L5 joint moments across all participants.

Table C-1: Comparison of dynamic and quasi-static sagittal plane L4/L5 joint moments in TST 1. See Fig. 4-6 for a description of |ΔDyn| and |ΔQ|.

Participant #	***|ΔDyn| (Nm)***	***|ΔQ| (Nm)***	***|ΔDyn-ΔQ | (Nm)***	***RMSE (Nm)***	***%Error***
1	106.5	64.6	41.8	13.8	15.8
2	102.6	65.8	36.8	12.7	34.2
3	161.0	110.1	50.9	19.1	34.6
4	87.5	58.7	28.8	10.8	14.5
5	98.7	66.8	32.0	11.8	15.6
6	57.2	31.2	26.0	9.3	16.1
7	69.7	41.4	28.3	10.2	13.8
8	61.4	36.8	24.6	8.4	12.4
9	61.9	39.5	22.5	7.9	10.8
10	55.1	29.9	25.2	9.3	13.3
Mean (SD)	**86.2 (32.9)**	**54.5 (24.4)**	**31.7 (9.0)**	**11.3 (3.3)**	**18.1 (8.7)**

Table C-2: Comparison of dynamic and quasi-static sagittal plane L4/L5 joint moments in TST 3. See Fig. 4-6 for a description of |ΔDyn| and |ΔQ|.

Participant #	***|ΔDyn| (Nm)***	***|ΔQ| (Nm)***	***|ΔDyn-ΔQ | (Nm)***	***RMSE (Nm)***	***%Error***
1	142.4	109.3	33.2	10.3	9.5
2	157.9	121.8	36.1	8.3	15.0
3	242.7	200.2	42.5	15.3	16.5
4	139.0	105.0	34.1	9.2	9.3
5	137.1	111.8	25.3	7.8	8.0
6	87.8	71.1	16.7	5.1	7.6
7	100.7	68.7	32.0	7.0	8.7
8	83.4	58.4	25.0	6.0	7.5
9	97.4	77.8	19.6	5.3	6.1
10	82.3	62.1	20.3	4.9	6.3
Mean (SD)	**127.1 (49.2)**	**98.6 (42.5)**	**28.5 (8.4)**	**7.9 (3.2)**	**9.5 (3.5)**

Table C-3: Difference between dynamic and quasi-static L4/L5 joint moments at the minima and maxima (Δmi) in TST 1. %Δmi was calculated by dividing Δmi by the peak to peak dynamic moment (Δdyn), and then multiplying the result by 100.

Participant #	***Δm1 (Nm)***	***%Δm1***	***Δm2 (Nm)***	***%Δm2***	***Δm3 (Nm)***	***%Δm3***
1	20.6	19.3	22.3	20.9	17.6	16.5
2	17.3	16.9	19.6	19.1	18.0	17.5
3	30.2	18.8	25.2	15.6	25.8	16.0
4	12.2	13.9	16.6	19.0	13.0	14.9
5	13.9	14.1	19.4	19.6	12.9	13.1
6	11.7	20.5	15.0	26.3	8.5	14.9
7	8.7	12.4	19.7	28.3	9.4	13.5
8	10.2	16.6	17.5	28.5	10.2	16.5
9	8.6	13.8	14.4	23.3	8.2	13.2
10	9.9	17.9	16.8	30.5	8.4	15.3
Mean (SD)	14.3 (6.8)	16.4 (2.7)	18.7 (3.3)	23.1 (5.0)	13.2 (5.7)	15.1 (1.5)

Table C-4: Difference between dynamic and quasi-static L4/L5 joint moments at the minima and maxima (Δmi) in TST 3. %Δmi was calculated by dividing Δmi by the peak to peak dynamic moment (Δdyn), and then multiplying the result by 100.

	Δm1 (Nm)	***% Δm1***	***Δm2 (Nm)***	***% Δm2***	***Δm3 (Nm)***	***% Δm3***	***Δm4 (Nm)***	***% Δm4***	***Δm5 (Nm)***	***% Δm5***
1	19.9	14.0	20.0	14.0	14.6	10.2	21.5	15.1	18.0	12.6
2	11.5	7.3	13.0	8.3	17.9	11.4	18.5	11.7	13.4	8.5
3	22.6	9.3	24.7	10.2	20.3	8.4	25.1	10.4	31.7	13.1
4	9.7	7.0	15.3	11.0	18.6	13.4	16.5	11.9	10.8	7.8
5	9.2	6.7	14.1	10.3	11.9	8.7	16.6	12.1	11.7	8.5
6	8.5	9.7	12.1	13.8	6.8	7.8	9.2	10.5	4.5	5.1
7	8.0	8.0	16.2	16.1	16.0	15.9	12.7	12.6	3.5	3.5
8	8.1	9.7	13.5	16.2	13.9	16.7	9.8	11.7	6.3	7.6
9	7.3	7.5	10.0	10.2	11.3	11.7	9.1	9.3	4.4	4.5
10	7.3	8.9	12.7	15.4	8.4	10.2	5.4	6.5	3.3	4.1
Mean	11.2	8.8	15.2	12.6	14.0	11.4	14.4	11.2	10.8	7.5
(SD)	(5.5)	(2.1)	(4.3)	(2.9)	(4.4)	(3.1)	(6.2)	(2.3)	(8.9)	(3.4)

APPENDIX D DYNAMIC MOMENT W/ AND WO/ GRF

Tables below illustrate the results of comparison of dynamic L4/L5 joint moments with and without GRF data across all participants.

Table D-1: Comparison of dynamic sagittal plane L4/L5 joint moments with and without GRF in TST 1.

Participant #	***|ΔDyn| (Nm)***	***|ΔQ| (Nm)***	***|ΔDyn-ΔQ | (Nm)***	***RMSE (Nm)***	***%Error***
1	106.5	101.8	4.7	14.3	16.3
2	102.6	103.0	0.4	8.9	23.9
3	161.0	169.1	8.1	6.8	12.3
4	87.5	87.2	0.3	8.8	11.8
5	98.7	104.5	5.8	14.6	19.2
6	57.2	64.5	7.3	16.0	27.9
7	69.7	68.3	1.4	9.7	13.1
8	61.4	73.0	11.6	17.4	25.8
9	61.9	63.2	1.3	11.7	15.9
10	55.1	55.7	0.6	9.7	13.9
Mean (SD)	**86.2 (32.9)**	**89.0 (33.5)**	**4.2 (4.0)**	**11.8 (3.6)**	**18.0 (5.9)**

Table D-2: Comparison of dynamic sagittal plane L4/L5 joint moments with and without GRF in TST 3.

Participant #	***|ΔDyn| (Nm)***	***|ΔQ| (Nm)***	***|ΔDyn-ΔQ | (Nm)***	***RMSE (Nm)***	***%Error***
1	142.4	138.3	4.1	13.2	12.2
2	157.9	154.1	3.8	9.8	17.7
3	242.7	239.4	3.2	4.8	5.2
4	139.0	137.6	1.4	8.4	8.5
5	137.1	133.2	3.9	13.4	13.7
6	87.8	88.2	0.4	14.7	22.1
7	100.7	99.9	0.7	9.6	11.8
8	83.4	85.9	2.5	16.1	19.9
9	97.4	94.6	2.8	10.4	11.9
10	82.3	79.6	2.8	8.7	11.1
Mean (SD)	**127.1 (49.2)**	**125.1 (48.1)**	**2.6 (1.3)**	**10.9 (3.4)**	**13.4 (5.2)**

Table D-3: Difference between dynamic L4/L5 joint moments with and without GRF at the locations shown in Fig. 4-7 in TST 1 (Δmi). %Δmi was calculated by dividing Δmi by the peak to peak dynamic moment (Δdyn), and then multiplying the result by 100.

Participant #	***Δm1(Nm)***	***%Δm1***	***Δm2(Nm)***	***%Δm2***	***Δm3(Nm)***	***%Δm3***
1	17.8	16.7	14.3	13.4	23.0	21.6
2	13.1	12.8	10.3	10.0	14.2	13.8
3	19.8	12.3	6.2	3.9	10.0	6.2
4	12.8	14.6	9.7	11.1	14.3	16.4
5	26.5	26.8	14.6	14.8	25.5	25.8
6	26.9	47.0	16.0	28.0	23.4	40.8
7	20.8	29.9	10.2	14.7	19.4	27.8
8	30.5	49.6	17.6	28.7	22.9	37.3
9	19.5	31.5	12.5	20.2	17.3	27.9
10	20.4	37.0	10.0	18.2	19.4	35.2
Mean (SD)	20.8 (5.8)	27.8 (13.8)	12.1 (3.5)	16.3 (7.8)	18.9 (5.0)	25.3 (11.0)

Table D-4: Difference between dynamic L4/L5 joint moments with and without GRF at the locations shown in Fig. 4-7 in TST 3 (Δmi). %Δmi was calculated by dividing Δmi by the peak to peak dynamic moment (Δdyn), and then multiplying the result by 100.

	Δm1 (Nm)	***%Δm1***	***Δm2 (Nm)***	***%Δm2***	***Δm3 (Nm)***	***%Δm3***	***Δm4 (Nm)***	***%Δm4***	***Δm5 (Nm)***	***%Δm5***
1	19.8	13.9	14.9	10.5	14.0	9.9	17.0	11.9	19.2	13.5
2	14.4	9.1	11.7	7.4	9.5	6.0	12.4	7.8	16.6	10.5
3	17.7	7.3	5.7	2.4	4.0	1.6	4.8	2.0	10.0	4.1
4	11.4	8.2	10.4	7.5	8.4	6.1	9.7	7.0	14.3	10.3
5	27.7	20.2	14.7	10.8	14.2	10.4	14.3	10.4	26.7	19.5
6	23.6	26.9	15.5	17.7	14.7	16.8	15.6	17.8	21.9	25.0
7	19.2	19.1	10.1	10.0	9.5	9.4	9.9	9.8	26.3	26.1
8	28.3	33.9	17.6	21.1	17.5	21.0	15.1	18.1	21.6	25.9
9	19.8	20.4	11.7	12.0	10.0	10.3	11.6	12.0	16.9	17.4
10	25.8	31.3	9.9	12.1	7.7	9.4	8.4	10.2	20.9	25.4
Mean	20.8	19.0	12.2	11.2	11.0	10.1	11.9	10.7	19.4	17.8
(SD)	(5.6)	(9.5)	(3.5)	(5.3)	(4.0)	(5.5)	(3.8)	(4.8)	(5.2)	(7.9)